AN ABSTRACT OF THE THESIS OF

Hosung Chang for the degree of Doctor of Philosophy in

Electrical and Computer Engineering presented on

Mar. 5, 1993

Title: ANALYSIS OF LINEAR AND NONLINEAR COUPLED DIELECTRIC WAVEGUIDES

Abstract approved: Signature redacted for privacy.

Prof. Vijai K. Tripathi

Multiport network functions, such as impedance matrix parameters and scattering parameters, of general multiple coupled slab waveguides are derived in terms of the normal mode parameters of the system. These characteristic normal mode parameters include the propagation constants, the modal impedances, and the eigenvector matrices. It is shown that the results of the analysis for four and six port optical directional couplers based on this approach are in good agreement with those based on the conventional coupled mode theory for matched systems. In addition, unlike the coupled mode theory, this approach allows for the inclusion of the structure terminations or the boundary conditions and can be readily used to calculate the near and far end crosstalk in optical interconnects. Examples

of general asymmetric two-waveguide and symmetric three-waveguide couplers are included to demonstrate the applications and usefulness of this method.

The conventional matrix method algorithm which has been used to study graded index and nonlinear waveguides is modified here for enhanced accuracy and efficiency. This enhanced algorithm is used to investigate the propagation characteristics and the nonlinear switching behavior of general five-layer waveguide structures with self-defocusing nonlinear coupling media. The saturation effects of the nonlinear media are incorporated by using a two-level saturation model. The numerical results obtained for a multiple quantum well directional coupler are shown to be in agreement with published experimental data. This method is also applied to analyze a nonlinear three-waveguide coupler with self-defocusing coupling media. The results show the power dependent switching characteristics when the light is coupled to the input of an outside guide, whereas a quasi-linear switching behavior is obtained for excitation to the center guide.

# Analysis of Linear and Nonlinear Coupled Dielectric Waveguides

by

Hosung Chang

A Thesis

submitted to

Oregon State University

in partial fulfillment of
the requirements for the
degree of

Doctor of Philosophy

Completed March 5, 1993

Commencement June 1993

APPROVED:

Signature redacted for privacy.

Professor of Electrical and Computer Engineering in charge of major

Signature redacted for privacy.

Head of Department of Electrical and Computer Engineering

Signature redacted for privacy.

Dean of Graduate School

Date thesis is presented March 5, 1993

Typed by : Hosung Chang

ACKNOWLEDGEMENTS

The author wishes to express his most sincere appreciation to his major professor, Dr. Vijai K. Tripathi, for invaluable counsel during the course of this study and for many hours spent in the preparation of this manuscript. The writer extends thanks to his doctoral committee: Dr. Thomas Plant who served as a major professor in his master's program, Dr. Ronald Mohler, Dr. Flanklin Flaherty, and Dr. White Warnes.

Conversations with Dr. Youn K. Chin, Dr. Andreas Weisshaar, and a fellow graduate student, Sung K. Lim, were helpful and appreciated. The author would like to thank his parents for the tremendous support during his academic career. Finally, special thanks go to his wife, Kijung, for her patience and constant encouragement.

TABLE OF CONTENTS

LIST OF FIGURES

# Analysis of Linear and Nonlinear Coupled Dielectric Waveguides

## CHAPTER 1

## INTRODUCTION

### 1.1 Background

The field of integrated optics (IO) for signal processing and communication systems has experienced a rapid growth in recent years in view of the anticipated size advantages and cost reductions as well as reduced power consumption and performance superior to that of bulk optics. With the development of GaAs/AlGaAs hetero-junction lasers [1-3] which operate at room temperatures with low threshold currents and optical fibers [4] with an attenuation constant of 20 dB/km at the wavelength of 632.8 nm, there has been a revolution in the field of optical communications.

For silica-based optical fibers, attenuation loss minima have been found at 1.2 $\mu$m (0.47 dB/km), 1.3 $\mu$m (0.6 dB/km), and 1.55 $\mu$m (0.2 dB/km) [5-7]. These advances in optical fiber development have enabled the coterminous development of long wavelength (e.g., from 1.0 to 1.7 $\mu$m)

semiconductor lasers [8-17]. Accompanying this progress in fiber technology, a number of complementary devices have been developed to provide light sources and detectors, modulators and couplers, and the integration of opto-electronic components.

Optical directional couplers, which consist of more than two closely-spaced, single-mode waveguides, are important components of almost all integrated optical circuits. Directional couplers can be used as power dividers or combiners, modulators and switches [18-24], and samplers and filters [25-27]. A primary technique for the analysis and design of such optical multiports has been the coupled mode theory. Coupled mode theory was first formulated by Pierce [28] in 1954 for the analysis of coupled electron beams in microwave travelling-wave tubes. Miller [29] subsequently applied the principle to the analysis and design of microwave waveguide structures, and Marcuse [30-31], Snyder [32], Yariv [33], and Kogelnik [34], in turn, provided implementations of conventional coupled mode theory for optical waveguides. The theory has since been widely applied to numerous optoelectronic components and fiber optic devices, including optical directional couplers which can perform optical logic functions [35-36].

Conventional coupled mode theory is based upon the assumption that uncoupled waveguide modes are orthogonal to

one another. Hardy and Streifer [37-39] introduced cross-power terms which are based on the nonorthogonality of modes for conventional coupled mode theory and Haus et al. [40-42] developed the method derived from variational principle and power nonorthogonality. These nonorthogonal formulations have been shown to yield more accurate results for weakly-coupled waveguides and TE (transverse electric) modes than the conventional method. However, the numerical accuracy of the coupled-mode analysis has not yet been determined for strongly coupled cases and for TM (transverse magnetic) modes [40,43].

A finite length coupled transmission system can be characterized in terms of multiport network functions such as an immittance matrix, a chain matrix, or scattering parameters. Explicit closed form expressions of scattering parameters of asymmetric two-line and symmetric three-line structures were derived by Tripathi [44-47] in terms of normal mode parameters of coupled systems. This form of coupled line analysis which has been applied to numerous active and passive coupled distributed parameter circuits [48-54] can be used as an alternative analytical tool for the study and design of multiple weakly or strongly coupled optical waveguides.

Single and coupled waveguides imbedded in a nonlinear media such as a Kerr-like nonlinear medium whose refractive index changes in proportion to optical intensities has

attracted increased interest. Nonlinear dielectric constant (i.e., the optical Kerr effect) originates from the third-order susceptibility term of nonlinear polarization expansions. Most studies of the intensity-dependent characteristics of nonlinear guided waves have been based on theoretical analyses, but a number of all-optical devices [55-57] for single waveguide schemes, including optical limiters, lower threshold devices, spatial scanners, and optically tunable optical filters, have been proposed. Materials such as silicate glasses, ZnS, and liquid crystal MBBA, have been considered as the primary nonlinear material choices for self-focusing media where the refractive indices increase with optical intensities, exhibit such weak nonlinearities that applications of these materials to optical signal processing has been restricted due to high power consumption and large device dimensions.

The nonlinear directional coupler (NLDC), capable of performing novel all-optical switching and logic operations, was first proposed and analyzed based on the coupled mode theory by Jensen [58]. The semiconductor multiple quantum-well (MQW) layer is a self-defocusing medium whose refractive index decreases in proportion to optical intensity, exhibiting high nonlinearity due to excitonic absorption [59-60] near the bandgap in multiple quantum-wells. Power dependent switching characteristics at substantial reductions of switching power were first

demonstrated by Li Kam Wa *et al.* [61] for a strain-induced GaAs-AlGaAs multiple quantum-well coupler. The coupled mode theory provides an analytical tool for the description of intensity-dependent switching behaviors, and had been almost exclusively applied to the analysis and design of nonlinear directional couplers. Recently, Ghatak *et al.* [62-63] have developed a convenient matrix method for the analysis of linear planar waveguides with inhomogeneous refractive index profiles as well as three-layer nonlinear planar waveguides. In addition, Cada *et al.* [64] have used a mode combination method based on a combination of perturbed symmetric and antisymmetric modes of a multiple quantum well directional coupler and have shown that coupling length is power dependent.

Recently, experimental results [65-66] for GaAs-based multiple quantum-well directional couplers have shown that at high input powers, the results based on coupled mode theory are not in good agreement with the measured data. Saturation effects, thermal nonlinearity fluctuation, material losses, and fabrication errors were suggested as possible sources of this discrepancy [65]. In practical terms, however, maximum changes in the refractive indices of a nonlinear medium were evidenced, and the dielectric constants did not change in proportion to the optical intensities. Two saturation models [67-71], the exponential saturable and the two-level saturable models, have

also been proposed to model this refractive index variation with electric field. At high powers, the saturation of nonlinearity serves to degrade the switching characteristics of a nonlinear directional coupler. Although, improved versions [72-74] of the coupled mode theory have been proposed that include saturation effects and absorption losses [75-76], the results obtained by using these techniques have not clearly explained the experimental data.

Over the next few years, based upon the demands for the realization of ultrafast optical signal processing and optical computing methodologies, the area of nonlinear integrated optics based on the third-order nonlinearities is expected to be an active area of research.

## 1.2 Organization of the Study

The current investigation is presented in six chapters. Chapter 1 includes a brief historical background of the development of linear and nonlinear directional couplers, as well as the summary of the organizational structure of the present study, as described in this section.

In the second chapter, normal mode analysis of coupled guided wave transmission line structures (i.e., coupled transmission line analysis) is reviewed and then applied to the case of general multiple coupled optical waveguides.

The method of analysis includes the derivation of the scattering parameters expressed in terms of normal mode parameters for asymmetric two-line and symmetric three-line structures with nonmode converting terminations. Multiport impedance matrix parameters and the scattering parameters for a general n-waveguide coupler are derived from the normal mode analysis by following the same procedure that used for multiple coupled transmission lines. In addition, procedures for the determination of normal mode parameters for optical coupled waveguides, based upon the solution of the field equations obtained by solving the standard boundary value problem and transverse resonance technique, are also presented.

The normal mode parameters for asymmetric two-waveguide and symmetric three-waveguide directional couplers are calculated in Chapter 3. Numerical results for the output power distributions of asymmetric two-waveguide and symmetric three-waveguide couplers, based upon calculation of the scattering parameters derived in Chapter 2, are obtained and are compared to those obtained from the implementation of coupled mode theory.

In chapter 4, analytic solutions for nonlinear wave equations in relation to various waveguide structures are considered. For the analysis and design of nonlinear directional couplers with saturable nonlinear coupling media, the matrix method is modified to provide better

accuracy and efficiency. To obtain the power-dependent characteristics of the couplers with saturable coupling media, procedures for the determination of unperturbed and perturbed modes of nonlinear two-waveguide directional couplers are illustrated.

Numerical results for the power-dependent characteristics of the unperturbed modes, as obtained from the application of extended matrix methods, are compared with those for exact analyses in Chapter 5. Nonlinear switching behaviors which can be explained by combinations of perturbed modes in the presence of saturation in multiple quantum well coupling medium are compared to the experimental data. The system consisting of symmetric two-waveguide couplers bounded by two self-focusing nonlinear media is also considered. In addition, the analysis of a three-waveguide coupler with two multiple quantum-well nonlinear coupling regions is presented together with the numerical results.

The final chapter includes concluding remarks as well as suggestions for future research directions for the improvement or extension of the techniques developed in the course of the present investigation.

# CHAPTER 2

# LINEAR MULTIPLE COUPLED DIELECTRIC WAVEGUIDES

## 2.1 Introduction

A multiport structure which consists of two or more uniformly coupled waveguides leads to power exchange between the guided modes of the individual waveguides and can be used as a directional coupler. The system considered in this chapter consists of such parallel dielectric waveguides with linear and lossless media.

Coupled mode theory has been the predominant tool used for the analysis of optical directional couplers since the first coupled mode formulations for optical circuits were developed by Marcus, Snyder, Yariv, and Kogelnik [30-34]. This method employs perturbation theory to calculate the coupling coefficients, $k_{12}$ and $k_{21}$, from one guide to the next for two-waveguide couplers. The principle of power conservation requires that $k_{12}$ and $k_{21}$ be complex conjugate of one another. However, this method provides accurate results for identical waveguides or weakly coupled waveguides only, and may not be applied, in general, to nonidentical or strongly coupled waveguides.

Conventional coupled mode theory for coupled guided wave structure is based upon the assumption that the uncoupled waveguide modes are orthogonal to one another. Nonorthogonal coupled mode theory, as investigated by Haus *et al*. [40-42], has resulted in more accurate dispersion relations for weakly coupled waveguides and TE modes. Though coupled mode formulation has been significantly improved over the years, the method dose not lead to accurate results for strongly coupled waveguides and TM modes [40,43].

At microwave and millimeter wave frequencies uniformly coupled transmission line circuits have also been used for various applications, including filters, couplers, and impedance matching networks. Circuits have been designed by using network functions such as impedance, admittance, scattering, and other parameters to represent multi-port networks. Closed form expressions for the scattering parameters of two- and three-line multiports were derived by Tripathi [44-47] in terms of the normal mode parameters for coupled transmission line structures with nonmode converting terminations encompassing the excitation of the individual normal modes of the coupled systems. General expressions for the network functions of n-line structures were developed by Chin [48]. Normal mode parameters consist of the ratios of line voltages, propagation constants, and characteristic line impedances for normal

modes. Analogous normal mode parameters can also be defined for coupled optical waveguides. These normal mode parameters consisting of the ratios of the peak amplitudes for electric fields within guiding layers, propagation constants, and wave impedances for the guided modes can be used to evaluate the scattering matrix of the coupled waveguide multiports.

The basic parameters used for characterizing coupled transmission lines such as characteristic impedances are, in general, not defined for inhomogeneous guided wave structures including coupled optical waveguides. This is primarily because the characteristic impedance or wave impedance does not have a unique definition for inhomogeneous structures. However, a set of equations representing waveguide fields can be obtained from the application of an analogy between normal mode waveguide solutions and those for transmission lines. This form of normal mode analysis can be used as an alternative tool for the analysis of general and multiple coupled optical waveguides.

The coupled mode theory which is most frequently used for the analysis and design of optical devices is briefly reviewed in the following section. The normal mode analysis of coupled transmission lines and coupled waveguides are then considered in the subsequent sections.

## 2.2 Coupled Mode Theory

Based upon the use of conventional coupled mode theory as a starting point, TE modes, lossless media, and two single-mode individual waveguides are considered in this section without loss of generality. For planar optical waveguides, z is considered to be the direction of propagation and x the direction perpendicular to the interfaces of the dielectric media. With propagation constants $\beta_1$ and $\beta_2$, $E_1(x)$ and $E_2(x)$ are the individual modes which satisfy the wave equations

$$\nabla_t^2 E_1 + [k_o^2 \epsilon_1(x) - \beta_1^2] E_1 = 0 \qquad (2\text{-}1a)$$

$$\nabla_t^2 E_2 + [k_o^2 \epsilon_2(x) - \beta_2^2] E_2 = 0 \ , \qquad (2\text{-}1b)$$

where

$$\nabla_t^2 = \nabla^2 - \frac{\partial^2}{\partial z^2} \qquad (2\text{-}2)$$

and $k_o^2 = \omega^2 \mu_o \epsilon_o$. The field in a coupled structure is approximated by a summation of the individual waveguide modes as

$$E_y = A_1(z) E_1(x) e^{j(\omega t - \beta_1 z)} + A_2(z) E_2(x) e^{j(\omega t - \beta_2 z)} \ , \qquad (2\text{-}3)$$

where $A_1(z)$ and $A_2(z)$ are the expansion coefficients which describe possible changes in field amplitudes as the superposition modes propagate along the guide. The total field satisfies

$$\nabla_t^2 E + \frac{\partial^2 E}{\partial z^2} + k_o^2 \epsilon(x) E = 0 \ . \qquad (2\text{-}4)$$

Substituting eq. (2-3) into eq. (2-4) with a slowly varying approximation (SVA), given by

$$\left| \frac{d^2 A_i}{dz^2} \right| \ll \beta_i \left| \frac{dA_i}{dz} \right| , \qquad (2\text{-}5)$$

leads to the well-known coupled mode equations [77]:

$$\frac{dA_1}{dz} = -jk_{11}A_1 - jk_{12}A_2 e^{j(\beta_1 - \beta_2)z} \qquad (2\text{-}6a)$$

$$\frac{dA_2}{dz} = -jk_{22}A_2 - jk_{21}A_1 e^{-j(\beta_1 - \beta_2)z} , \qquad (2\text{-}6b)$$

where

$$K_{ij} = \frac{\omega}{4} \int_{-\infty}^{\infty} \Delta\epsilon_j \, E_i E_j \, dx \qquad (2\text{-}7)$$

and $\Delta\epsilon_j(x) = \epsilon(x) - \epsilon_j(x)$. Solutions for $A_i(z)$ are obtained from eqs. (2-6) with initial conditions $A_1(0) = 1$ and $A_2(0) = 0$ when the power is excited into guide 1. The output power from guides 1 and 2 along the direction of propagation is proportional to $A_1 A_1^*$ and $A_2 A_2^*$, respectively. The power conservation condition for real values of $k_{12}$ and $k_{21}$ is given by

$$\frac{d}{dz}\left( |A_1|^2 + |A_2|^2 \right) = 2Im\left[ A_1^* A_2 e^{j(\beta_1 - \beta_2)z} \right](k_{12} - k_{21}) = 0 \ . \qquad (2\text{-}8)$$

Power is conserved when the structure is symmetric ($k_{12} = k_{21}$). Power conservation is violated for asymmetric struc-

tures in this approximate formulation, since calculation of coupling coefficients using eq. (2-7) shows $k_{12} \neq k_{21}$.

Conventional coupled mode theory is based upon three assumptions: 1) The cross-power terms (i.e., the overlap integrals of the uncoupled modes) are neglected, 2) slowly varying approximation (the second derivatives of amplitudes are neglected), and 3) the coupled system field is expressed as the sum of the individual waveguide modes. This method is thus improved by the exclusion of assumptions 1 and 2, and by the application of the variational principle. Though the accuracy of nonorthogonal coupled mode theory has been demonstrated for weakly coupled waveguides, the same approach may result in inaccuracies when very strongly coupled waveguides and TM modes are considered.

## 2.3 Normal Mode Analysis of Coupled Transmission Lines

An asymmetric two-waveguide directional coupler can be represented as a coupled two-line structure, as shown in Fig. 2-1(a). The reflection and transmission coefficients for the individual modes of each line are given as [78]

$$\Gamma_{xj} = \frac{j(Z_{xj}/Z_j - Z_j/Z_{xj})\sin\theta_x}{\phi_{xj}} \qquad (2\text{-}9a)$$

$$T_{xj} = \frac{2}{\phi_{xj}} , \qquad (2\text{-}9b)$$

where

$$\phi_{xj} = 2\cos\theta_x + j(Z_{xj}/Z_j + Z_j/Z_{xj})\sin\theta_x \qquad (2\text{-}10)$$

and where x represents the two normal modes (c and $\pi$) of the coupled waveguide, j symbolizes the lines (1 and 2), $\theta_x$ is the electrical length ($\beta_x$L) of the line for mode x, $Z_j$ is the termination impedance for line j, and $Z_{xj}$ is the characteristic impedance of the line j for mode x. The ratios of the line impedances for the two normal modes and the voltage eigenvectors are obtained from the coupled-line analysis [44] and are given by

$$\frac{Z_{c2}}{Z_{c1}} = \frac{Z_{\pi 2}}{Z_{\pi 1}} = -R_c R_\pi \qquad (2\text{-}11a)$$

$$[M_v] = \begin{bmatrix} a & b \\ aR_c & bR_\pi \end{bmatrix}, \qquad (2\text{-}11b)$$

where $R_c$ and $R_\pi$ represent the ratio of the voltage of line 2 to line 1 for the c and $\pi$ modes, respectively. The ratio can be measured directly from the electric field distributions for the coupled dielectric waveguide and line impedances can be replaced by wave impedances for given waveguide modes. Terminating with $Z_2/Z_1 = -R_cR_\pi$, the so-called nonmode converting termination, enables the excitation of individual normal modes. Since the ratios of the mode impedances for the two lines are the same for all the modes, line reflection and transmission coefficients calculated from eqs. (2-9) for both modes are found identical.

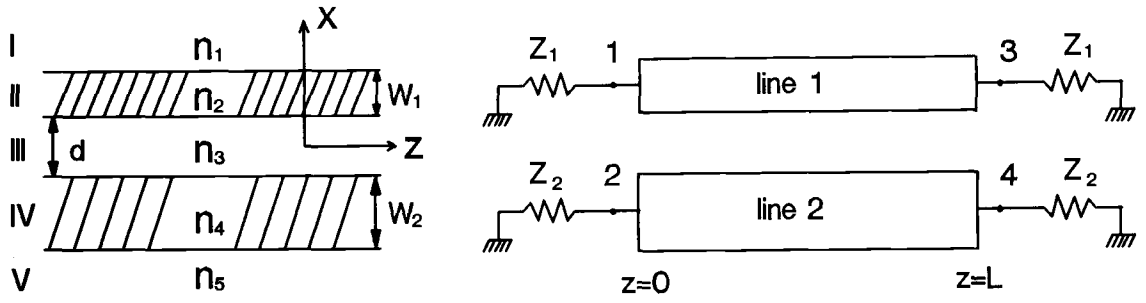


(a)

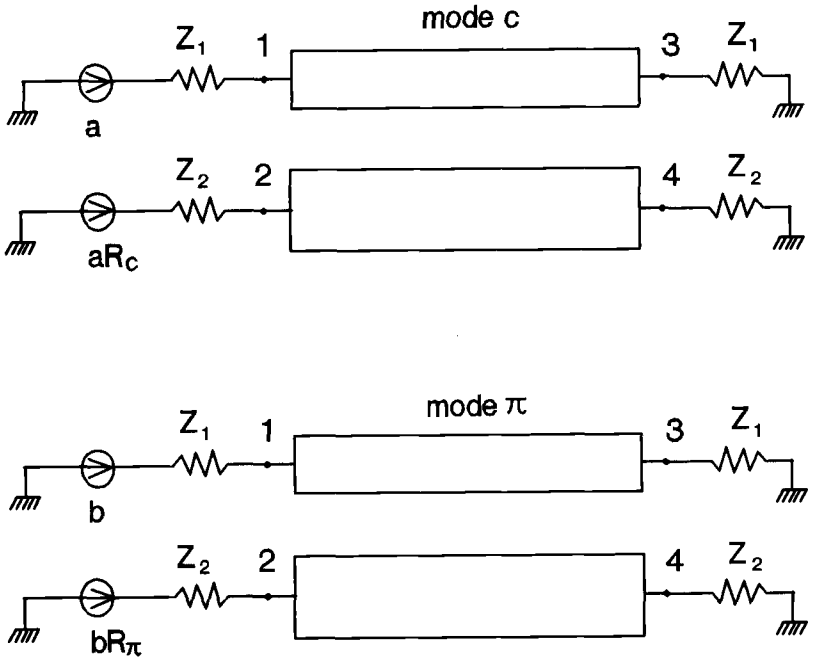


(b)

Fig. 2-1 (a) An asymmetric two-waveguide coupler and its equivalent transmission line structure. (b) Configurations of sources and terminations.

When the power is initially launched into guide 1, that is,

$$V_1 = 1,\ V_2 = V_3 = V_4 = 0\ ,$$

the settings $a + b = 1$ and $aR_c + bR_\pi = 0$ determines the constants a and b as

$$a = -\frac{R_\pi}{R_c - R_\pi}\ , \qquad b = \frac{R_c}{R_c - R_\pi}\ . \tag{2-12}$$

The scattering parameters are then obtained from the source configurations and terminations shown in Fig. 2-1(b). The scattering parameters are

$$S_{11} = S_{33} = \frac{R_c\Gamma_\pi - R_\pi\Gamma_c}{R_c - R_\pi}\ , \tag{2-13a}$$

$$S_{21} = S_{12} = S_{34} = S_{43} = \sqrt{-R_cR_\pi}\,\frac{\Gamma_c - \Gamma_\pi}{R_c - R_\pi}\ , \tag{2-13b}$$

$$S_{41} = S_{14} = S_{23} = S_{32} = \sqrt{-R_cR_\pi}\,\frac{T_c - T_\pi}{R_c - R_\pi}\ , \tag{2-13c}$$

$$S_{31} = S_{13} = \frac{R_cT_\pi - R_\pi T_c}{R_c - R_\pi}\ . \tag{2-13d}$$

When the power is excited into guide 2, that is,

$$V_2 = 1,\ V_1 = V_3 = V_4 = 0\ ,$$

the constants a and b are determined from $a + b = 0$ and $aR_c + bR_\pi = 1$. The remainder of the scattering parameters are similarly obtained as

$$S_{22} = S_{44} = \frac{R_c\Gamma_c - R_\pi\Gamma_\pi}{R_c - R_\pi}\ , \tag{2-14a}$$

$$S_{42} = S_{24} = \frac{R_cT_c - R_\pi T_\pi}{R_c - R_\pi}\ . \tag{2-14b}$$

For a symmetric two-waveguide coupler, as a special case of the asymmetric two-waveguide structure, even simpler expressions for the scattering parameters may be found for the values of $R_c = 1$ and $R_\pi = -1$.

A symmetric three-waveguide coupler, represented as a coupled three-lines structure, as shown in Fig. 2-2(a), is also considered. The line impedance ratios for the three normal modes (A, B, and C) and the voltage eigenvectors are obtained from the coupled-line analysis [46] by a process similar to that previously described for the two-waveguide coupler:

$$Z_{x1} = Z_{x3} \ , \quad \frac{Z_{x2}}{Z_{x1}} = -\frac{R_B R_C}{2} \ , \tag{2-15a}$$

$$[M_v] = \begin{bmatrix} a & b & c \\ 0 & bR_B & cR_C \\ -a & b & c \end{bmatrix} , \tag{2-15b}$$

where $R_B$ and $R_C$ are ratios of the amplitudes of the electric fields for guide 2 to those for guide 1 for the even-even and even-odd modes (respectively, B and C). The scattering parameters are then determined by calculating a, b, and c from the input conditions. Based upon the configuration of sources and terminations shown in Fig. 2-2(b), the results are

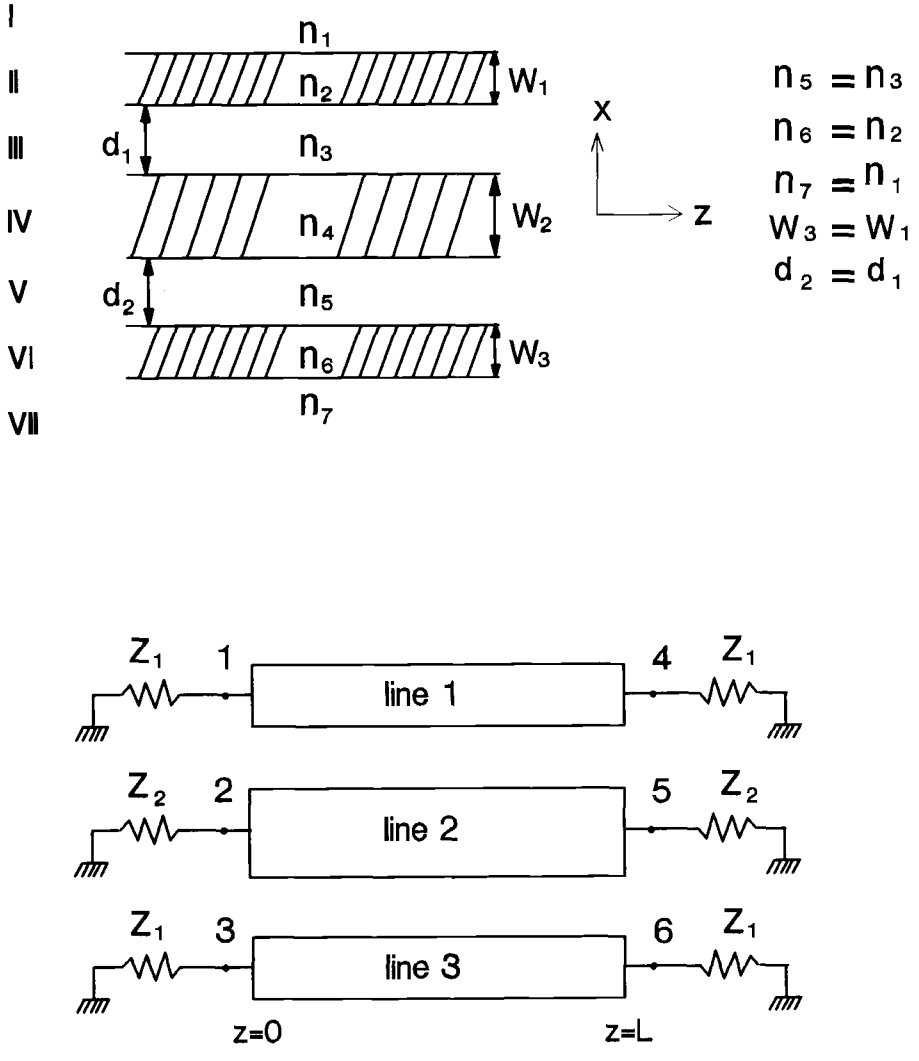


(a)

Fig. 2-2 (a) A symmetric three-waveguide coupler and its equivalent transmission line structure.

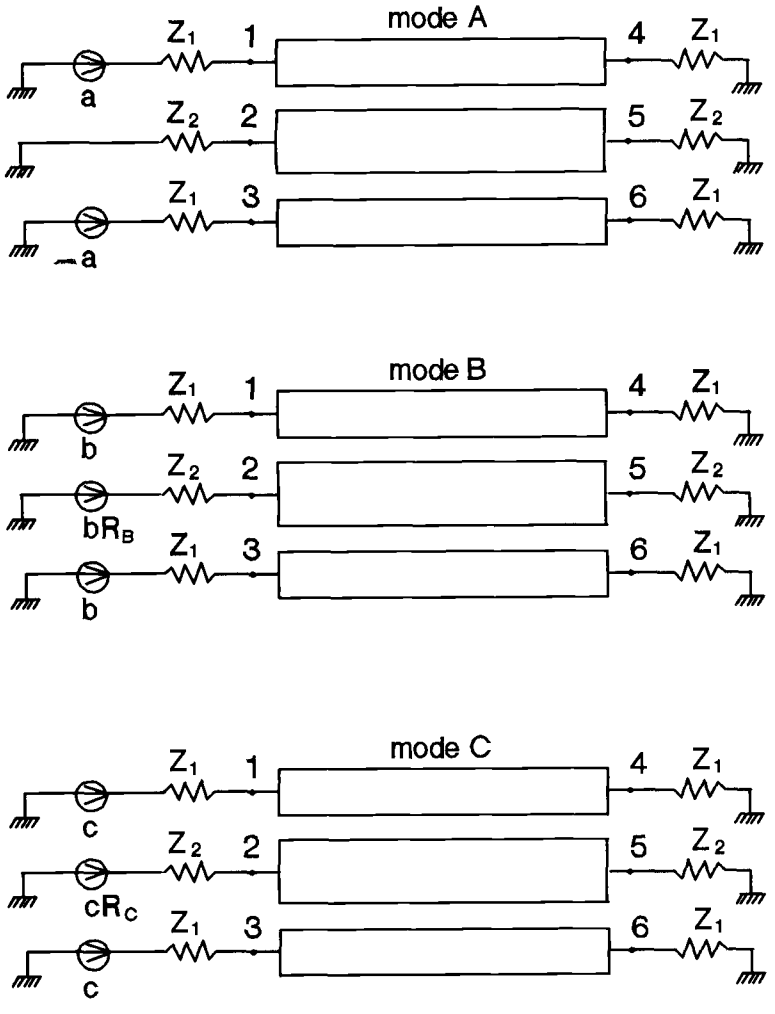


(b)

Fig. 2-2 (b) Configurations of sources and terminations for a symmetric three-line structure.

$$S_{11} = S_{33} = S_{44} = S_{66} = -\frac{\Gamma_A}{2} + \frac{R_B\Gamma_C - R_C\Gamma_B}{2(R_B - R_C)} , \tag{2-16a}$$

$$S_{21} = S_{12} = S_{23} = S_{32} = S_{45} = S_{54} = S_{56} = S_{65} ,$$

$$= \sqrt{\frac{-R_BR_C}{2}}\frac{\Gamma_B - \Gamma_C}{R_B - R_C} , \tag{2-16b}$$

$$S_{31} = S_{13} = S_{46} = S_{64} = -\frac{\Gamma_A}{2} + \frac{R_B\Gamma_C - R_C\Gamma_B}{2(R_B - R_C)} , \tag{2-16c}$$

$$S_{61} = S_{16} = S_{34} = S_{43} = -\frac{T_A}{2} + \frac{R_BT_C - R_CT_B}{2(R_B - R_C)} , \tag{2-16d}$$

$$S_{51} = S_{115} = S_{35} = S_{53} = S_{24} = S_{42} = S_{26} = S_{62}$$

$$= \sqrt{-\frac{R_BR_C}{2}}\frac{T_B - T_C}{R_B - R_C} , \tag{2-16e}$$

$$S_{41} = S_{14} = S_{36} = S_{63} = \frac{T_A}{2} + \frac{R_BT_C - R_CT_B}{2(R_B - R_C)} , \tag{2-16f}$$

$$S_{22} = S_{55} = \frac{R_B\Gamma_B - R_C\Gamma_C}{R_B - R_C} , \tag{2-16g}$$

$$S_{52} = S_{25} = \frac{R_BT_B - R_CT_C}{R_B - R_C} . \tag{2-16h}$$

Setting $R_B = \sqrt{2}$ and $R_C = -\sqrt{2}$ for a symmetric three-waveguide directional coupler consisting of three identical waveguides simplifies the expressions for the scattering parameters.

The properties of coupled two-line and symmetric three-line structures are governed by eqs. (2-11a) and (2-15a), respectively. The normal mode analysis with

nonmode converting terminations provides compact expressions of output power distributions and yields very accurate results. The nonmode converting termination technique may not be directly applicable to general multiple coupled structures with arbitrary terminations. However, based upon analogy between transmission lines and optical waveguides, a method for general coupled optical waveguides can be developed.

## 2.4 Normal Mode Analysis of Multiple Coupled Waveguides

As shown in Figure 2-3, TE modes and a general asymmetric coupled waveguide consisting of n waveguides are considered. Fields in each guide can be expressed as a linear combination of forward and backward travelling guided modes. The electric and magnetic fields can be written as

$$
\begin{aligned}
e_1 &= A_1 R_{11} e^{-j\beta_1 z} + A_2 R_{12} e^{-j\beta_2 z} + \cdots + A_n R_{1n} e^{-j\beta_n z} \\
&\quad + A_{n+1} R_{11} e^{j\beta_1 z} + A_{n+2} R_{12} e^{j\beta_2 z} + \cdots + A_{2n} R_{1n} e^{j\beta_n z} \\
e_2 &= A_1 R_{21} e^{-j\beta_1 z} + A_2 R_{22} e^{-j\beta_2 z} + \cdots + A_n R_{2n} e^{-j\beta_n z} \\
&\quad + A_{n+1} R_{21} e^{j\beta_1 z} + A_{n+2} R_{22} e^{j\beta_2 z} + \cdots + A_{2n} R_{2n} e^{j\beta_n z} \\
&\vdots \\
e_n &= A_1 R_{n1} e^{-j\beta_1 z} + A_2 R_{n2} e^{-j\beta_2 z} + \cdots + A_n R_{nn} e^{-j\beta_n z} \\
&\quad + A_{n+1} R_{n1} e^{j\beta_1 z} + A_{n+2} R_{n2} e^{j\beta_2 z} + \cdots + A_{2n} R_{nn} e^{j\beta_n z} ,
\end{aligned}
\qquad (2\text{-}17a)
$$

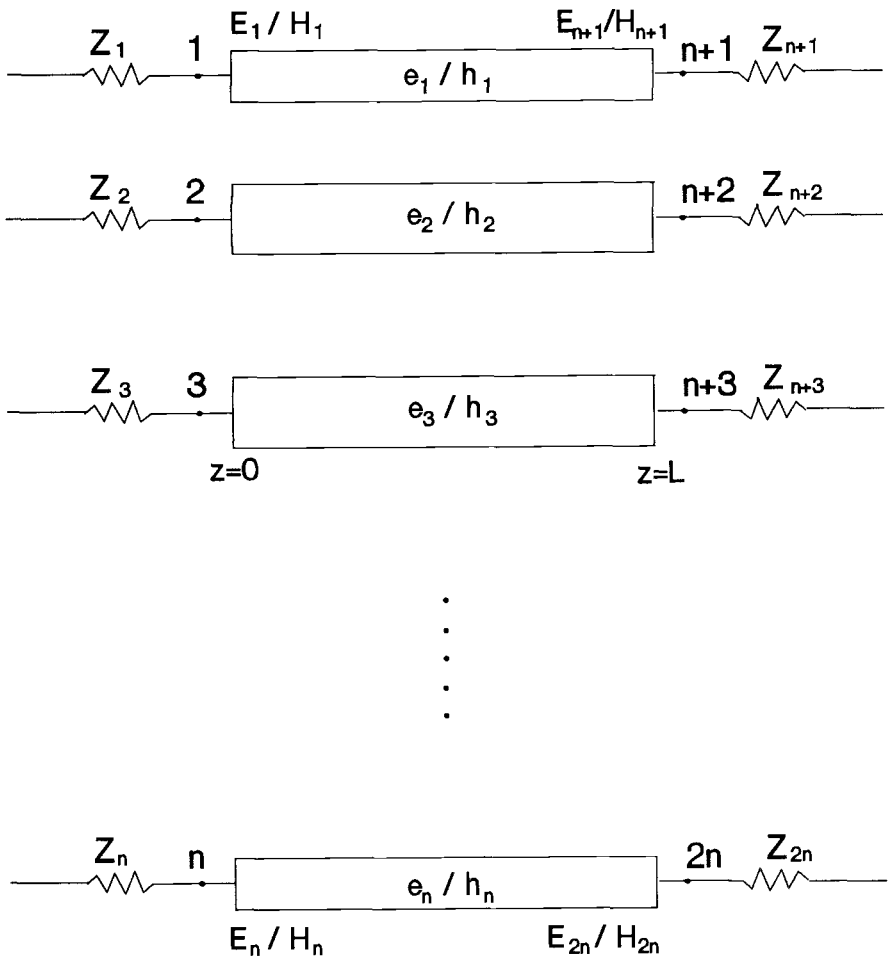


Fig. 2-3. An asymmetric coupled n-waveguide structure.

$$
\begin{aligned}
h_1 &= -A_1R_{11}Y_{11}e^{-j\beta_1 z} - A_2R_{12}Y_{12}e^{-j\beta_2 z} - \cdots - A_nR_{1n}Y_{1n}e^{-j\beta_n z} \\
&\quad + A_{n+1}R_{11}Y_{11}e^{j\beta_1 z} + A_{n+2}R_{12}Y_{12}e^{j\beta_2 z} + \cdots + A_{2n}R_{1n}Y_{1n}e^{j\beta_n z} \\
h_2 &= -A_1R_{21}Y_{21}e^{-j\beta_1 z} - A_2R_{22}Y_{22}e^{-j\beta_2 z} - \cdots - A_nR_{2n}Y_{2n}e^{-j\beta_n z} \\
&\quad + A_{n+1}R_{21}Y_{21}e^{j\beta_1 z} + A_{n+2}R_{22}Y_{22}e^{j\beta_2 z} + \cdots + A_{2n}R_{2n}Y_{2n}e^{j\beta_n z} \qquad (2\text{-}17b) \\
&\vdots \\
h_n &= -A_1R_{n1}Y_{n1}e^{-j\beta_1 z} - A_2R_{n2}Y_{n2}e^{-j\beta_2 z} - \cdots - A_nR_{nn}Y_{nn}e^{-j\beta_n z} \\
&\quad + A_{n+1}R_{n1}Y_{n1}e^{j\beta_1 z} + A_{n+2}R_{n2}Y_{n2}e^{j\beta_2 z} + \cdots + A_{2n}R_{nn}Y_{nn}e^{j\beta_n z} \ ,
\end{aligned}
$$

where for TE modes,

$$
Y_{ji} = \mp \frac{h_j}{e_j}\bigg|_i = \frac{\beta_i}{\omega\mu_o} \ , \qquad (2\text{-}18)
$$

and where j = guides and i = modes. The negative and positive signs in eq. (2-18) indicate, respectively, the forward and the backward travelling waves. Eqs. (2-17a) and (2-17b) can be conveniently denoted as

$$
e_j = \sum_{i=1}^{n} A_i R_{ji} e^{-j\beta_i z} + A_{n+i} R_{ji} e^{j\beta_i z} \ , \qquad (2\text{-}19a)
$$

$$
h_j = \sum_{i=1}^{n} -A_i R_{ji} Y_{ji} e^{-j\beta_i z} + A_{n+i} R_{ji} Y_{ji} e^{j\beta_i z} \ . \qquad (2\text{-}19b)
$$

Positive values are assumed for both wave admittances and impedances. For the circuit parameters, it is necessary to specify the fields at both the input (z = 0) and output (z = L) ends, which are then expressed in matrix form as:

$$\begin{bmatrix} E_1 \\ E_2 \\ \cdot \\ \cdot \\ E_n \\ E_{n+1} \\ E_{n+2} \\ \cdot \\ \cdot \\ E_{2n} \end{bmatrix} = \begin{bmatrix} [M_E] & [M_E] \\ & \\ & \\ & \\ [M_E][e^{-j\theta_i}]_d & [M_E][e^{j\theta_i}]_d \\ & \end{bmatrix} \begin{bmatrix} A_1 \\ A_2 \\ \cdot \\ \cdot \\ A_n \\ A_{n+1} \\ A_{n+2} \\ \cdot \\ \cdot \\ A_{2n} \end{bmatrix} \qquad (2\text{-}20a)$$

and

$$\begin{bmatrix} H_1 \\ H_2 \\ \cdot \\ \cdot \\ H_n \\ -H_{n+1} \\ -H_{n+2} \\ \cdot \\ \cdot \\ -H_{2n} \end{bmatrix} = \begin{bmatrix} -[M_H] & [M_H] \\ & \\ & \\ & \\ [M_H][e^{-j\theta_i}]_d & -[M_H][e^{j\theta_i}]_d \\ & \end{bmatrix} \begin{bmatrix} A_1 \\ A_2 \\ \cdot \\ \cdot \\ A_n \\ A_{n+1} \\ A_{n+2} \\ \cdot \\ \cdot \\ A_{2n} \end{bmatrix} \qquad (2\text{-}20b)$$

where a matrix with subscript d represents a diagonal matrix and $\theta_i = \beta_i L$. $[M_E]$ and $[M_H]$ are the eigenvectors corresponding to the eigenvalues and are given by

$$[M_E] = \begin{bmatrix} R_{11} & R_{12} & \cdots & R_{1n} \\ R_{21} & R_{22} & \cdots & R_{2n} \\ \vdots & & & \vdots \\ R_{n1} & R_{n2} & \cdots & R_{nn} \end{bmatrix}, \quad [M_H] = \begin{bmatrix} R_{11}Y_{11} & R_{12}Y_{12} & \cdots & R_{1n}Y_{1n} \\ R_{21}Y_{21} & R_{22}Y_{22} & \cdots & R_{2n}Y_{2n} \\ \vdots & & & \vdots \\ R_{n1}Y_{n1} & R_{n2}Y_{n2} & \cdots & R_{nn}Y_{nn} \end{bmatrix} \tag{2-21}$$

The impedance or admittance matrix can then be obtained by eliminating the constants $A_i$ and by solving for the electric and magnetic field relationships:

$$[E] = \begin{bmatrix} [M_E] & [M_E] \\ [M_E][e^{-j\theta_i}]_d & [M_E][e^{j\theta_i}]_d \end{bmatrix} \begin{bmatrix} -[M_H] & [M_H] \\ [M_H][e^{-j\theta_i}]_d & -[M_H][e^{j\theta_i}]_d \end{bmatrix}^{-1} [H] \tag{2-22}$$

By rearranging eq. (2-22), the impedance matrix then becomes

$$[Z] = \begin{bmatrix} [M_E] & [0] \\ [0] & [M_E] \end{bmatrix} \begin{bmatrix} [U] & [U] \\ [e^{-j\theta_i}]_d & [e^{j\theta_i}]_d \end{bmatrix} \begin{bmatrix} -[U] & [U] \\ [e^{-j\theta_i}]_d & [e^{j\theta_i}]_d \end{bmatrix}^{-1} \begin{bmatrix} [M_H] & [0] \\ [0] & [M_H] \end{bmatrix}^{-1}$$

$$= \begin{bmatrix} [M_E] & [0] \\ [0] & [M_E] \end{bmatrix} \begin{bmatrix} [j\cot\theta_i]_d & [j\csc\theta_i]_d \\ [j\csc\theta_i]_d & [j\cot\theta_i]_d \end{bmatrix} \begin{bmatrix} [M_H]^{-1} & [0] \\ [0] & [M_H]^{-1} \end{bmatrix}$$

$$= \begin{bmatrix} [M_E][j\cot\theta_i]_d[M_H]^{-1} & [M_E][j\csc\theta_i]_d[M_H]^{-1} \\ [M_E][j\csc\theta_i]_d[M_H]^{-1} & [M_E][j\cot\theta_i]_d[M_H]^{-1} \end{bmatrix} . \qquad (2\text{-}23)$$

Eq. (2-23) represents a general expression of the impedance matrix for an n-waveguide coupler; the admittance matrix can be obtained in a similar manner. The impedance matrix for the TM case can be derived in the same manner and is included in Appendix A.

The scattering matrix [S] is defined by [b] = [S][a], where [a] and [b] are column vectors. The terms $a_i$ and $b_i$ are normalized so that $a_i a_i^*/2$ and $b_i b_i^*/2$ are, respectively, time-averaged incident power and reflected power at port i. Thus, $a_i$ and $b_i$ can be defined as

$$a_i = \frac{1}{2}\left(\frac{E_i}{\sqrt{Z_{oi}}} + \sqrt{Z_{oi}}H_i\right) , \qquad (2\text{-}24a)$$

$$b_i = \frac{1}{2}\left(\frac{E_i}{\sqrt{Z_{oi}}} - \sqrt{Z_{oi}}H_i\right) , \qquad (2\text{-}24b)$$

where $Z_{oi}$ is the terminating impedance at port i. Using the normalized impedance and admittance matrices,

$$[Z_n] = [\sqrt{Z_o}\,]^{-1}[Z][\sqrt{Z_o}\,]^{-1} , \qquad (2\text{-}25a)$$

$$[Y_n] = [\sqrt{Z_o}\,][Y][\sqrt{Z_o}\,] , \qquad (2\text{-}25b)$$

the scattering matrix is then expressed in terms of the normalized immittance matrix,

$$[S] = ([Z_n] - [U])([Z_n] + [U])^{-1} = ([Z_n] + [U])^{-1}([Z_n] - [U])$$
$$= ([U] - [Y_n])([U] + [Y_n])^{-1} = ([U] + [Y_n])^{-1}([U] - [Y_n]) \ . \qquad (2\text{-}26)$$

Eq. (2-26) can be used to calculate the scattering parameters $S_{ij}$ or normalized output power distributions $|S_{ij}|^2$ at output port i for input to port j.

## 2.5 Normal Mode Parameters

### 2.5.1 Asymmetric Two-Waveguide Couplers

Consideration is given to a dielectric slab waveguide consisting of homogeneous and lossless media, as illustrated in Fig. 2-1(a). Based upon the assumption of a structural wave equation solution, $E_y = E_y(x) \exp[j(\omega t - \beta z)]$, the wave equation is reduced to

$$\left[\frac{\partial^2}{\partial^2 x} + (k_o^2 n^2(x) - \beta^2)\right] E_y(x) = 0 \ , \qquad (2\text{-}27)$$

where $k_o = \omega/c = \omega(\mu_o \epsilon_o)^{1/2}$ is the free space wave number and c is the speed of light in free space. Eq. (2-27) holds for each homogeneous region and the determination of solutions for this equation is subject to the application of appropriate boundary conditions. Boundary conditions state that tangential components $E_y$ and $H_z$ must be continuous at each boundary for TE modes and that tangential components $H_y$ and $E_z$ are contnuous for TM modes. When solutions for

guided TE modes are considered, the mode function $E_y(x)$ in different regions can be written as

$$E_y = \begin{cases} Ae^{-\gamma_1(x - W_1 - d/2)} & Reg.I \\ B\cos\gamma_2(x - d/2) + C\sin\gamma_2(x - d/2) & Reg.II \\ De^{-\gamma_3 x} + Ee^{\gamma_3 x} & Reg.III \\ F\cos\gamma_4(x + d/2) + G\sin\gamma_4(x + d/2) & Reg.IV \\ He^{\gamma_5(x + W_2 + d/2)} & Reg.V \end{cases} \qquad (2\text{-}28)$$

where $\gamma_i^2 = \beta^2 - k_o^2 n_i^2$ for i = 1, 3, 5 and

$\gamma_i^2 = k_o^2 n_i^2 - \beta^2$ for i = 2, 4.

Applying boundary conditions yields eight equations for eight unknowns (respectively, A through H). The system of the equations is abbreviated in the form

$$\mathbf{Mx} = \mathbf{0}, \quad \mathbf{x} = [A\ B\ C\ \ldots\ H]^T$$

and

$$\boldsymbol{M} = \begin{bmatrix} 1 & -\cos q_o & -\sin q_o & 0 & 0 & 0 & 0 & 0 \\ \gamma_1 & -\gamma_2 \sin q_o & \gamma_2 \cos q_o & 0 & 0 & 0 & 0 & 0 \\ 0 & -1 & 0 & e^{-q_1} & e^{q_1} & 0 & 0 & 0 \\ 0 & 0 & \gamma_2 & \gamma_3 e^{-q_1} & -\gamma_3 e^{q_1} & 0 & 0 & 0 \\ 0 & 0 & 0 & e^{q_1} & e^{-q_1} & -1 & 0 & 0 \\ 0 & 0 & 0 & -\gamma_3 e^{q_1} & \gamma_3 e^{-q_1} & 0 & -\gamma_4 & 0 \\ 0 & 0 & 0 & 0 & 0 & \cos 2q_2 & -\sin 2q_2 & -1 \\ 0 & 0 & 0 & 0 & 0 & \gamma_4 \sin 2q_2 & \gamma_4 \cos 2q_2 & -\gamma_5 \end{bmatrix}$$

(2-29)

where $q_o = \gamma_2 W_1$, $q_1 = \gamma_3 d/2$, and $q_2 = \gamma_4 W_2$. For the eight unknowns to be linearly dependent, det **M** = 0, which results in the following eigenvalue equation

$$tan2q_2 = \frac{(h_1\gamma_2 + h_2\gamma_5) + (h_1\gamma_2\gamma_5/\gamma_3 + h_2\gamma_3)\,tanh2q_1}{(h_2\gamma_4 - h_1\gamma_2\gamma_5/\gamma_4) + (h_1\gamma_2\gamma_4/\gamma_3 - h_2\gamma_3\gamma_5/\gamma_4)\,tanh2q_1} \tag{2-30}$$

where $h_1 = \gamma_1 cosq_o - \gamma_2 sinq_o$ and $h_2 = \gamma_2 cosq_o + \gamma_1 sinq_o$. The propagation constants, $\beta$, are determined from the eq. (2-30), whereas the values of the unknown constants are determined from the boundary conditions and the normalization condition

$$-\frac{1}{2}\int_{-\infty}^{\infty} E_y H_x^*\, dx = \frac{\beta}{2\omega\mu_o}\int_{-\infty}^{\infty} E_y^2(x)\, dx = 1\ , \tag{2-31}$$

where

$$\mathbf{H}_x = -j(\omega\mu_o)^{-1}\partial\mathbf{E}_y/\partial z,$$

and wave impedance is obtained from

$$Z_{TE} = -E_y/H_x = \omega\mu_o/\beta.$$

Thus, the propagation constants, the wave impedances, and the field distributions for the guided modes are obtained. In turn, $R_c$ and $R_\pi$ are defined as the ratios of the peak amplitudes of the fields in guide 2 to the fields in guide 1 for, respectively, c and $\pi$ modes. These ratios are measured from the field distributions of the guided modes, as shown in Fig. 2-4(a). The normal mode parameters (i.e., $R_c$ and $R_\pi$, the propagation constants, and the wave

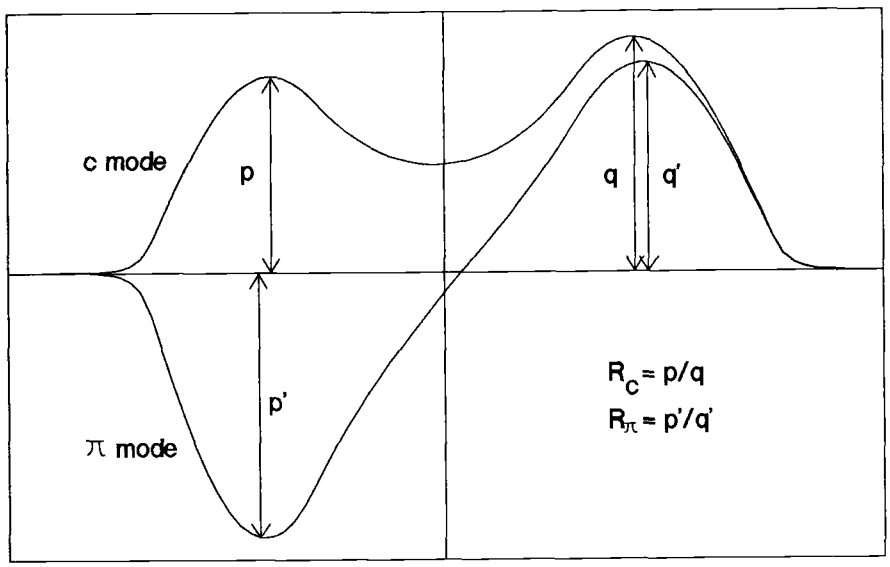


(a)

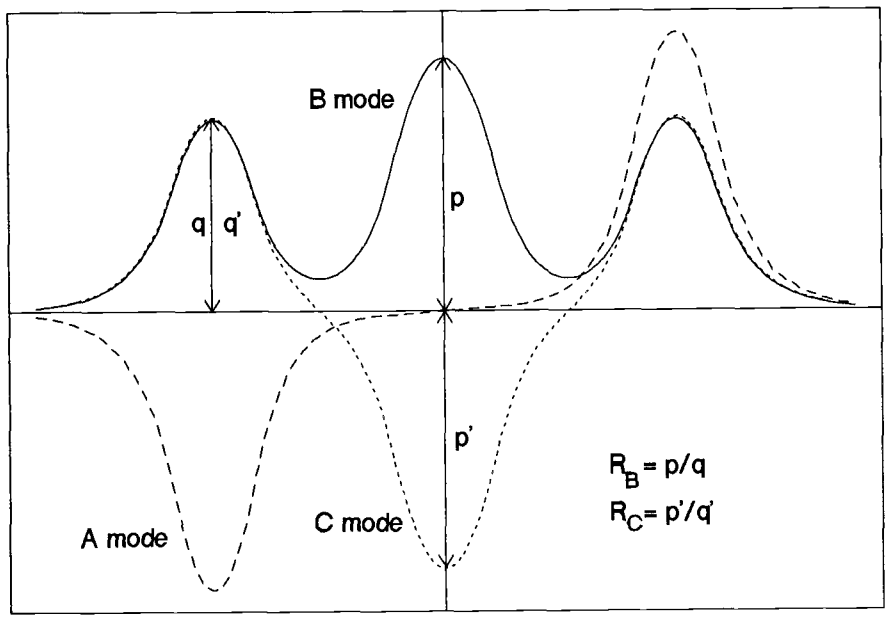


(b)

Fig. 2-4. Typical field distributions of (a) asymmetric two-waveguide couplers and (b) symmetric three-waveguide couplers.

impedances) are substituted into the expressions for the scattering parameters previously considered to obtain normalized output power from the output ends of an optical two-waveguide directional coupler.

### 2.5.2 Symmetric Three-Waveguide Couplers

The normal mode parameters for a symmetric three-waveguide coupler are calculated in the same manner as described in section 2.5.1. A symmetric three-waveguide coupler can be treated as a special case of an asymmetric three-waveguide coupler. Therefore, a general three-waveguide coupler, as shown in Fig. 2-2(a), is considered. For the given structure, $E_y$ for different regions is given by

$$E_y = \begin{cases} Ae^{-\gamma_1(x - W_1 - W_2/2 - d_1)} & I \\ B\cos\gamma_2(x - W_2/2 - d_1) + C\sin\gamma_2(x - W_2/2 - d_1) & II \\ De^{-\gamma_3(x - W_2/2)} + Ee^{\gamma_3(x - W_2/2)} & III \\ F\cos\gamma_4 x + G\sin\gamma_4 x & IV \\ He^{\gamma_5(x + W_2/2)} + Ie^{\gamma_5(x + W_2/2)} & V \\ J\cos\gamma_6(x + W_2/2 + d_2) + K\sin\gamma_6(x + W_2/2 + d_2) & VI \\ Le^{\gamma_7(x + W_2/2 + W_3 + d_2)} & VII \end{cases} \quad (2\text{-}32)$$

where

$\gamma_i^2 = \beta^2 - k_o^2 n_i^2$ for i = 1, 3, 5, 7 and

$\gamma_i^2 = k_o^2 n_i^2 - \beta^2$ for i = 2, 4, 6.

By applying boundary conditions successively and setting

$q_o = \gamma_2 W_1$, $q_1 = \gamma_6 W_3$, $q_2 = \gamma_4 W_2/2$, $q_3 = \gamma_3 d_1$, $q_4 = \gamma_5 d_2$ ,

the matrix **M**, as listed in Table 2-1, is obtained. From det **M** = 0, the eigenvalue equation is derived as

$$\tan 2q_2 = \frac{h_1 h_3 + h_2 h_4}{h_2 h_3 - h_1 h_4} , \qquad (2\text{-}33)$$

where

$$\begin{aligned}
h_1 &= \gamma_3(\gamma_3 t_1 \sinh q_3 + \gamma_2 t_2 \cosh q_3) \\
h_2 &= \gamma_4(\gamma_3 t_1 \cosh q_3 + \gamma_2 t_2 \sinh q_3) \\
h_3 &= \gamma_4(-\gamma_6 t_3 \sinh q_4 + \gamma_5 t_4 \cosh q_4) \\
h_4 &= \gamma_5(-\gamma_6 t_3 \cosh q_4 + \gamma_5 t_4 \sinh q_4) \\
t_1 &= \gamma_1 \sin q_o + \gamma_2 \cos q_o \\
t_2 &= \gamma_1 \cos q_o - \gamma_2 \sin q_o \\
t_3 &= \gamma_6 \sin q_1 - \gamma_7 \cos q_1 \\
t_4 &= \gamma_6 \cos q_1 + \gamma_7 \sin q_1 .
\end{aligned} \qquad (2\text{-}34)$$

The propagation constants for the three normal modes are calculated from the eigenvalue eq. (2-33). Field distributions and the wave impedances are determined for the given propagation constants. Then, $R_B$ and $R_C$ are defined as the ratios of the peak amplitudes of the fields in the center guide to those for the fields in one of the outside guides for, respectively, B and C modes. They may also be

$$
\boldsymbol{M} = \begin{bmatrix}
1 & -\cos\theta_o & -\sin\theta_o & 0 & 0 & 0 & 0 & 0 & 0 & 0 & 0 & 0 \\
\gamma_1 & -\gamma_2\sin\theta_o & \gamma_2\cos\theta_o & 0 & 0 & 0 & 0 & 0 & 0 & 0 & 0 & 0 \\
0 & 1 & 0 & -e^{-\theta_3} & -e^{\theta_3} & 0 & 0 & 0 & 0 & 0 & 0 & 0 \\
0 & 0 & \gamma_2 & \gamma_3 e^{-\theta_3} & -\gamma_3 e^{\theta_3} & 0 & 0 & 0 & 0 & 0 & 0 & 0 \\
0 & 0 & 0 & 1 & 1 & -\cos\theta_2 & -\sin\theta_2 & 0 & 0 & 0 & 0 & 0 \\
0 & 0 & 0 & -\gamma_3 & \gamma_3 & \gamma_4\sin\theta_2 & -\gamma_4\cos\theta_2 & 0 & 0 & 0 & 0 & 0 \\
0 & 0 & 0 & 0 & 0 & \cos\theta_2 & -\sin\theta_2 & -1 & -1 & 0 & 0 & 0 \\
0 & 0 & 0 & 0 & 0 & \gamma_4\sin\theta_2 & \gamma_4\cos\theta_2 & \gamma_5 & -\gamma_5 & 0 & 0 & 0 \\
0 & 0 & 0 & 0 & 0 & 0 & 0 & e^{\theta_4} & e^{-\theta_4} & -1 & 0 & 0 \\
0 & 0 & 0 & 0 & 0 & 0 & 0 & -\gamma_5 e^{\theta_4} & \gamma_5 e^{-\theta_4} & 0 & -\gamma_6 & 0 \\
0 & 0 & 0 & 0 & 0 & 0 & 0 & 0 & 0 & \cos\theta_1 & -\sin\theta_1 & -1 \\
0 & 0 & 0 & 0 & 0 & 0 & 0 & 0 & 0 & \gamma_6\sin\theta_1 & \gamma_6\cos\theta_1 & -\gamma_7
\end{bmatrix}
$$

Table 2-1. Matrix **M** for an asymmetric three-waveguide coupler.

measured from the field distributions of the guided modes, as illustrated in Fig. 2-4(b).

### 2.5.3 Transverse Resonance Technique

The transverse resonance technique (TRT) also provides an alternative procedure for evaluating the propagation constants for slab waveguide. The technique [79-80] was initially used for the evaluation of the dispersion characteristics of waveguides with discontinuities placed in a direction perpendicular to the propagation axis. As an example, for a planar waveguide with three dielectric layers, when propagation along the x direction occurs, the waveguide can be represented by a transverse equivalent transmission line circuit, as shown in Fig. 2-5(a).

For this planar structure, $d_1$ and $d_3$ extend to $\infty$ and $x_1 = x_2 = 0$. We have $Z_{oi} = \omega\mu_o/k_i$, $k^2_i = k^2_o(n^2_i - \beta^2)$, and input impedance $Z_{in}(x = W + d_1) \propto j/k_3$. At $x = d_1$, The resonant condition, $Z_{in1} + Z_{in2} = 0$, gives

$$-\frac{j}{k_1} + \frac{1}{k_2}\frac{\frac{j}{k_3} + \frac{j}{k_2}\tan k_2 W}{\frac{1}{k_2} - \frac{1}{k_3}\tan k_2 W} = 0. \qquad (2\text{-}35)$$

Solving eq. (2-35) yields the eigenvalue equation

$$\tan k_2 W = \frac{k_2(k_1 + k_3)}{(k_2^2 - k_1 k_3)} . \qquad (2\text{-}36)$$

The eigenvalue equations for two-waveguide and three-

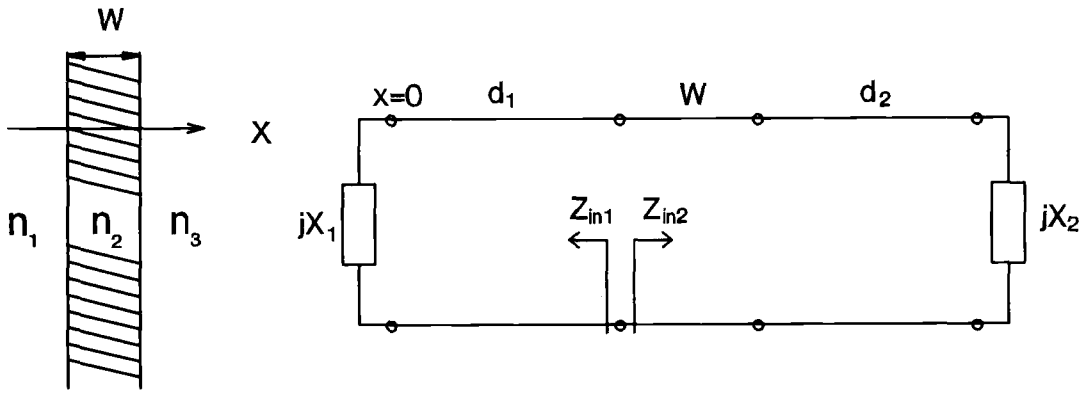


(a)

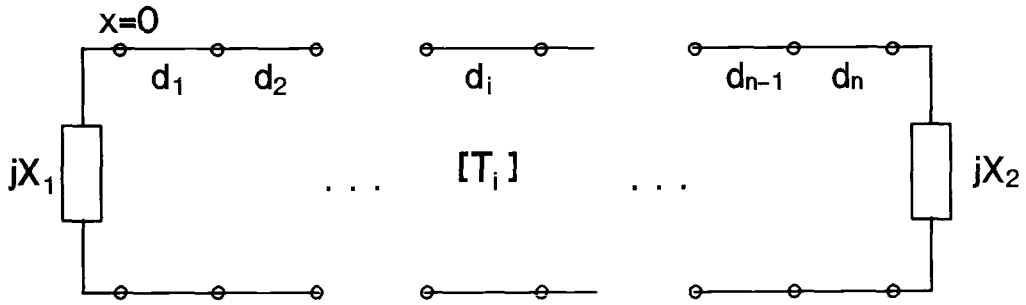


(b)

Fig. 2-5. (a) A three-layer waveguide and an equivalent transverse network. (b) An equivalent transverse network for a general slab waveguide.

waveguide couplers can be obtained in a similar fashion and the transverse resonance technique yields the same results obtained from the method as described in sections 2.5.1 and 2.5.2.

Chain matrix representation is helpful for the evaluation of propagation constants of general slab waveguides and the chain matrix is given by

$$[T_i] = \begin{bmatrix} \cos\theta_i & jZ_{oi}\sin\theta_i \\ jY_{oi}\sin\theta_i & \cos\theta_i \end{bmatrix}, \tag{2-37}$$

where $Z_{oi} = \omega\mu_o/k$, $k_i^2 = k_o^2(n_i^2 - \beta^2)$, $Y_{oi} = Z_{oi}$, and $\theta_i$ is the electrical length. The trigonometric functions in eq. (2-37) are replaced by hyperbolic functions for cladding layers. The overall chain matrix [80] is

$$[T] = \prod_{i=1}^{n} [T_i] = \begin{bmatrix} t_{11} & jt_{12} \\ jt_{21} & t_{22} \end{bmatrix}. \tag{2-38}$$

For terminations of $jX_1$ and $jX_2$, The resonant condition is

$$-jX_1 = \frac{jX_2t_{11} + jt_{12}}{jX_2t_{21} + jt_{22}}. \tag{2-39}$$

For a planar waveguide ($X_1 = X_2 = 0$), from eq. (2-37) the resonant condition becomes $t_{12} = 0$, and $\tanh(k_1d_1)$ and $\tanh(k_nd_n)$ converge to unity as $d_1$ and $d_n$ approach infinity. The propagation constants are then obtained from the eigenvalue equation $t_{12} = 0$.

## 2.6 Concluding Remarks

The procedure for the derivation of closed form expressions for scattering parameters for asymmetric two-line and symmetric three-line structures, expressed in terms of the normal mode parameters for coupled systems, has been presented. This normal mode analysis can be applied to analyze coupled waveguide structures including general two-waveguide and symmetrical three-waveguide optical couplers.

General expressions for the scattering parameters of asymmetric multiple coupled optical waveguides were also derived. The scattering parameters have been obtained from impedance matrices which are expressed in terms of the normal mode parameters.

The proceures for the evaluation of the normal mode parameters, including the propagation constants, the wave impedances, and eigenvectors, were also presented. Eigen-value equations for asymmetric two-waveguide and three-waveguide coupler were derived for the calculation of the propagation constants of TE modes.

The formulations for the scattering parameters are general, with various applications for multiple coupled guided wave structures operating at microwave or optical frequencies. The advantage of normal mode analysis with

respect to coupled mode theory is that the use of normal mode parameters provides more accurate results.

For the greater part, the analyses provided in this chapter has been concentrated upon TE modes. The normal mode analysis for TM modes is treated in Appendix A. The numerical results for the computation of the scattering parameters for general two-waveguide and symmetric three-waveguide couplers are considered in the next chapter.

# CHAPTER 3

# NUMERICAL RESULTS ON LINEAR MULTIPLE COUPLED DIELECTRIC WAVEGUIDES

## 3.1 Introduction

The normal mode analysis of the coupled waveguide system presented in chapter 2 is used to study propagation characteristics and circuit properties of coupled optical waveguides. The scattering parameters are expressed in terms of the characteristic normal mode parameters and results obtained from the normal mode analysis are compared with those based on the coupled mode theory for typical waveguide multiports.

## 3.2 Symmetric Two-Waveguide Couplers

As the first example we consider a symmetric two-waveguide directional coupler consisting of two identical slabs with $n_1 = n_3 = n_5 = 3.2$, $n_2 = n_4 = 3.3$, $W_1 = W_2 = 0.8$ $\mu$m, $d = 1$ $\mu$m, and $\lambda = 1.5$ $\mu$m as shown in Fig. 3-1(a). The electric field component $E_y$ associated with TE modes of the coupler is shown in Fig. 3-1(b). The structure exhibits perfect symmetry and we have a symmetric (even) mode and an antisymmetric (odd) mode, while there exist a symmetric-

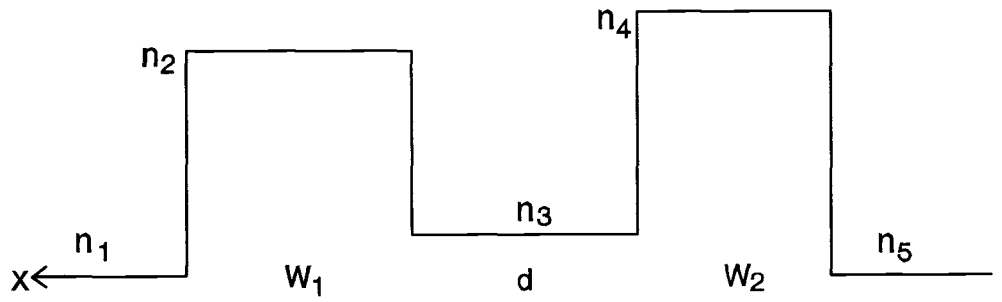


(a)

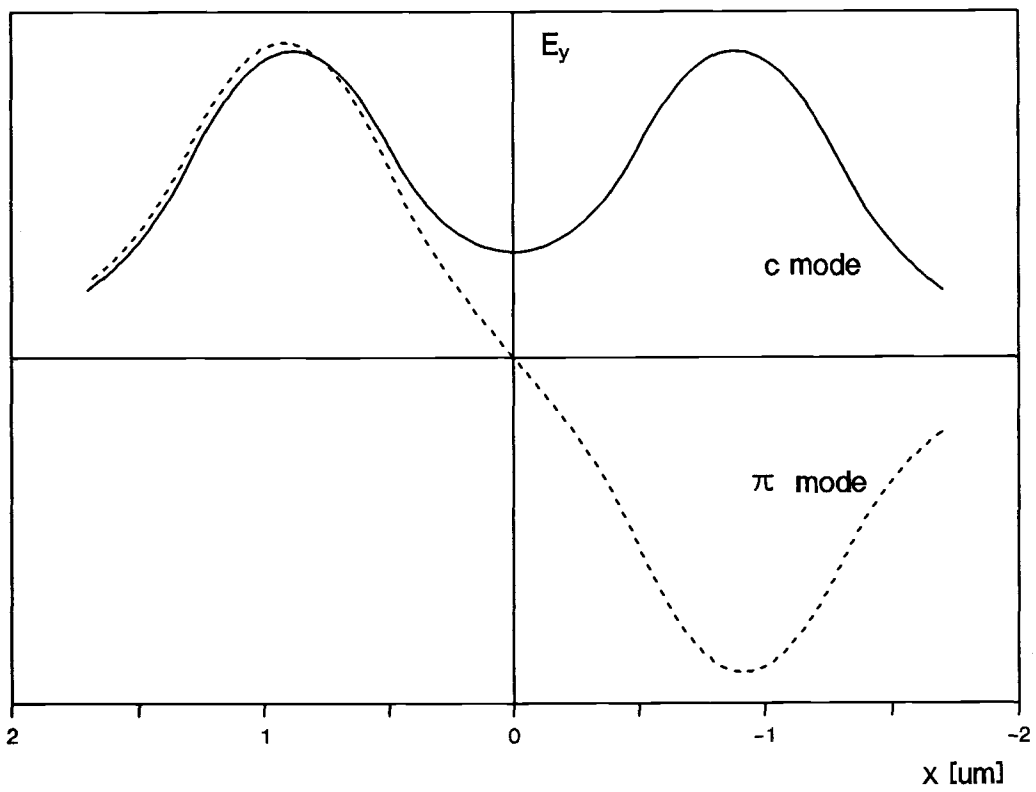


(b)

Fig. 3-1. (a) A refractive index profile of a two-waveguide directional coupler. (b) A symmetric and an antisymmetric modes of a symmetric two-waveguide coupler.

like mode (even-like or c mode) and an antisymmetric-like mode ( odd-like or $\pi$ mode) for an asymmetric two-waveguide coupler. We refer symmetric or symmetric-like modes as c modes, since symmetric modes can be treated as a special case of symmetric-like modes. We also refer antisymmetric or antisymmetric-like modes as $\pi$ modes for this case. The effective indices (normalized propagation constants) obtained are $\beta_\pi$ = 3.2569640 and $\beta_c$ = 3.2605762. A coupling length $L_c$ is calculated from $\pi/k_o(\beta_c - \beta_\pi)$ and found to be $L_c$ = 207.63 $\mu$m. For TE modes, the wave impedance defined in terms of the ratio of electric to magnetic field in each waveguide, is give as $E_x/H_y = \beta/\omega\mu$ and the wave impedances are $Z_\pi$ = 115.672074 and $Z_c$ =115.543926. The ratios of peak amplitudes between guides are always $R_\pi$ = -1 and $R_c$ = 1 for a symmetric structure.

We consider first the normal mode analysis with nonmode converting terminations which is $Z_1 = Z_2$ for the symmetric structure. This condition can be realized into the geometry of a structure with characteristically terminated ($Z_1 = Z_2 = (Z_c Z_\pi)^{1/2}$) as shown Fig. 3-2(a). When we assume the guide 1 is excited, from eqs. (2-13) and eqs. (2-14), the scattering parameters are simplified to

$$\begin{aligned} S_{11} &= (\Gamma_c + \Gamma_\pi)/2 \\ S_{21} &= (\Gamma_c - \Gamma_\pi)/2 \\ S_{31} &= (T_c + T_\pi)/2 \\ S_{41} &= (T_c - T_\pi)/2 \end{aligned} \qquad (3\text{-}1)$$

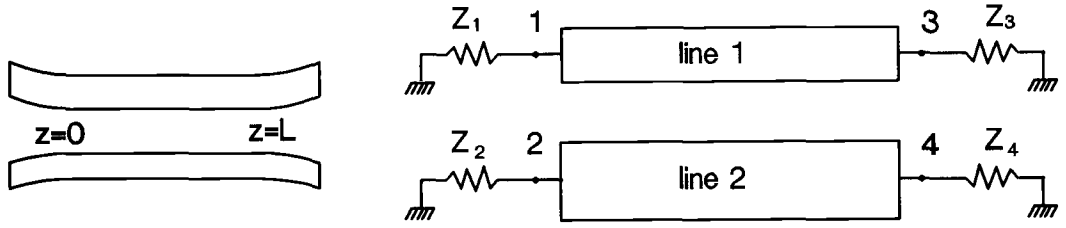


(a)

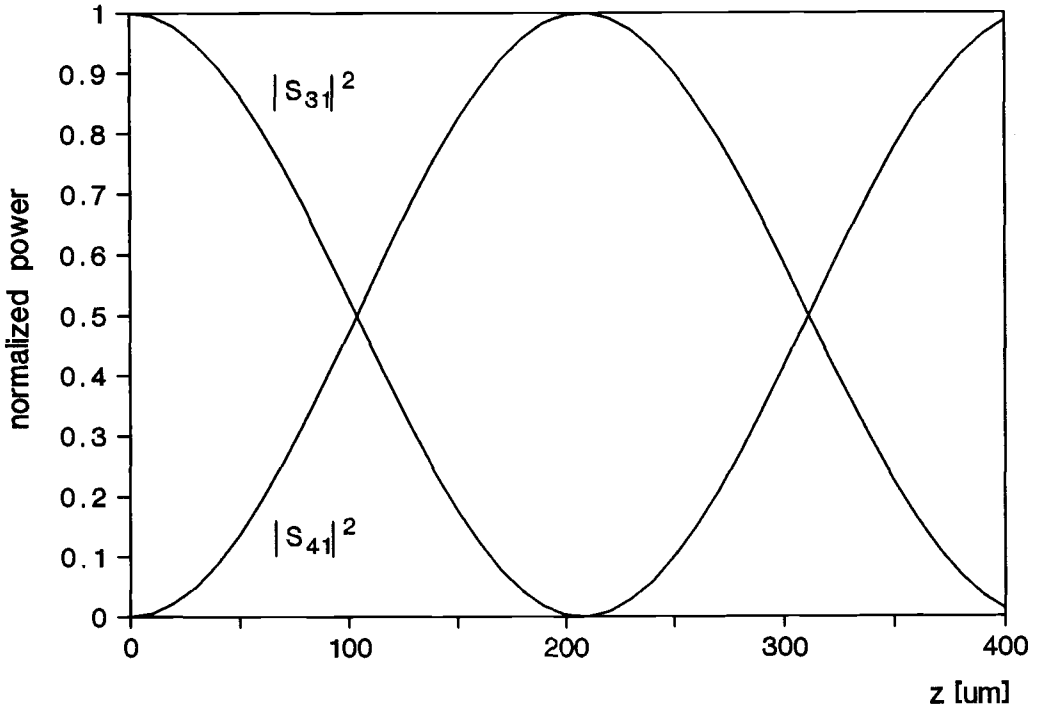


(b)

Fig. 3-2. (a) A general two-waveguide coupler and an equivalent transmission line structure. (b) Normalized output power distributions along the waveguide.

Normalized power at port i for the given input to port j is $|S_{ij}|^2$.

The scattering parameters can also be obtained from the generalized expressions for arbitrary terminations and we have $R_{11} = R_{12} = 1$, $R_{21} = R_c$, $R_{22} = R_\pi$, $Y_{11} = Y_{21} = Y_c = 1/Z_c$, and $Y_{12} = Y_{22} = Y_\pi = 1/Z_\pi$. $[M_E]$ and $[M_H]^{-1}$ becomes

$$[M_E] = \begin{bmatrix} 1 & 1 \\ R_C & R_\pi \end{bmatrix} \qquad [M_H]^{-1} = \frac{1}{\Delta} \begin{bmatrix} R_\pi Y_\pi & -Y_\pi \\ -Y_C & Y_C \end{bmatrix} \tag{3-2}$$

where $\Delta = (R_\pi - R_c) Y_c Y_\pi$. The impedance matrix parameters and the scattering parameters are then obtained from eq. (2-23) and eq. (2-26), respectively.

The numerical result on power flows along the coupler is shown in Fig. 3-2(b). There exhibits complete power transfer between guides at a coupling length $L_c$. The results calculated from the normal mode analysis and the coupled mode theory are almost indistinguishable for this symmetric structure with the characteristic terminations. For this matched system, we have vanishing values of $|S_{11}|^2$ and $|S_{21}|^2$.

For a mismatched system, we consider a waveguide with large refractive index difference between guiding layers ($n_2 = n_4 = 3.8$) and non-guiding layers ($n_1 = n_3 = n_5 = 3$) as shown in Fig. 3-2(c). Port 2 and port 4 are terminated with the substrate material. The termination impedance is assumed to be equal to the intrinsic impedance of the

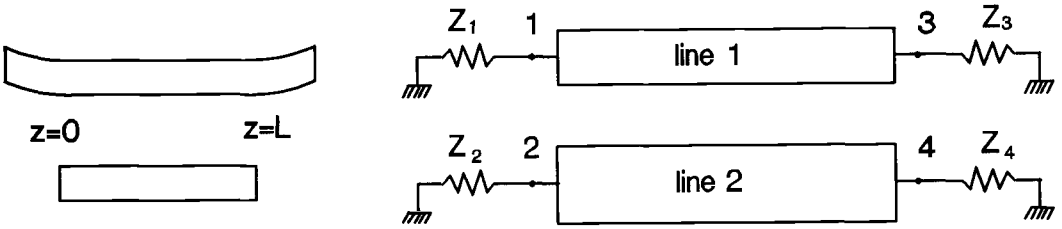


(c)

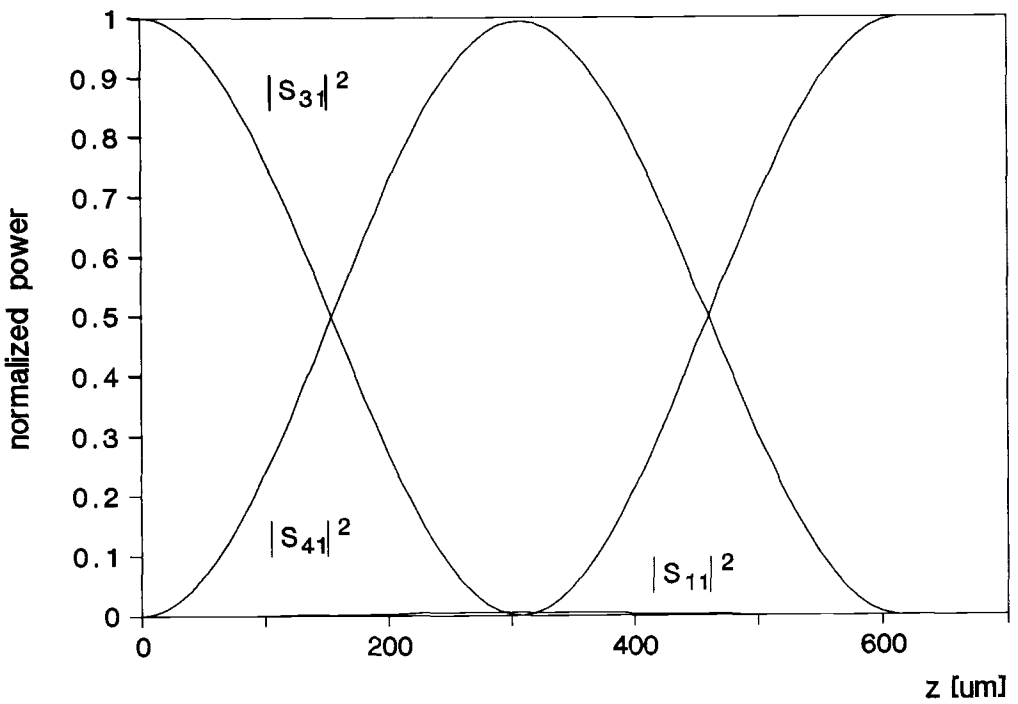


(d)

Fig. 3-2. (c) A mismatched symmetric two-waveguide coupler. (d) Normalized output power distributions along the waveguide.

substrate which is given by $(\mu_o/\epsilon_o)^{1/2}/n_5$. Normalized power at port 1, $|S_{11}|^2$ is shown in Fig. 3-2(d) and the normal mode analysis yields $|S_{11}|^2_{max} \approx 6 \times 10^{-3}$ and $|S_{21}|^2_{max} \approx 1.5 \times 10^{-3}$.

## 3.3 Asymmetric Two-Waveguide Couplers

From the coupled-line analysis, the property of a coupled line is given by $Z_{c2}/Z_{c1} = Z_{\pi 2}/Z_{\pi 1} = -R_c R_\pi$ as described in section 2.4. Nonmode converting terminations must satisfy the condition $Z_2/Z_1 = -R_c R_\pi$. For an asymmetric coupled optical waveguide, mode impedances are given by $\omega\mu_o/\beta$ and $\beta/\omega\epsilon$ for TE modes and TM modes, respectively and we have $Z_{c2}/Z_{c1} = Z_{\pi 2}/Z_{\pi 1} = 1$ for TE modes and generally $Z_{c2}/Z_{c1} = Z_{\pi 2}/Z_{\pi 1} \neq 1$ for TM modes if the dielectric constants of the two guides are not equal. From the normal mode analysis, for the given electric field and magnetic field eigenvectors, the impedance matrix parameters for TE modes are

$$
\begin{aligned}
Z_{11} &= Z_{33} = R_\pi Y_\pi \cot\theta_1 - R_c Y_c \cot\theta_2, \\
Z_{12} &= Z_{34} = -Y_\pi \cot\theta_1 + Y_c \cot\theta_2, \\
Z_{21} &= Z_{43} = R_c R_\pi (Y_\pi \cot\theta_1 - Y_c \cot\theta_2), \\
Z_{22} &= Z_{44} = -R_c Y_\pi \cot\theta_1 + R_\pi Y_c \cot\theta_2, \\
Z_{13} &= Z_{31} = R_\pi Y_\pi \csc\theta_1 - R_c Y_c \csc\theta_2, \\
Z_{14} &= Z_{32} = -Y_\pi \csc\theta_1 + Y_c \csc\theta_2, \\
Z_{23} &= Z_{41} = R_c R_\pi (Y_\pi \cot\theta_1 - Y_c \cot\theta_2), \\
Z_{24} &= Z_{42} = -R_c Y_\pi \csc\theta_1 + R_\pi Y_c \csc\theta_2,
\end{aligned}
\qquad (3\text{-}3)
$$

where $Y_c = \beta_c/\omega\mu_o$, $Y_\pi = \beta_\pi/\omega\mu_o$. Here, $j/\Delta$ was assumed and $\Delta = (R_\pi - R_c)Y_cY_\pi$. Since there is no loss or gain involved, we must have $Z_{ij} = Z_{ji}$ by reciprocity. Thus, we have a relationship $-R_cR_\pi = 1$ which is the required condition for the normal mode parameters of TE modes. Therefore, the normal mode analysis can be applied to coupled waveguides since the product $-R_cR_\pi$ is approximately equal to unity.

For an asymmetric structure as shown in Fig. 3-1(a), the structural parameters used are $n_1 = n_3 = n_5 = 3.4$, $n_2 = n_4 = 3.6$, $W_1 = 0.15$ $\mu$m, $W_2 = 0.14$ $\mu$m, $d = 0.4$ $\mu$m, and $\lambda = 0.8$ $\mu$m. For TE modes, electric field distributions are shown in Fig. 3-3(a) and calculated normal mode parameters are

$\beta_c = 3.4667519$, $\beta_\pi = 3.4486981$, $R_c = 0.7305947$,

$R_\pi = -1.3621991$, $1/Y_c = 108.6722643$, $1/Y_\pi = 109.2411601$.

The accuracy of the coupled mode theory is often checked by comparing calculated values of effective indices with the normal mode parameters $\beta_c$ and $\beta_\pi$. The effective indices obtained from the nonorthogonal coupled mode theory are $\beta_c = 3.4663470$, $\beta_\pi = 3.4487641$. The output power profile along the waveguide obtained from the normal mode analysis is shown in Fig. 3-3(b) and is in good agreement with that of the coupled mode theory. Incomplete power transfer

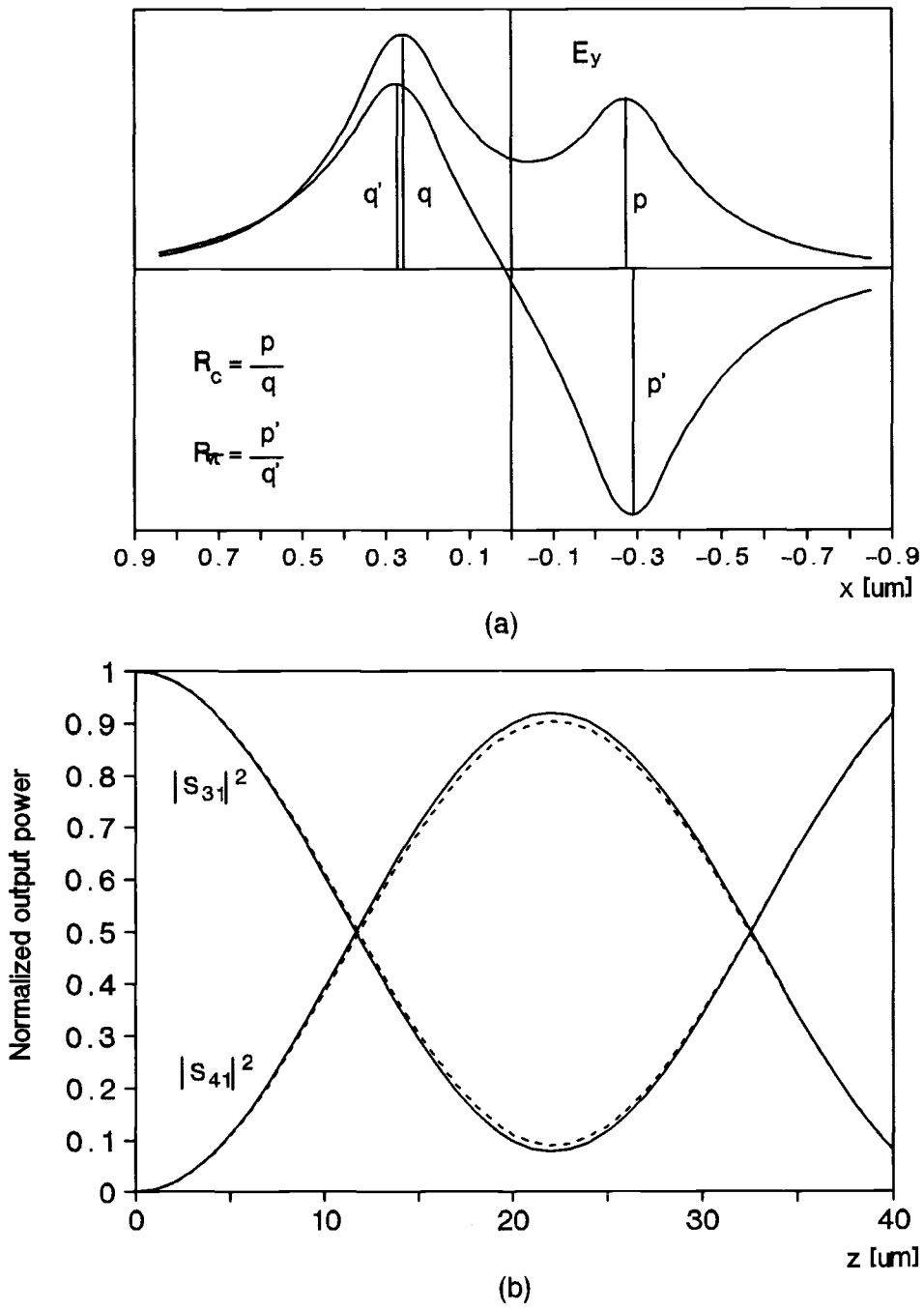


Fig. 3-3. (a) c mode and $\pi$ mode of an asymmetric coupled waveguide. (b) Output power distributions obtained from coupled mode theory (solid lines) and normal mode analysis (dotted lines).

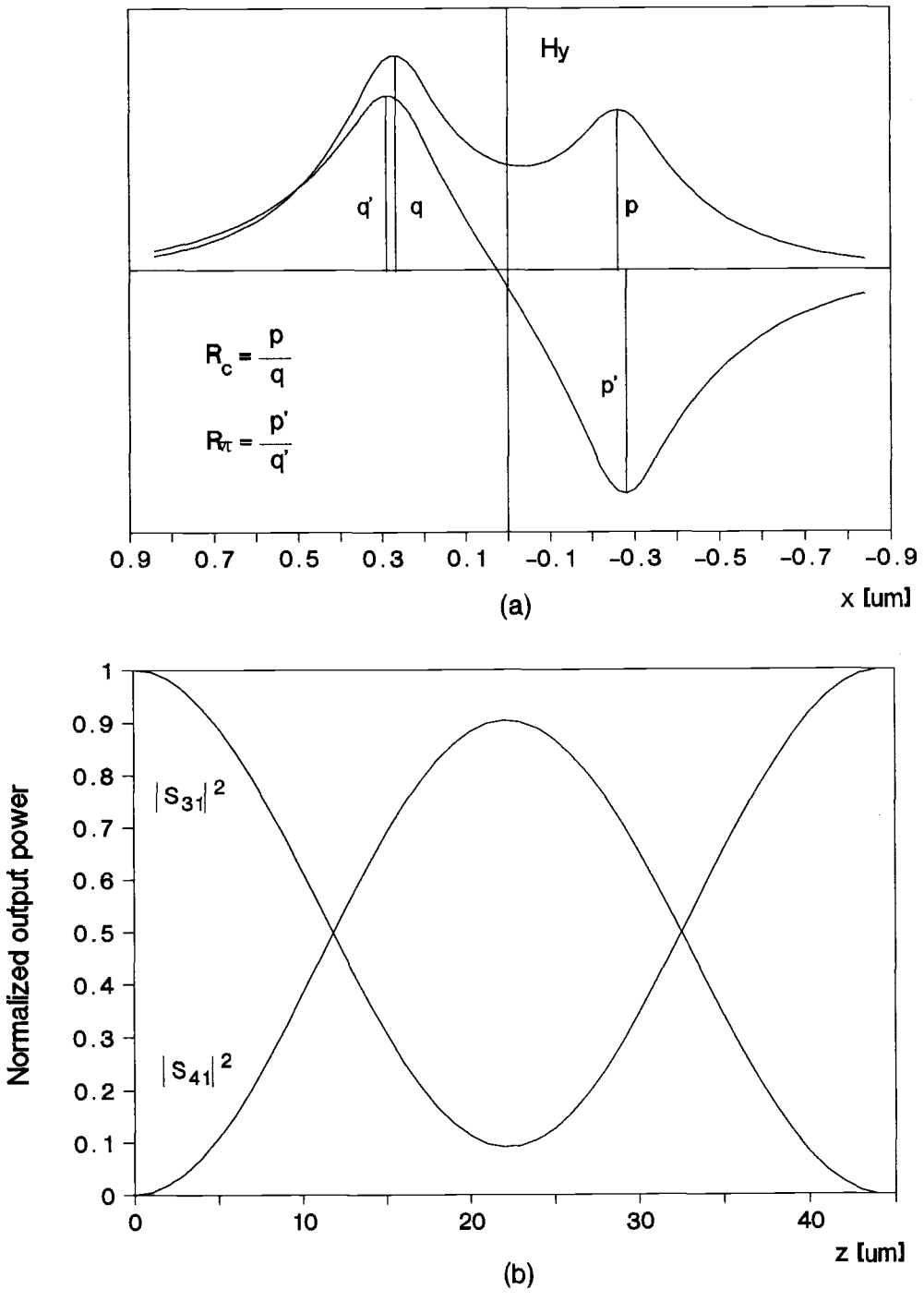


Fig. 3-4. (a) Magnetic field distributions for TM modes of an asymmetric coupled waveguide. (b) Normalized output power distributions obtained from normal mode analysis.

between guides occurs for this asymmetric coupled waveguide.

The elements of the impedance matrix and the property for TM modes of a two-waveguide coupler are shown in Appendix A. The required condition for the normal mode parameters of TM modes is given by

$$R_c R_\pi \frac{Z_{m21}}{Z_{m11}} = R_c R_\pi \frac{\epsilon_{g1}}{\epsilon_{g2}} = -1 \qquad (3\text{-}4)$$

where wave impedances $Z_{mji} = \beta_i/\omega\epsilon_{gj}$, and $\epsilon_{g1}$ and $\epsilon_{g2}$ are dielectric constants of guide 1 and guide 2, respectively. Here, $R_c$ and $R_\pi$ are the elements of magnetic field eigenvectors. For TM modes, the normal mode parameters of the same structure are

$\beta_c = 3.4603795$, $\beta_\pi = 3.4409762$, $Z_{m11} = Z_{m21} = 100.5861972$,
$Z_{m12} = Z_{m22} = 100.0221829$, $R_c = 0.7535940$, $R_\pi = -1.3188956$.

Magnetic field profiles and the output power distribution calculated from the normal mode method are shown in Fig. 3-4(a) and (b), respectively. The result also exhibits incomplete switching.

For asymmetric coupled waveguides where the refractive indices or widths of two guiding layers have considerable difference, the product $-R_cR_\pi$ deviates from given conditions for this asymmetric waveguides. In this case, $R_c$ and $R_\pi$ can be defined differently from the usual

definition used here. One of the possible definitions for $R_c$ and $R_\pi$ is discussed in Appendix B.

## 3.4 Symmetric Three-Waveguide Couplers

The circuit parameters of a symmetric three-waveguide coupler can be similarly obtained as described in sections 3.1, 3.2, and Appendix A. Electric field and magnetic field eigenvectors for TE modes can be written as

$$[M_E] = \begin{bmatrix} 1 & 1 & 1 \\ 0 & R_B & R_C \\ -1 & 1 & 1 \end{bmatrix} \qquad [M_H] = \begin{bmatrix} Y_1 & Y_2 & Y_3 \\ 0 & R_B Y_2 & R_C Y_3 \\ -Y_1 & Y_2 & Y_3 \end{bmatrix} \tag{3-5}$$

Then, the elements of the impedance matrix are expressed as

$$\begin{aligned} Z_{11} &= \frac{\cot\theta_1}{2Y_1} - \frac{R_C \cot\theta_2}{2(R_B - R_C)Y_2} + \frac{R_B \cot\theta_3}{2(R_B - R_C)Y_3} \\ Z_{12} &= \frac{1}{R_B - R_C}\left(\frac{\cot\theta_2}{Y_2} - \frac{\cot\theta_3}{Y_3}\right) \\ Z_{21} &= \frac{-R_B R_C}{2(R_B - R_C)}\left(\frac{\cot\theta_2}{Y_2} - \frac{\cot\theta_3}{Y_3}\right) \\ &\vdots \end{aligned} \tag{3-6}$$

Here, j is assumed. The condition to be a reciprocal system is $-R_B R_C = 2$. This condition holds for TE modes of a symmetric three-waveguide coupler either with identical guides or with nonidentical guides.

We consider first a symmetric three-waveguide where all three waveguides are identical. From Fig. 3-5(a), the

structural parameters are $n_1 = n_3 = n_5 = n_7 = 3.4$, $n_2 = n_4 = n_6 = 3.6$, $W_1 = W_2 = W_3 = 0.15$ $\mu$m, $d_1 = d_2 = 0.4$ $\mu$m, and $\lambda = 0.8$ $\mu$m. Computed values of the normal mode parameters are

$\beta_a = 3.4612656$, $\beta_b = 3.4473212$, $\beta_c = 3.4714101$

$1/Y_1 = 108.8445158$, $1/Y_2 = 109.2847905$, $1/Y_3 = 108.5264396$

$R_B = 1.3904038$, $R_C = -1.4432537$.

The numerical results obtained from the normal mode analysis for different input conditions are shown in Fig. 3-6. For excitation to center guide, as shown in Fig. 3-6(a), power flows are periodic. For excitation to an outer guide, power flows of outer guides are not periodic while output power distribution of center guide is periodic. The results are in very good agreement with those obtained by Hardy and Streifer [38] using the coupled mode theory.

The parameters used for a symmetric three-waveguide coupler with nonidentical guides are $n_1 = n_3 = n_5 = n_7 = 3.4$, $n_2 = n_6 = 3.6$, $n_4 = 3.58$, $W_1 = W_3 = 0.15$ $\mu$m, $W_2 = 0.14$ $\mu$m, $d_1 = d_2 = 0.4$ $\mu$m, and $\lambda = 1.05$ $\mu$m. The normal mode parameters are calculated as

$\beta_A = 3.4396584$, $\beta_B = 3.4018417$, $\beta_C = 3.4551154$

$1/Y_1 = 109.5282535$, $1/Y_2 = 110.7458265$, $1/Y_3 = 109.0382609$

$R_B = 1.0230693$, $R_C = -1.9594716$.

The optical input power is not completely transferred to outer guides for excitation to the center guide as shown in

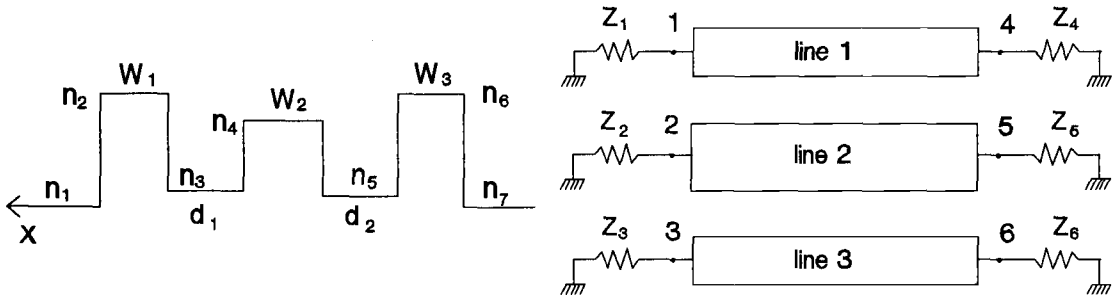


(a)

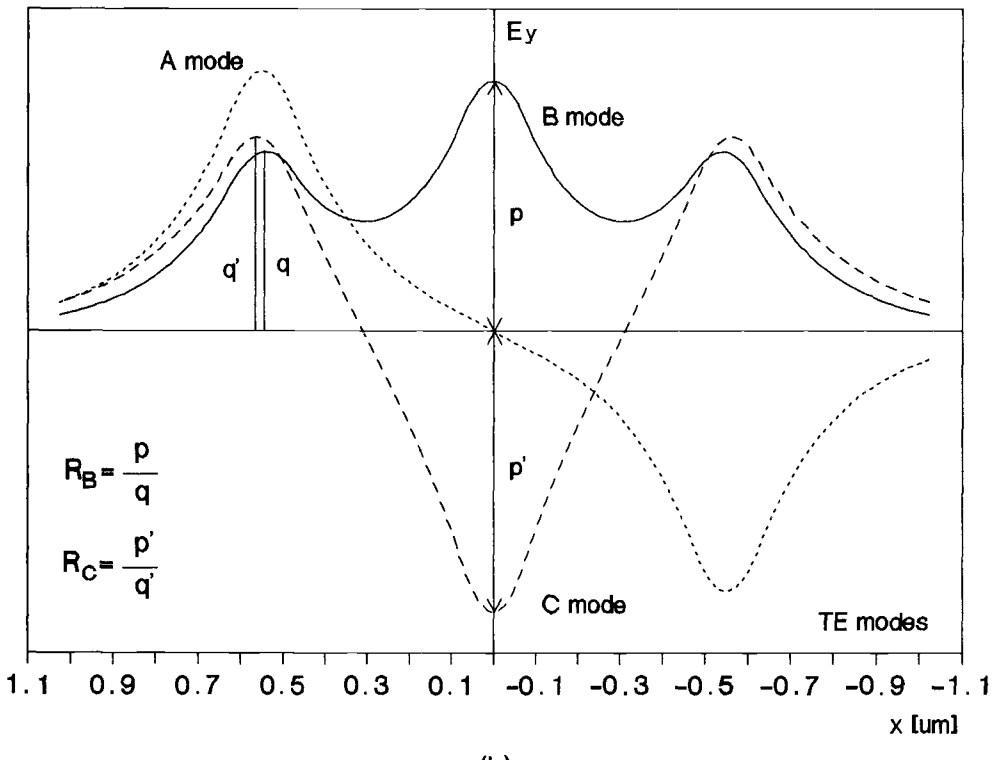


(b)

Fig. 3-5. (a) A structure of a symmetric three-waveguide coupler and an equivalent transmission line. (b) Electric field distributions for TE modes of a symmetric coupler which consists of three identical waveguides.

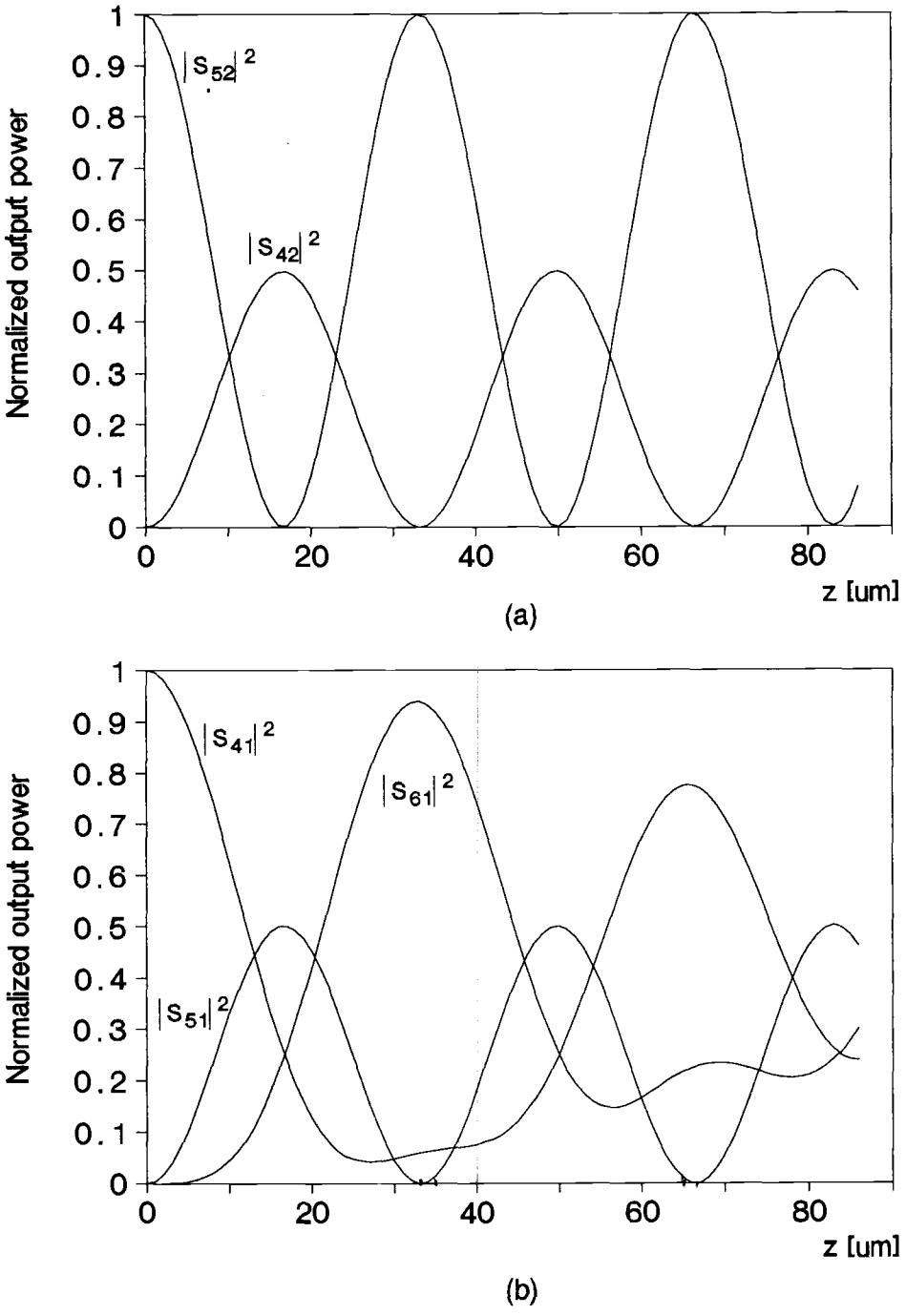


Fig. 3-6. Variation of output power along the coupler with three identical waveguides for (a) excitation to center guide and (b) excitation to an outside guide.

Fig. 3-7(a). The normalized power flows for asymmetric excitation are plotted in Fig. 3-7(b). Again, the input power is not completely delivered to the central guide and the other outside guide. Power conservation is satisfied with the condition $-R_B R_C = 2$ which is required by reciprocity. The normal mode analysis maintains high accuracy as long as $-R_B R_C \approx 2$ holds for symmetric three-waveguide directional couplers.

When an outside guide is excited, output powers from the output ports are non-periodic and the input power is not completely transferred to the other outside guide. The output power distributions can be periodic, if the following conditions are met [81] :

$$2\beta_A - \beta_B - \beta_C = 0. \qquad (3\text{-}7)$$

To realize eq. (3-7), the center guide must be wider than the outside ones. We consider TM modes, as an example, and the parameters are $n_1 = n_3 = n_5 = n_7 = 3.4$, $n_2 = n_4 = n_6 = 3.6$, $d_1 = d_2 = 0.4\ \mu m$, $\lambda = 0.8\ \mu m$, $W_1 = W_3 = 0.15\ \mu m$, and $W_2 = 0.1585\ \mu m$. The impedance matrix is similarly obtained and the required condition for the normal mode parameters of TM modes of this symmetric three-waveguide is given by

$$-R_B R_C \frac{\epsilon_{g1}}{\epsilon_{g2}} = 2. \qquad (3\text{-}8)$$

The effective indices for the three normal modes are $\beta_C = 3.44141286$, $\beta_A = 3.45433667$, and $\beta_B = 3.46725440$. The

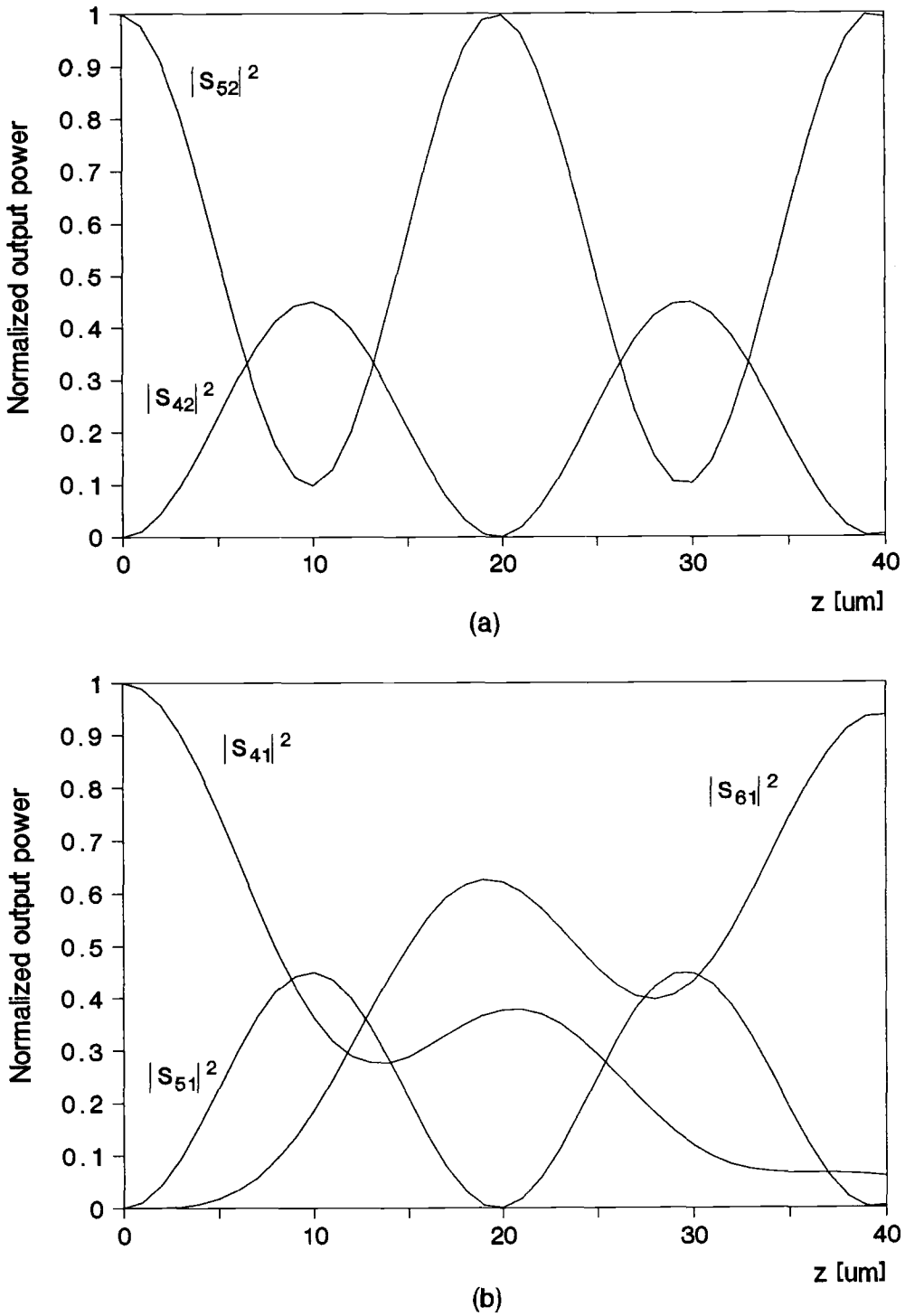


Fig. 3-7. Power distributions along the symmetric three-waveguide coupler for (a) excitation to center guide and (b) excitation to an outside guide.

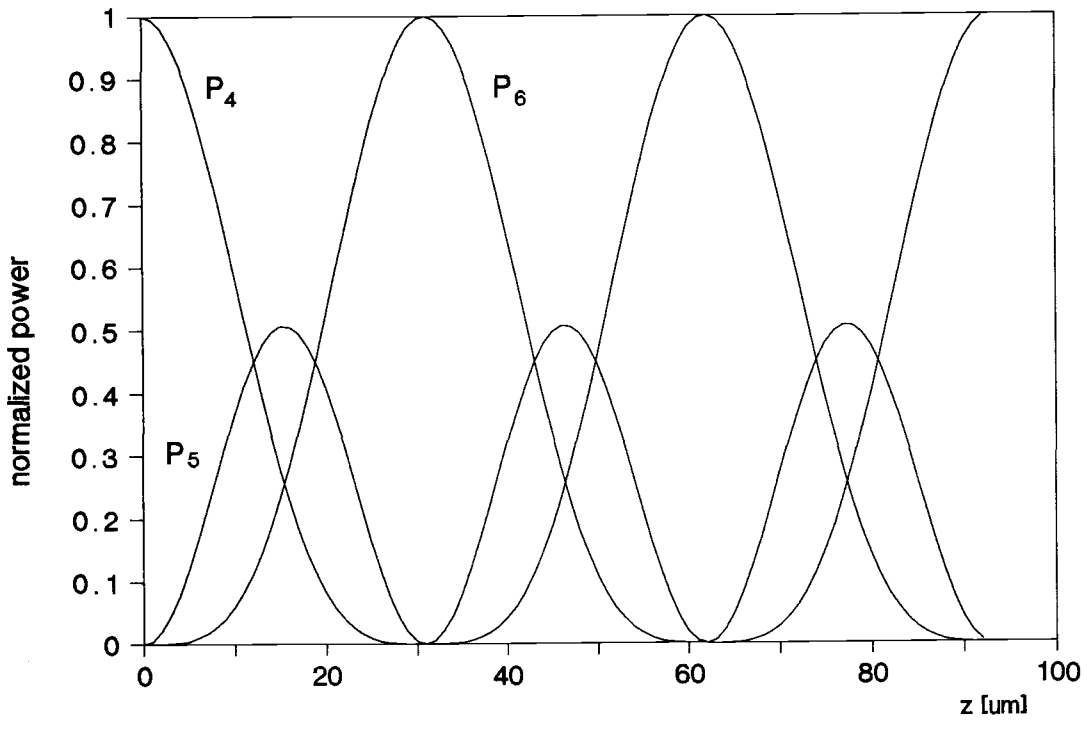


Fig. 3-8. Output powers emerging from ports 4, 5, and 6 for TM modes and for asymmetric excitation.

result obtained from the normal mode analysis is shown in Fig. 3-8. The power distribution along the coupler is periodic and full power transfer from one outside guide to another is achieved.

## 3.5 Concluding Remarks

Numerical calculations on output power distributions for two-waveguide couplers and symmetric three-waveguide couplers using the normal mode analysis have been performed. The numerical results of the normal mode analysis has shown to be in good agreement with those of the coupled mode analysis.

For the normal mode analysis, high accuracy and power conservation are achieved when the conditions, which is required by reciprocity, are satisfied. Those conditions may be violated for asymmetric structures where the refractive index or width of one waveguide shows large difference from that of others. An improved definition of $R_c$ or $R_\pi$ ($R_B$ or $R_C$) can be devised in order for the normal mode method to maintain high accuracy for such structures.

The normal mode analysis can be applied for the analysis and design of asymmetric three-waveguide couplers and multiple coupled waveguides which consist of more than three waveguides. The normal mode method for the analysis of optical coupled waveguides has advantage of simplicity, accuracy, and power conservation over the coupled mode

theory and the normal mode analysis can be used to investigate impedance mismatching problems which may develop in interconnecting optical components.

# CHAPTER 4

# ANALYSIS OF NONLINEAR DIRECTIONAL COUPLERS

## 4.1 Introduction

A great deal of attention has been given to the development of a low power, all-optical switch operating at faster speeds than electronic counterparts. Such a device first analyzed by Jensen [58] based upon coupled mode formulations is a nonlinear directional coupler (NLDC) composed of Kerr-like nonlinear media, whose refractive indices change linearly with optical intensity. Large nonlinearity is required to obtain appreciable switching at low optical powers.

One of the most promising materials is GaAs-AlGaAs multiple quantum-well (MQW) layer. The radius of a bound electron-hole pair, the so-called exciton, is reduced due to confinement in a narrow well. Therefore, there is an increase in binding energy, resulting in a clear excitonic absorption spectrum near the bandgap even at room temperatures [59-60]. Since a high density of photogenerated free carriers serves to screen out the excitons, nonlinear optical effects are induced as the intensity of the light is increased. The absorption spectrum is thus intensity

dependent and results in the phenomenon of an intensity-dependent refractive index. However, though large nonlinearity can be achieved in the MQW layer by operating at frequencies near the band edge, the application of this technology has resulted in increased absorption losses. Thus, for the reduction of absorption losses, Cada *et al.* [64] proposed a coupler structure based upon the use of a multiple quantum well layer in the coupling region only.

Since the nonlinear wave equation has been analytically solved only for Kerr-like nonlinearity, most of the investigations related to the use of nonlinear waveguides have been based on the use of Kerr-like nonlinear media. Coupled mode theory has been used exclusively for the development of nonlinear and linear directional couplers, and is presently the only analytical method which has been used to describe the power-dependent coupling behavior of nonlinear structures. Even when losses and saturation [75-76] are considered, analyses of the coupled mode theory have not been in agreement with experimental results [65-66] obtained for GaAs-based MQW directional couplers with high input powers. Saturation effects, thermal nonlinearity fluctuation, material losses, and fabrication errors have been suggested as the possible sources of this discrepancy [65].

Ghatak *et al.* [63] developed a matrix approach for the investigation of linear planar waveguides with inhomogeneous refractive index profiles and three-layer nonlinear

waveguides with both Kerr-like and non-Kerr-like nonlinear media. Applying the original matrix method to a five-layer NLDC, especially when the nonlinear coupling medium is bounded by two linear guiding layers of finite thickness or when two linear guiding films are bounded by two outside semi-infinite nonlinear media, leads to inaccurate results.

In the present investigation, an extended matrix method for NLDC analysis, where the value of the nonlinear refractive index is calculated in terms of the average field amplitude for each stratified nonlinear layer, is considered. For any material, there are maximum changes in the refractive index which do not increase or decrease in precise linearity to the level of optical intensity. For the consideration of saturation effects, both an exponential and a two-level system model have been proposed. The two-level system model can be readily incorporated into the matrix method. The numerical results obtained have suggested that the saturation effects must be considered in the analysis and design of nonlinear directional couplers.

## 4.2 Nonlinear Wave Equations

Consider a three-layer waveguide consisting of a linear guiding film bounded by one or two nonlinear media, as shown in Fig. 4-1(a) and (b). The refractive index of the Kerr-like nonlinear region is given by

$$n^2 = (n_o + n_{nl}I)^2 \approx n_o^2 + \alpha E^2 \ , \qquad (4\text{-}1)$$

where $\alpha = n_o^2 n_{nl}/Z_o$, $n_o$ is the refractive index at zero light power, $Z_o$ is the free-space impedance, and I represents the intensity of the light; nonlinear media can be either self-focusing ($\alpha > 0$) or self-defocusing ($\alpha < 0$). The nonlinear wave equation for guided TE modes, $E(x,z,t) = E(x)\exp(j\omega t)\exp(-jk_o\beta z)$, reduces to [64]

$$d^2E(x)/dx^2 - k^2E(x) + 2\Lambda E^3(x) = 0 \ , \qquad (4\text{-}2)$$

where $k^2 = k_o^2(\beta^2 - n_o^2)$, $k_o$ is the free-space wave number, $\Lambda = \alpha k_o^2/2$, and $\beta$ is the effective index. Integration of eq. (4-2) gives

$$(E_x)^2 - k^2E^2 + \Lambda E^4 = C \ , \qquad (4\text{-}3)$$

where $E_x = dE/dx$. Since fields vanish for $x \to \pm\infty$, the constant C must be zero for semi-infinite nonlinear media. The solutions for eq. (4-2) are given by [81-84]

$$E(x) = \pm\sqrt{\frac{2}{\alpha}}\frac{k}{k_o}\,sechk(x - x_o) \ , \qquad \alpha > 0 \qquad (4\text{-}4a)$$

$$= \pm\sqrt{\frac{2}{|\alpha|}}\frac{k}{k_o}\,cschk(x - x_o) \ , \qquad \alpha < 0 \qquad (4\text{-}4b)$$

where $x_o$ is a constant of integration.

For example, when structures are similar to the illustration in Fig. 4-1(a), the remainder of the modal fields in the linear regions are given by

$$E(x) = A\cos k_2x + B\sin k_2x \ , \qquad 0 \le x < d \qquad (4\text{-}5a)$$

$$= C\exp[k_3(x - d)] \ , \qquad x > d \qquad (4\text{-}5b)$$

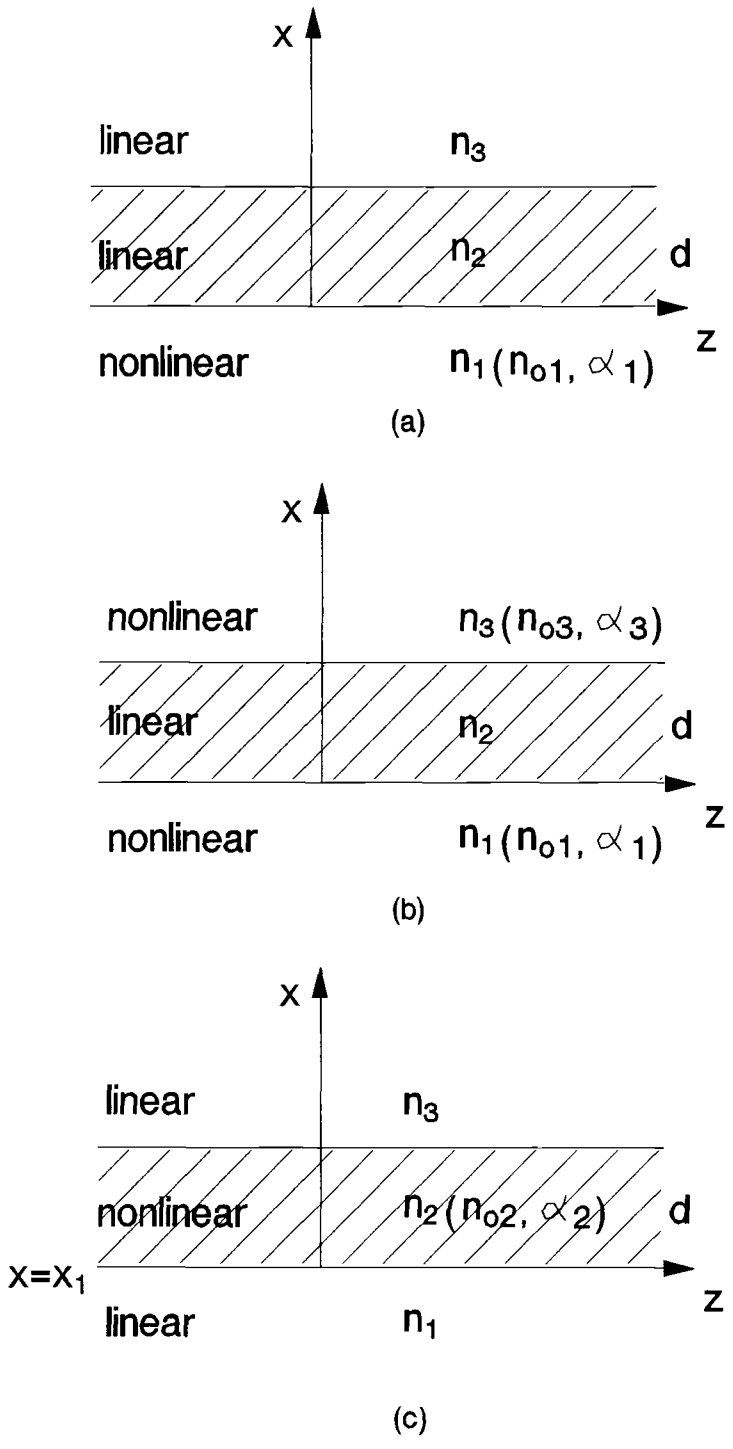


Fig. 4-1. A three-layer waveguide (a) with a semi-infinite nonlinear medium. (b) bounded by two nonlinear media. (c) with nonlinear medium bounded by two linear media.

From the boundary conditions, the eigenvalue equation may be obtained as

$$\tan k_2 d = \frac{k_2(k_1 \tanh k_1 x_o - k_3)}{k_2^2 + k_1 k_3 \tanh k_1 x_o} \quad . \tag{4-6}$$

The parameters A, B, C, $x_o$, and $\beta$ are involved in four algebraic equations and an eigenvalue equation. When $x_o$ is arbitrarily chosen, the remainder of the parameters and the mode power can be determined. For structures with a linear film bounded by two nonlinear media (e.g., Fig. 4-1(b)), power dependent dispersion may be similarly obtained.

When a nonlinear film is sandwiched between two linear media, as shown in Fig. 4-1(c), the constant c has nonzero value. The integration constant C is evaluated from

$$C = E_x^2(x_1) - k^2E^2(x_1) + \Lambda E^4(x_1) \quad , \tag{4-7}$$

where $x_1$ can be chosen conveniently at the linear-nonlinear layer boundary, and where the first derivative of E is known. Then, from eq. (4-7):

$$\int dx = \int \frac{dE}{\sqrt{C + k^2E^2 - \Lambda E^4}}$$

$$= \int \frac{dE}{\sqrt{-\Lambda\left(E^2 - \frac{k^2}{2\Lambda} + \sqrt{\frac{4\Lambda C + k^4}{4\Lambda^2}}\right)\left(E^2 - \frac{k^2}{2\Lambda} - \sqrt{\frac{4\Lambda C + k^4}{4\Lambda^2}}\right)}} \quad . \tag{4-8}$$

Solutions are then expressed in terms of Jacobian elliptic functions [85-86] for differences dependent upon on the signs for $\Lambda$ and C. To obtain real solutions for the E fields, we have $4\Lambda C + k^4 \geq 0$, which is otherwise a cutoff

condition for a certain mode. For a self-defocusing medium ($\alpha$, $\Lambda < 0$) with an antisymmetric mode ($C > 0$), the solution is

$$E(x) = p\ sc[q(x - x_o)|m] \ , \tag{4-9}$$

where

$$p^2 = (q^2 - k^2)/\Lambda \ , \tag{4-10a}$$

$$q^2 = [k^2 + (k^4 + 4\Lambda C)^{1/2}]/2 \ , \tag{4-10b}$$

$$m = 2 - k^2/q^2 \ , \tag{4-10c}$$

and where $x_o$ is another constant of integration, determined by substituting $E(x = x_1)$ into eq. (4-7). Different combinations of the signs for $\Lambda$ and $C$ yield different solutions [87-88], as shown in Table 4-1.

| | |
|---|---|
| $\Lambda < 0$<br>$C > 0$ | $E(x) = p\ sc[q(x - x_o)\|m]$<br>$p^2 = (q^2 - k^2)/\Lambda$<br>$q^2 = [k^2 + (k^4 + 4\Lambda C)^{1/2}]/2$<br>$m = 2 - k^2/q^2$ |
| $\Lambda < 0$<br>$C < 0$ | $E(x) = p\ nc[q(x - x_o)\|m]$<br>$p^2 = (k^2 - q^2)/2\Lambda$<br>$q^2 = (k^4 + 4\Lambda C)^{1/2}$<br>$m = (k^2 + q^2)/2q^2$ |
| $\Lambda > 0$<br>$C < 0$ | $E(x) = p\ nd[q(x - x_o)\|m]$<br>$p^2 = (k^2 - q^2)/\Lambda$<br>$q^2 = [k^2 + (k^4 + 4\Lambda C)^{1/2}]/2$<br>$m = 2 - k^2/q^2$ |
| $\Lambda > 0$<br>$C > 0$ | $E(x) = p\ cn[q(x - x_o)\|m]$<br>$p^2 = (k^2 + q^2)/2\Lambda$<br>$q^2 = (k^4 + 4\Lambda C)^{1/2}$<br>$m = (k^2 + q^2)/2q^2$ |

Table 4-1. Guided TE mode solutions of nonlinear equations for different types of bounded nonlinear media.

## 4.3 Extended Matrix Method

Consider a two-waveguide coupler consisting of a nonlinear coupling medium bounded by two linear guiding layers, as shown in Fig. 4-2(a). The nonlinear region is divided into a large number of layers, each with identical thicknesses, to obtain the approximate electrical field distributions for each layer, as shown in Fig. 4-2(b). For the $i^{th}$ layer of a guided TE mode, Eq. (4-2) can be approximated as

$$\begin{aligned} & d^2E_i/dx^2 - k_o^2(\beta_i^2 - n_o^2 - \alpha E_i^2)E_i \\ & \quad = d^2E_i/dx^2 - k_o^2(\beta_i^2 - n_i^2)E_i = 0 \ , \end{aligned} \tag{4-11}$$

which provides solutions in terms of the trigonometric or hyperbolic functions, given by

$$\begin{aligned} E_i &= A_i \cos[k_i(x - d_{i-1})] \\ &\quad + B_i \sin[k_i(x - d_{i-1})] \ , \qquad \text{for } k_i^2 > 0 \end{aligned} \tag{4-12a}$$

$$\begin{aligned} &= A_i \cosh[k_i(x - d_{i-1})] \\ &\quad + B_i \sinh[k_i(x - d_{i-1})] \ , \qquad \text{for } k_i^2 < 0 \end{aligned} \tag{4-12b}$$

where $k_i^2 = k_o^2(n_i^2 - \beta_i^2)$. Then, since the field decays to zero as x goes to $-\infty$ and $\infty$, $A_1 = B_1$ and $A_N + B_N = 0$ for the guided TE modes. The field amplitudes of the $i^{th}$ and the $(i+1)^{th}$ layers relate to the boundary conditions in the matrix form [63]:

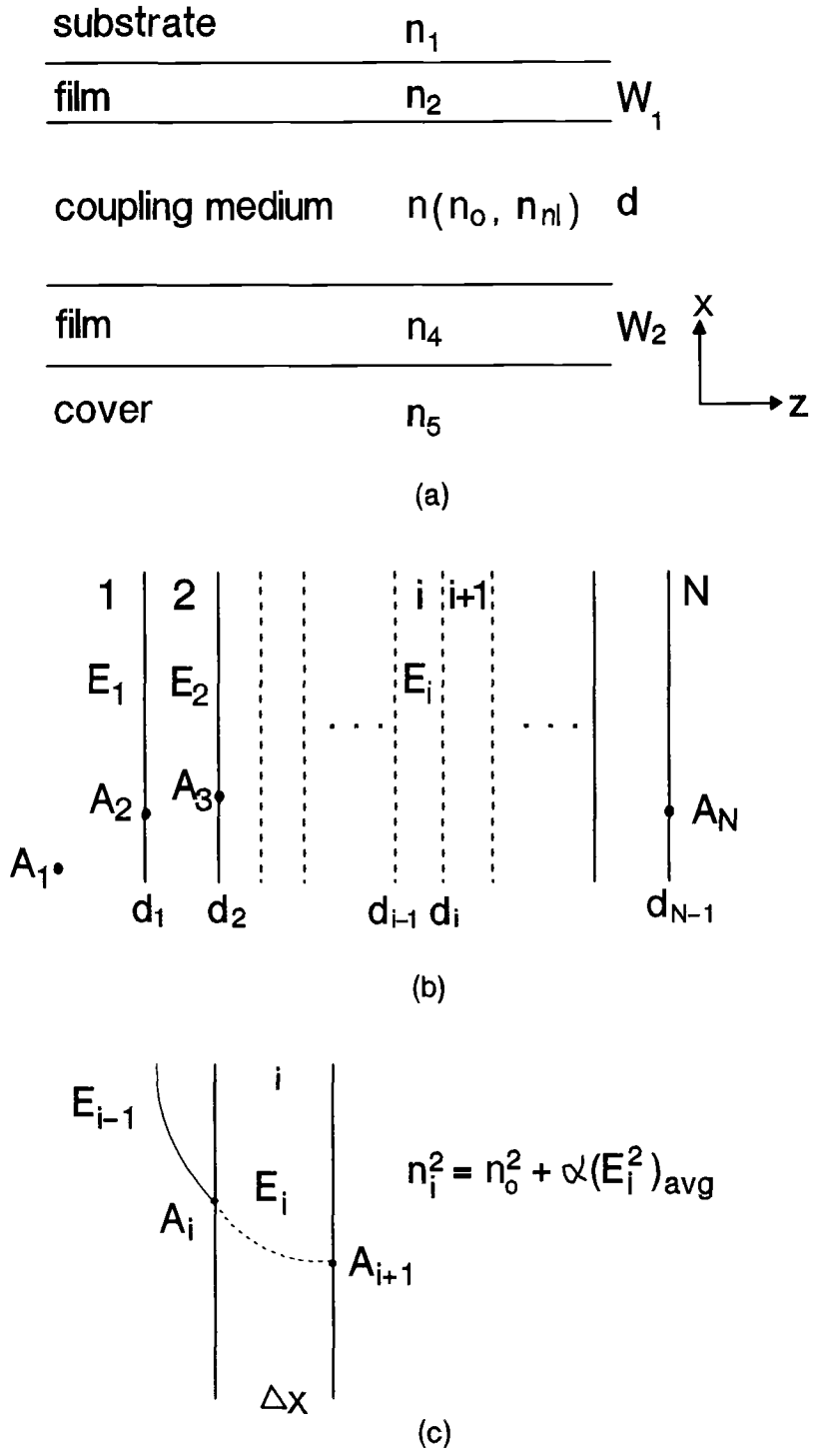


Fig. 4-2. (a) A structure of a nonlinear coupler. (b) A stratified nonlinear medium. (c) The $i^{th}$ nonlinear layer.

$$\begin{bmatrix} A_{i+1} \\ B_{i+1} \end{bmatrix} = S_i \begin{bmatrix} A_i \\ B_i \end{bmatrix} , \tag{4-13}$$

where

$$S_i = \begin{bmatrix} \cos\Delta_i & \sin\Delta_i \\ \frac{-k_i}{k_i+1}\sin\Delta_i & \frac{k_i}{k_i+1}\cos\Delta_i \end{bmatrix} , \qquad for\ k_i^2 > 0$$

$$= \begin{bmatrix} \cosh\Delta_i & \sinh\Delta_i \\ \frac{k_i}{k_i+1}\sinh\Delta_i & \frac{k_i}{k_i+1}\cosh\Delta_i \end{bmatrix} , \qquad for\ k_i^2 < 0 \tag{4-14}$$

and $\Delta_i = k_i(d_i - d_{i-1})$. Eq. (4-14) is useful for the computations of the field amplitudes. Each layer in the nonlinear region is assumed to be sufficiently thin to take the field amplitude within the layer as a constant. Since $A_i$ is already known from the boundary condition, $n_i^2$ is initially approximated (see Fig. 4-2(c)) as

$$n_i^2 = n_o^2 + \alpha(A_i^2) , \tag{4-15}$$

and $E_i$ ($A_i$, $B_i$, and $k_i$) can then be obtained from the initial value of $n_i^2$ and the refractive index of the $i^{th}$ layer, expressed as

$$n_i^2 = n_o^2 + \alpha(E_i^2)_{avg} , \tag{4-16}$$

where

$$(E_i^2)_{avg} = \frac{1}{\Delta x}\int E_i^2 \, dx , \tag{4-17}$$

for which $(E_i^2)_{avg}$ is conveniently written as

$$(E_i^2)_{avg} = \frac{1}{4\Delta_i}[2(A_i^2 - B_1^2)\Delta_i + (A_i^2 + B_i^2)sinh2\Delta_i + 2A_iB_i(cosh2\Delta_i - 1)] \quad . \tag{4-18}$$

For the given values of $A_1$ and the effective index, the averaging process is subject to iteration until the values of $n_i^2$ converge. After the process reaches a sufficient distance from the linear waveguide region, based upon the use of successive boundary conditions, the effective indices of the two independent guided modes for the fixed values of $A_1$ are then determined from the eigenvalue equation, $A_N + B_N = 0$ .

For the original matrix method, the refractive index of the $i^{th}$ nonlinear layer is assumed to be

$$n_i^2 = n_o^2 + \alpha(A_{i-1}^2) \quad . \tag{4-19}$$

It should be noted that when the nonlinear region is bounded by two linear guiding films of finite thickness, the use of eq. (4-19) leads to inaccurate results.

The guided wave power per unit length is expressed as

$$P = \frac{1}{2} Re\left( \int_{-\infty}^{\infty} (E \times H^*)_z \, dx \right) = \frac{\beta}{8}\sqrt{\frac{\epsilon_o}{\mu_o}} \sum_{i=1}^{N} \frac{q_i}{k_i} \quad , \tag{4-20}$$

where

$$q_i = A_i^2(2\Delta_i + \sin 2\Delta_i) + B_i^2(2\Delta_i - \sin 2\Delta_i) + 2A_iB_i(1 - \cos 2\Delta_i) \quad , \qquad \text{for } k_i^2 > 0 \tag{4-21a}$$

$$= A_i^2(2\Delta_i + \sinh 2\Delta_i) - B_i^2(2\Delta_i - \sinh 2\Delta_i) + 2A_iB_i(1 - \cosh 2\Delta_i) \quad , \qquad \text{for } k_i^2 < 0 \tag{4-21b}$$

$$\Delta_i = k_i(d_i - d_{i-1}) = k_i\Delta x \quad .$$

From eq. (4-3), the nonzero integration constant C is given by

$$C = E_x^2(x_o) - k^2E^2(x_o) + \Lambda E^4(x_o) \quad , \tag{4-22}$$

where $x_o$ is chosen at the linear-nonlinear layer boundary ($d_2$) for which the 1st derivative of E can be known. Thus, from eq. (4-22),

$$\int dx = \int \frac{dE}{\sqrt{C + k^2E^2 - \Lambda E^4}}$$

$$= \frac{1}{\sqrt{-\Lambda}} \int \frac{dE}{\sqrt{E^2 - \frac{k^2}{2\Lambda} + \sqrt{\frac{4\Lambda C + k^4}{4\Lambda^2}}} \sqrt{E^2 - \frac{k^2}{2\Lambda} - \sqrt{\frac{4\Lambda C + k^4}{4\Lambda^2}}}} \; . \tag{4-23}$$

To obtain real solutions for the E fields, $4\Lambda C + k^4 \geq 0$, which is otherwise the cutoff condition for antisymmetric modes.

Since the linear combinations of the two modes do not satisfy the nonlinear wave equation, these two independent modes cannot be used for coupler analysis. A nonlinear combination of these modes, as introduced by Cada *et al.* [64], expressed the total field as the sum of two perturbed modes such that $E(x,z) = Y_s(x,z) + Y_a(x,z)$. Thus, expressing the two perturbed modes as $Y_s(x,z) = y_s(x) \exp(-jk_o\beta_s z)$ and $Y_a(x,z) = y_a(x) \exp(-jk_o\beta_a z)$, respectively, results in two simultaneous nonlinear differential equations for the $i^{th}$ nonlinear layer:

$$d^2y_{si}/dx - k_{si}^2 y_{si} + \alpha k_o^2 (y_{si}^2 + 2y_{si}y_{ai}\cos\theta_i + y_{ai}^2) y_{si} = 0 \qquad (4\text{-}24)$$

and

$$d^2y_{ai}/dx - k_{ai}^2 y_{ai} + \alpha k_o^2 (y_{ai}^2 + 2y_{si}y_{ai}\cos\theta_i + y_{ai}^2) y_{ai} = 0 \ , \qquad (4\text{-}25)$$

where

$$k_{si}^2 = k_o^2(\beta_{si}^2 - n_o^2) \ , \quad k_{ai}^2 = k_o^2(\beta_{ai}^2 - n_o^2) \ , \quad \theta_i = k_o(\beta_{si} - \beta_{ai})\, z \ ,$$

and

$$y_{s,ai} = A_{s,ai} \cosh[k_{s,ai}(x-d_{i-1})] + B_{s,ai} \sinh[k_{s,ai}(x-d_{i-1})] \ .$$

It is convenient to calculate the propagation constants and the field distributions for the perturbed modes at the input end ($z = 0$). To obtain an initial field $y_{ai}$, the initial value of $n_i^2$ is evaluated from

$$n_i^2 = n_o^2 + \alpha (y_{si} + A_{ai})^2_{avg} \ , \qquad (4\text{-}26)$$

where $(y_{si} + A_{ai})^2_{avg}$ is expressed as

$$\frac{1}{4\Delta_{si}}\Big[2(A_{si}^2 - B_{sl}^2)\Delta_{si} + (A_{si}^2 + B_{si}^2)\sinh 2\Delta_{si} + 2A_{si}B_{si}(\cosh 2\Delta_{si} - 1) + 4A_{ai}^2\Delta_{si} + 8A_{ai}(A_{si}\sinh\Delta_{si} + B_{si}(\cosh\Delta_{si} - 1))\Big] \ , \qquad (4\text{-}27)$$

and where $\Delta_{si} = k_{si}\Delta x$. The refractive index of the $i^{th}$ nonlinear layer can then be calculated from

$$n_i^2 = n_o^2 + \alpha (y_{si} + y_{ai})^2_{avg} \ , \qquad (4\text{-}28)$$

where

$$(y_{si} + y_{ai})^2_{avg} = \frac{1}{4\Delta_{si}}[2(A_{si}^2 - B_{si}^2)\Delta_{si} + (A_{si}^2 + B_{si}^2)\sinh 2\Delta_{si} + 2A_{si}B_{si}(\cosh 2\Delta_{si} - 1)] + \frac{1}{4\Delta_{ai}}[2(A_{ai}^2 - B_{ai}^2)\Delta_{ai} + (A_{ai}^2 + B_{ai}^2)\sinh 2\Delta_{ai} + 2A_{ai}B_{ai}(\cosh 2\Delta_{ai} - 1)] + A_{si}A_{ai}\left(\frac{\sinh\Delta_{s+a,i}}{\Delta_{s+a,i}} + \frac{\sinh\Delta_{s-a,i}}{\Delta_{s-a,i}}\right) + A_{si}B_{ai}\left(\frac{\cosh\Delta_{s+a,i} - 1}{\Delta_{s+a,i}} - \frac{\cosh\Delta_{s-a,i} - 1}{\Delta_{s-a,i}}\right) + B_{si}A_{ai}\left(\frac{\cosh\Delta_{s+a,i} - 1}{\Delta_{s+a,i}} + \frac{\cosh\Delta_{s-a,i} - 1}{\Delta_{s-a,i}}\right) + B_{si}B_{ai}\left(\frac{\sinh\Delta_{s+a,i}}{\Delta_{s+a,i}} - \frac{\sinh\Delta_{s-a,i}}{\Delta_{s-a,i}}\right), \quad (4\text{-}29)$$

and where $\Delta_{s+a,i} = (k_{si} + k_{ai})\Delta x$ and $\Delta_{s-a,i} = (k_{si} - k_{ai})\Delta x$. The initial values of the propagation constant and the field profile for the independent symmetric mode ($y_{si}$), as previously determined, are then substituted into equation (4-25), from which calculations the results for the perturbed antisymmetric mode ($y_{ai}$) are substituted into equation (4-24) to obtain the propagation constant and the field distribution for the perturbed symmetric mode.

The procedure described above is subject to reiteration until the propagation constants for both modes converge. While the power of the perturbed symmetric mode is maintained during these iterations, because all the power is initially excited into a single waveguide, it is necessary to determine an antisymmetric mode with the ability to cancel a symmetric mode across one-half of the coupler cross section. The propagation constants for the perturbed

modes are calculated sequentially in terms of input power by increasing the power in small steps, modifying the modes to the end that the total power distribution at the input plane is in conformance with input excitation.

To consider saturation effects, a two-level saturation model is used, where $\alpha(E^2)_{avg}$ is replaced by

$$n^2 = n_o^2 + \frac{\epsilon_{sat}\,\alpha(E^2)_{avg}}{\epsilon_{sat} \pm \alpha(E^2)_{avg}} , \qquad (4\text{-}30)$$

and where + and - correspond to, respectively, self-focusing and self-defocusing media. The dielectric function is Kerr-like for low intensities, and for high intensities reaches the maximum or the minimum $n_o^2 \pm \varepsilon_{sat}$.

## 4.4 Concluding Remarks

In this chapter, the matrix method was extended to obtain the power-dependent switching characteristics for nonlinear two-waveguide directional couplers, based upon the assumption that nonlinear couplers may be characterized by combinations of the two perturbed modes. In addition, a two-level system model was incorporated with the extended matrix methods for consideration of the saturation effects.

The proposed method can be applied to NLDCs with non-Kerr-like coupling media, the refractive indices of which reflect arbitrary dependence upon electrical field amplitudes. The numerical calculations for the unperturbed and

perturbed modes for symmetric two-waveguide and three-waveguide couplers are described in Chapter 5.

# CHAPTER 5

# NUMERICAL RESULTS ON NONLINEAR DIRECTIONAL COUPLERS

## 5.1 Introduction

The matrix method for the analysis of nonlinear directional couplers described in chapter four is used to analyze nonlinear two-waveguide and three-waveguide couplers. The method represents an extension of the original matrix method and the method is based on an iterative averaging algorithm which calculates the average values of the dielectric constant and the field amplitude in each stratified nonlinear layer. The numerical results for a multiple quantum well two-waveguide coupler are compared with published experimental data.

## 5.2 A Multiple Quantum Well Directional Coupler

A system to be considered first is a structure of two waveguides coupled through a multiple quantum well (MQW) medium as depicted in Fig. 5-1. Only guided TE modes and homogeneous and lossless materials are considered here. The parameters for the GaAs-based MQW directional coupler are $n_1 = n_5 = 3.4576$, $n_2 = n_4 = 3.5336$, $n_{nl} = -1.88 \times 10^{-8}$ $m^2/W$,

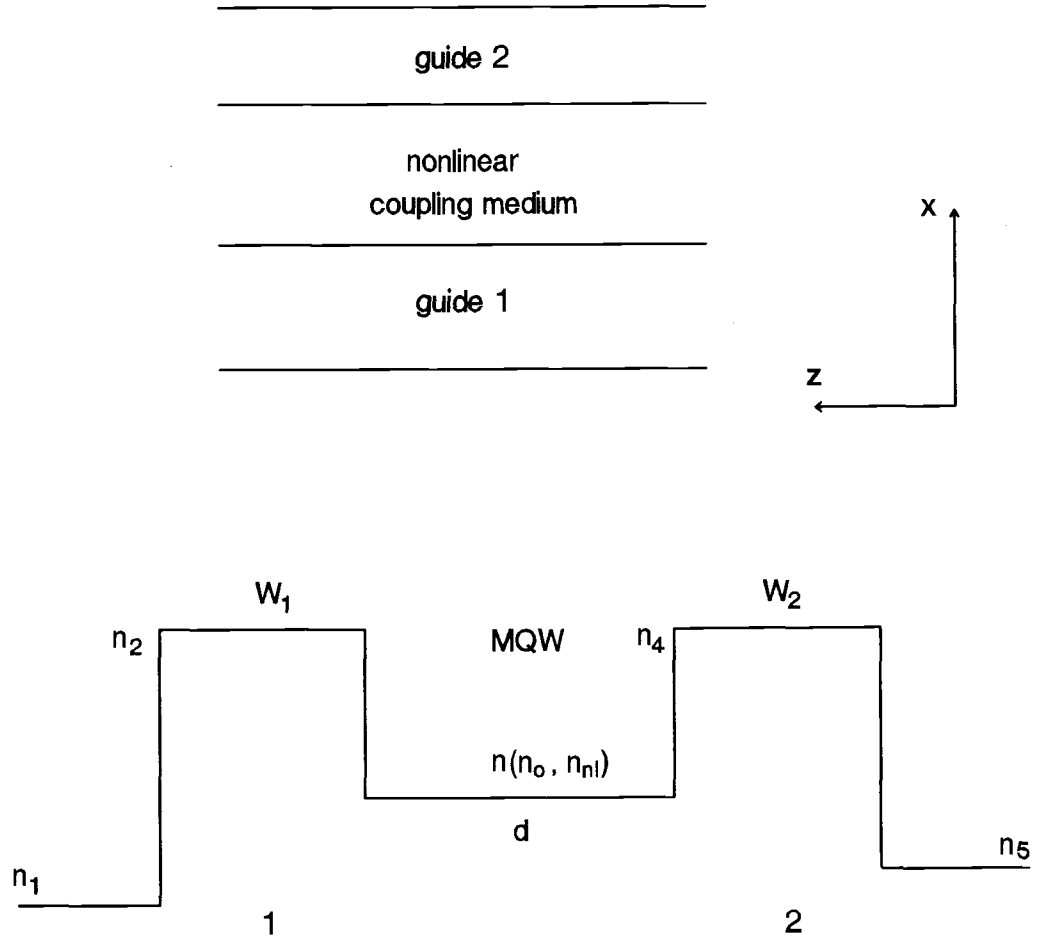


Fig. 5-1. A structure of a nonlinear two-waveguide directional coupler with a multiple quantum well (self-defocusing) coupling medium.

$W_1 = W_2 = 0.8\ \mu m$, $d = 1.2\ \mu m$, and $\lambda = 811.8$ nm. $n_o$ is taken as 3.48445 to yield a linear coupling length $Lc \approx 2.0$ mm.

Accuracy of numerical results obtained from the matrix method for a nonlinear coupler depends on the calculated value of the refractive index in each stratified nonlinear layer. From chapter four, the choices are

$$n_i^2 = n_o^2 + \alpha(A_{i-1}^2) \tag{5-1}$$

$$n_i^2 = n_o^2 + \alpha(A_i^2) \tag{5-2}$$

$$n_i^2 = n_o^2 + \alpha(E_i^2)_{avg}. \tag{5-3}$$

Eq. (5-1) has been used in the original matrix method to calculate the refractive index of nonlinear media. The equation cannot be utilized for a bounded nonlinear medium, since the refractive index of the first thin nonlinear layer is expressed in terms of the field amplitude in a linear region (see Fig. 4-2(b)). Using eq. (5-1) leads to inaccurate power dependent dispersion characteristics as shown in Fig. 5-2(a). In eq. (5-2), the refractive index of the $i^{th}$ layer is expressed in terms of its own amplitude at the boundary, since $A_i$ is already known from the boundary conditions. However, using eq. (5-2) yields a nonsymmetrical refractive index profile throughout the nonlinear region and therefore gives an asymmetric-like dispersion diagram for this symmetric coupler. The results obtained by using eq. (5-2) are shown in Fig. 5-2(b).

Using eq. (5-3) with calculations of $(E_i^2)_{avg}$ in an iterative manner generates a symmetric refractive index

distribution throughout the nonlinear medium and yields an accurate power dependent dispersion curve. There is excellent agreement between the exact analysis and the extended matrix method for the unperturbed modes as shown in Fig. 5-3(a). Cutoff for antisymmetric modes or asymmetric modes has not occurred yet in the range of input power as scaled in the figure and may appear at higher input powers. Typical field distributions for unperturbed symmetric modes, anti-symmetric modes, and asymmetric modes are shown in Fig. 5-3(b). The asymmetric modes disappear when saturation effect is taken into account and the dielectric constant change of 0.031 is allowed (see Fig. 5-3(a)). The dielectric constant changes with saturation and without saturation are shown in Fig. 5-4(a). The dielectric function is Kerr-like for low intensities and converges to a saturation level as the intensity increases. The power dependent switching characteristics of the coupler at guide length of $L = 2.73 \times L_c$ with saturation effects incorporated are shown in Fig. 5-4(b) and there is good agreement between the numerical results and the experimental data [66] for the same structure. A quasi-linear coupling behavior is expected at higher input intensities as the refractive index and the effective index (normalized propagation constant) saturate. The numerical results suggest that saturation effects must be considered in the analysis and design of the nonlinear waveguides.

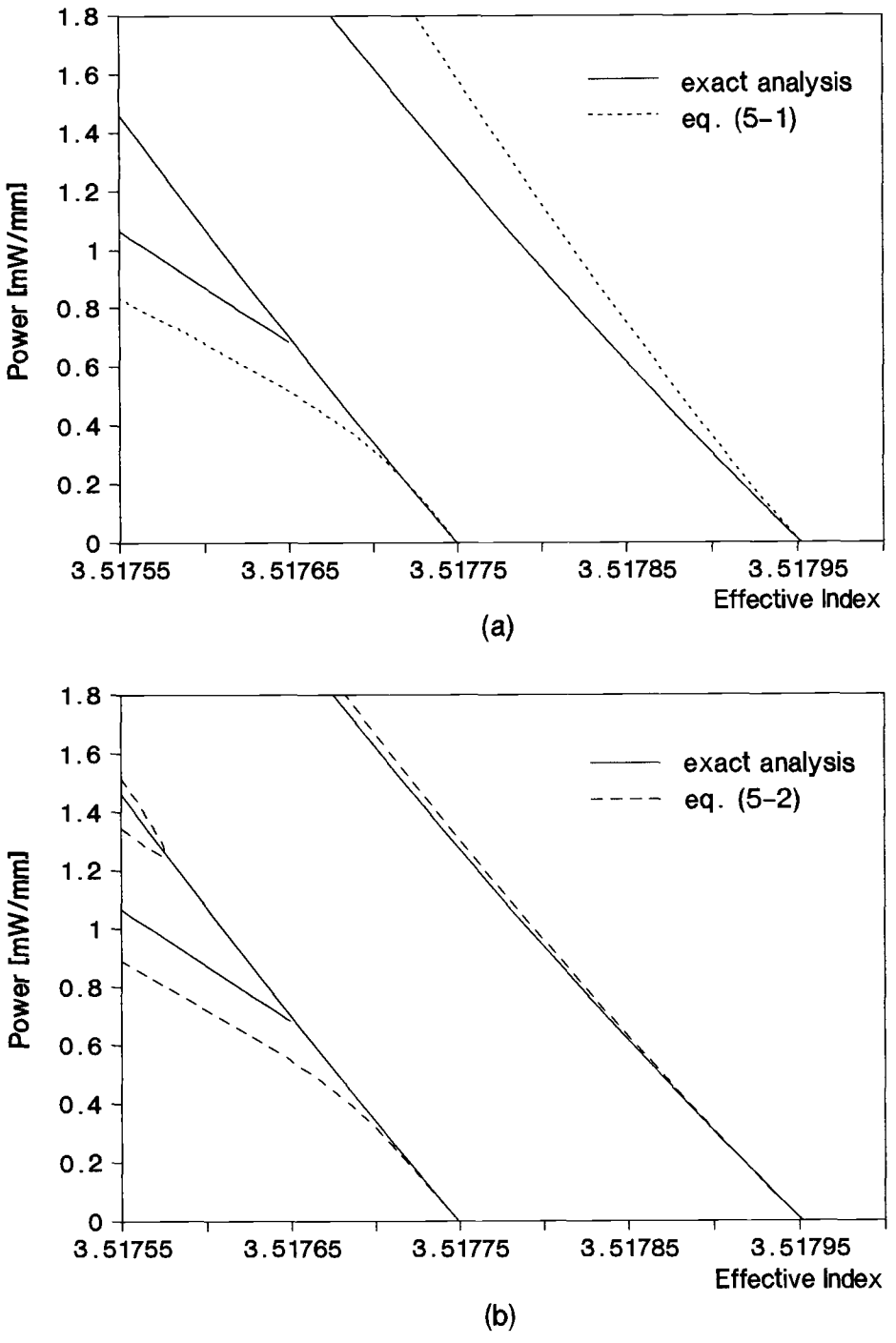


Fig. 5-2. Comparison of power dependent dispersion diagrams of unperturbed modes calculated from exact method and results (a) using original matrix method (dotted lines) and (b) using field amplitudes at each boundary (dashed lines).

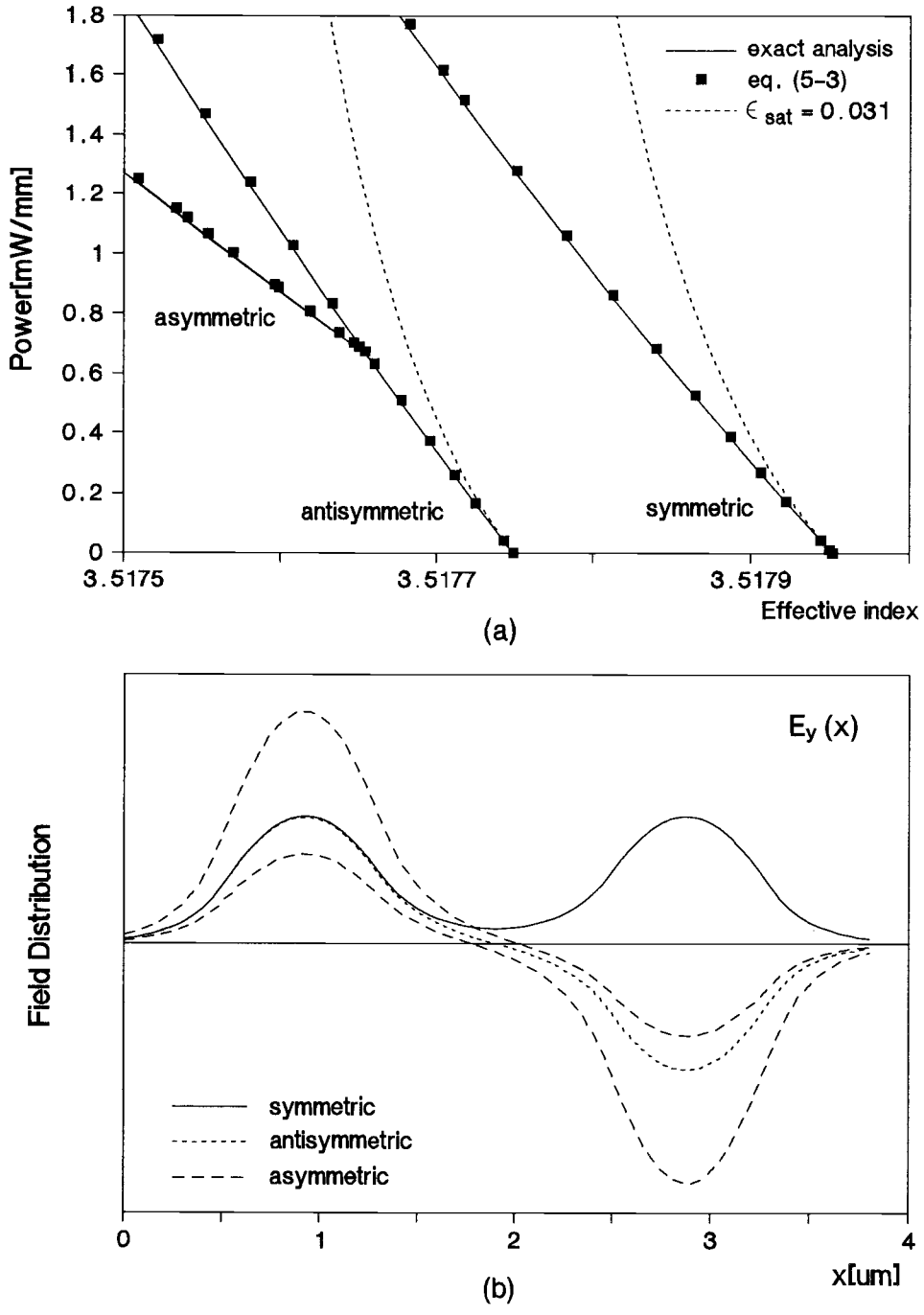


Fig. 5-3. (a) Power dependent dispersion characteristics of unperturbed modes obtained from exact analysis (solid lines) and extended matrix method (rectangles and dotted lines). (b) Typical field distributions of symmetric, antisymmetric, and asymmetric modes.

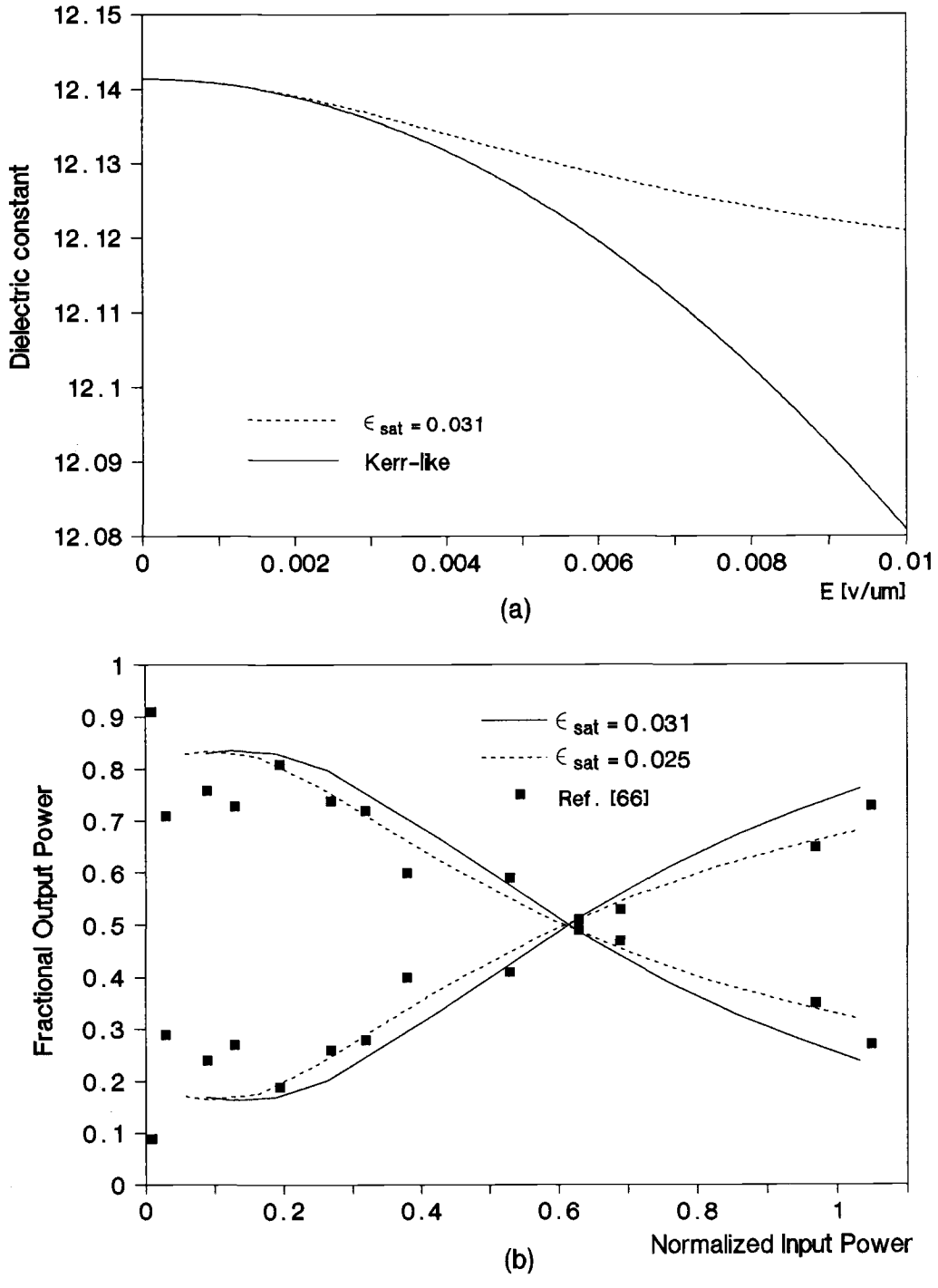


Fig. 5-4. (a) Variations of dielectric constants of a Kerr-like medium and a saturable medium. (b) Normalized ouptut power distributions obtained from matrix method with saturation effect ( ■ - experimental data [66]).

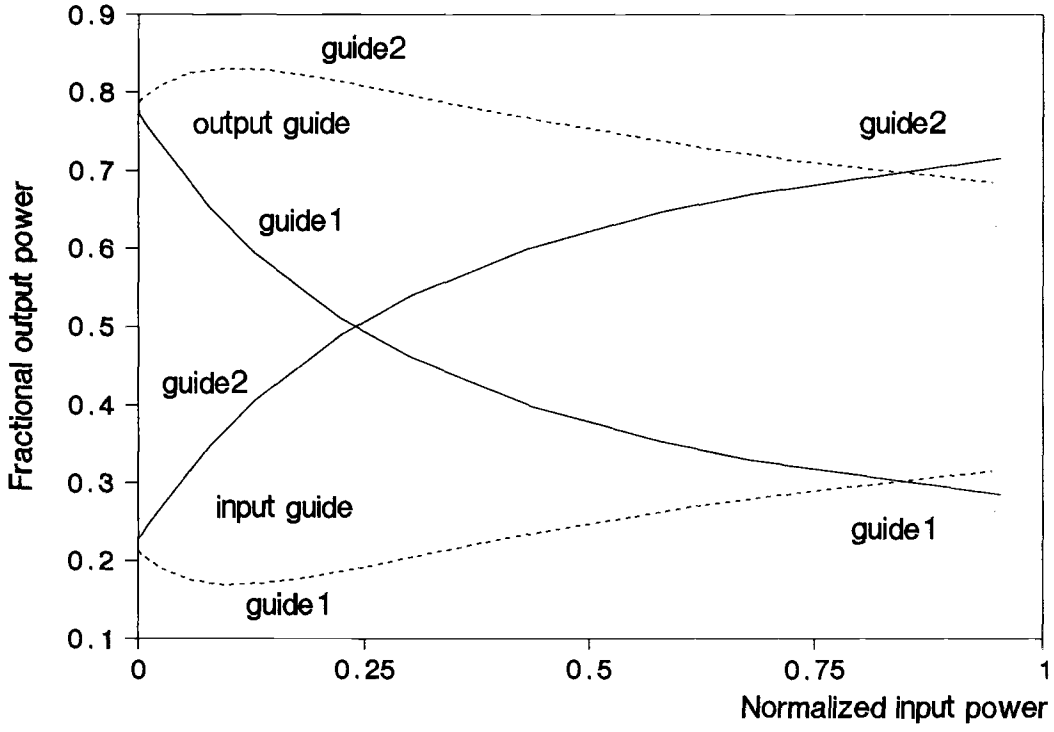


Fig. 5-5. Fractional output power vs. normalized input power for an asymmetric NLDC with $\epsilon_{sat}$ = 0.031 at guide length of 0.8 x $L_c$. Solid lines and dotted lines indicate fractional output power for input to guide 2 and input to guide 1, respectively.

Fractional output power of a nonsymmetric coupler ($n_1$ = 3.4576 and $n_5$ = 3.455) is shown in Fig. 5-5. Output power distribution is more sensitive to input power when the power is launched into guide 2, as compared to the case when the power is launched into guide 1. Excitation of either of the two waveguide results in over 70 % of input power remaining in guide 2 at guide length of 0.8 x $L_c$ for a normalized input power of about 0.85.

## 5.3 A Nonlinear Waveguide Bounded by Two Nonlinear Media

As shown in Fig. 5-6, a system to be analyzed is a symmetric two-waveguide nonlinear directional coupler with two outside self-focusing nonlinear layers. The parameters used are $n_1 = n_3 = 1.55$, $n_2 = 1{,}57$, $d = 2\ \mu m$, $W = \lambda = 1\ \mu m$, and $\alpha = 10^{-11}\ m^2/V^2$. Analytic solutions of nonlinear wave equations can be obtained since the nonlinear media are semi-infinite. For TE modes, electric fields are given by

$$E_y(x) = \begin{cases} \pm\sqrt{\dfrac{2}{\alpha}}\ \dfrac{\gamma_1 C}{\omega}\ sech\gamma_1(x + x_1 - W) & reg.(5) \\ A\cos\gamma_2 x + B\sin\gamma_2 x & reg.(4) \\ A\cosh\gamma_3 x + \dfrac{\gamma_2}{\gamma_3} B\sinh\gamma_3 x & reg.(3) \\ C\cos\gamma_2(x + d) + D\sin\gamma_2(x + d) & reg.(2) \\ \sqrt{\dfrac{2}{\alpha}}\ \dfrac{\gamma_1 C}{\omega}\ sech\gamma_1(x + x_2 + W + d) & reg.(1) \end{cases} \qquad (5\text{-}4)$$

where $\gamma_i^2 = k_o^2(\beta^2 - n_i^2)$ for i = 1, 3 and $\gamma_2^2 = k_o^2(n_2^2 - \beta^2)$.

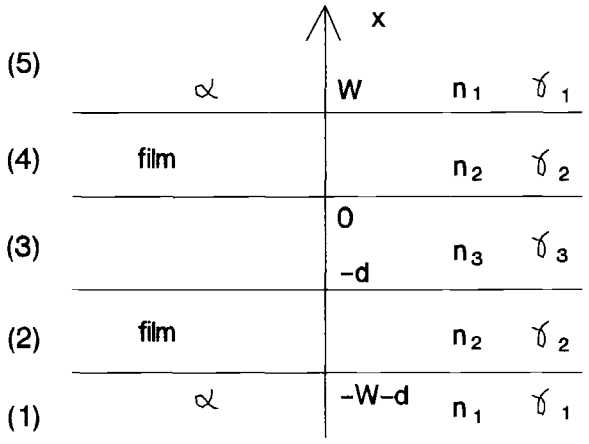


Fig. 5-6. A symmetric two-waveguide coupler with two outside nonlinear media.

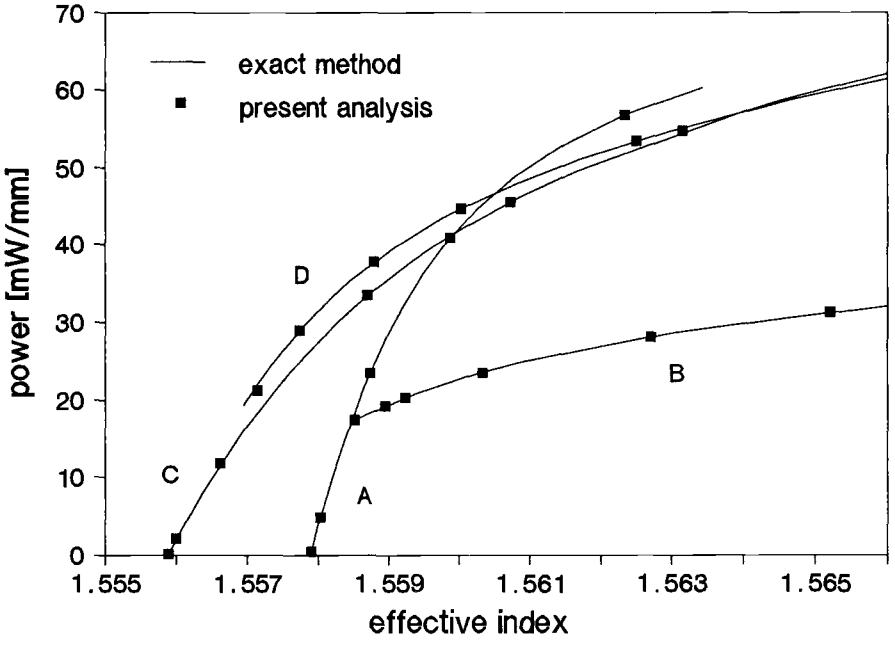


Fig. 5-7. Power dependent dispersion diagram of symmetric (branches A and B) and antisymmetric (branches C and D) modes.

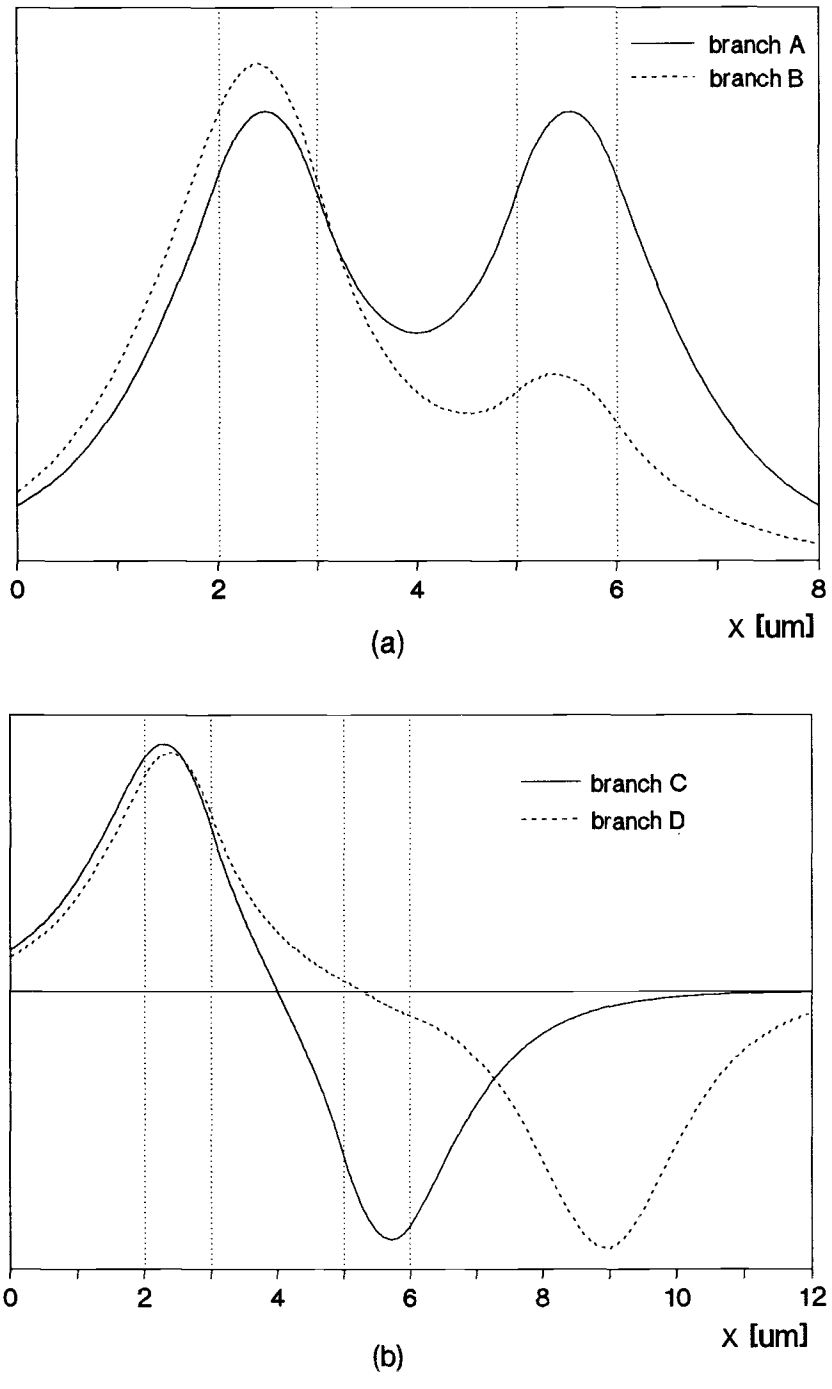


Fig. 5-8. (a) Typical field distributions of symmetric modes (branches A and B) and (b) antisymmetric modes (branches C and D).

In eq. (5-4), signs + and - indicate symmetric and antisymmetric modes, respectively. Applying appropriate boundary conditions yields two simultaneous eigenvalue equations:

$$\tan\gamma_2 W = \frac{1}{D}\left(C - \sqrt{\frac{2}{\alpha}}\,\frac{\gamma_1 C}{\omega}\,\frac{sech\gamma_1 x_2}{\cos\gamma_2 W}\right) \tag{5-5a}$$

$$\tan\gamma_2 W = -\frac{1}{C}\left(D + \sqrt{\frac{2}{\alpha}}\,\frac{\gamma_1^2 C}{\gamma_2\omega}\,\frac{sech\gamma_1 x_2\,\tanh\gamma_1 x_2}{\cos\gamma_2 W}\right) \tag{5-5b}$$

where

$$\begin{aligned} C &= A\cosh\gamma_3 d - \frac{\gamma_2}{\gamma_3} B\sinh\gamma_3 d \\ D &= B\cosh\gamma_3 d - \frac{\gamma_3}{\gamma_2} A\sinh\gamma_3 d \end{aligned} \tag{5-6}$$

and where

$$\begin{aligned} A &= \pm\sqrt{\frac{2}{\alpha}}\,\frac{\gamma_1 C}{\gamma_2\omega}\,sech\gamma_1 x_1\left(\gamma_2\cos\gamma_2 W + \gamma_1\sin\gamma_2 W\,\tanh\gamma_1 x_1\right) \\ B &= \pm\sqrt{\frac{2}{\alpha}}\,\frac{\gamma_1 C}{\gamma_2\omega}\,sech\gamma_1 x_1\left(\gamma_2\sin\gamma_2 W - \gamma_1\cos\gamma_2 W\,\tanh\gamma_1 x_1\right) \end{aligned} \tag{5-7}$$

Signs + and - indicate symmetric and antisymmetric modes. $x_1$ and $x_2$ are integration constants. In eqs. (5-5), we have two equations and three unknowns ($\beta$, $x_1$, and $x_2$). $\beta$ and $x_2$ can be calculated from the two eigenvalue equations for a given value of $x_1$. Power dependent dispersion characteristics of nonlinear guided modes are shown in Fig. 5-7 and the results of the matrix method are in excellent agreement

with those of the exact analysis. The results can also be compared with ref. [89]. Thus, the extended matrix method can lead to very accurate results for unperturbed modes. Symmetric mode solutions form a symmetric branch A and an asymmetric branch B (see Fig. 5-8(a)), while antisymmetric mode solutions generate an antisymmetric branch C and an asymmetric branch D as shown in Fig. 5-8(b). Branch D exhibits a field profile which has a soliton-like peak [89] in a nonlinear layer outside a guiding film.

## 5.4 A Nonlinear Three-Waveguide Directional Coupler

A structure to be analyzed is a three-waveguide coupler which consists of three identical waveguides with two self-defocusing nonlinear coupling media as shown in Fig. 5-9(a). The parameters are $n_1 = 3.48445$, $n_2 = 3.5336$, $n_o = 3.48445$, $n_{nl} = -1.88 \times 10^{-8}$ $m^2/W$, $W = 0.8$ $\mu m$, $d = 1.2$ $\mu m$, and $\lambda = 811.8$ nm. The extended matrix method yields power dependent dispersion characteristics of unperturbed modes, as depicted in Fig. 5-9(b), for the three-waveguide structure. There exist well-balanced modes (branches A, B, and C) and two asymmetric modes (branches $A_1$ and $C_1$) for Kerr-like media. These two asymmetric modes disappear for saturable media and the propagation constants of A, B, and C mode tend to saturate at high powers. Typical field profiles of unperturbed modes are shown in Fig. 5-9(c) and (d).

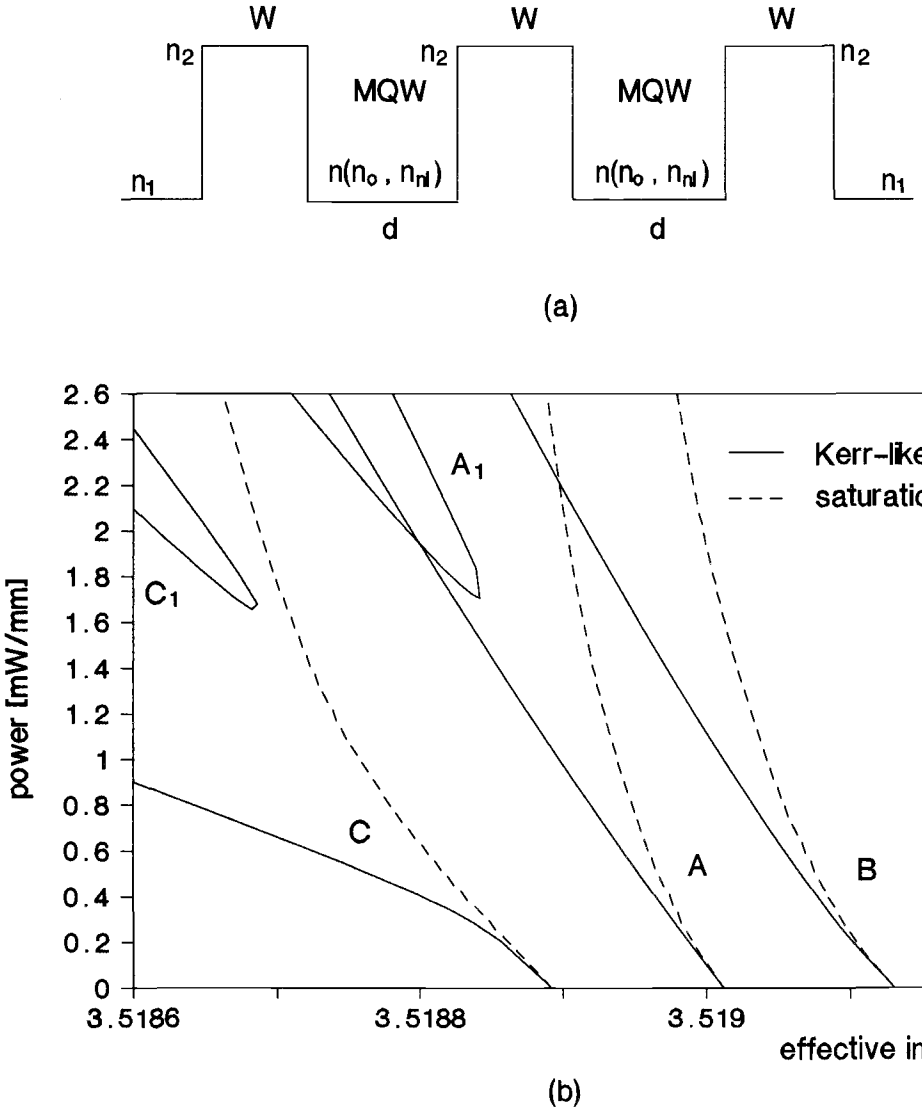


Fig. 5-9. (a) A symmetric three-waveguide coupler which consists of two MQW coupling media. (b) Power dependent dispersion diagram of unperturbed modes.

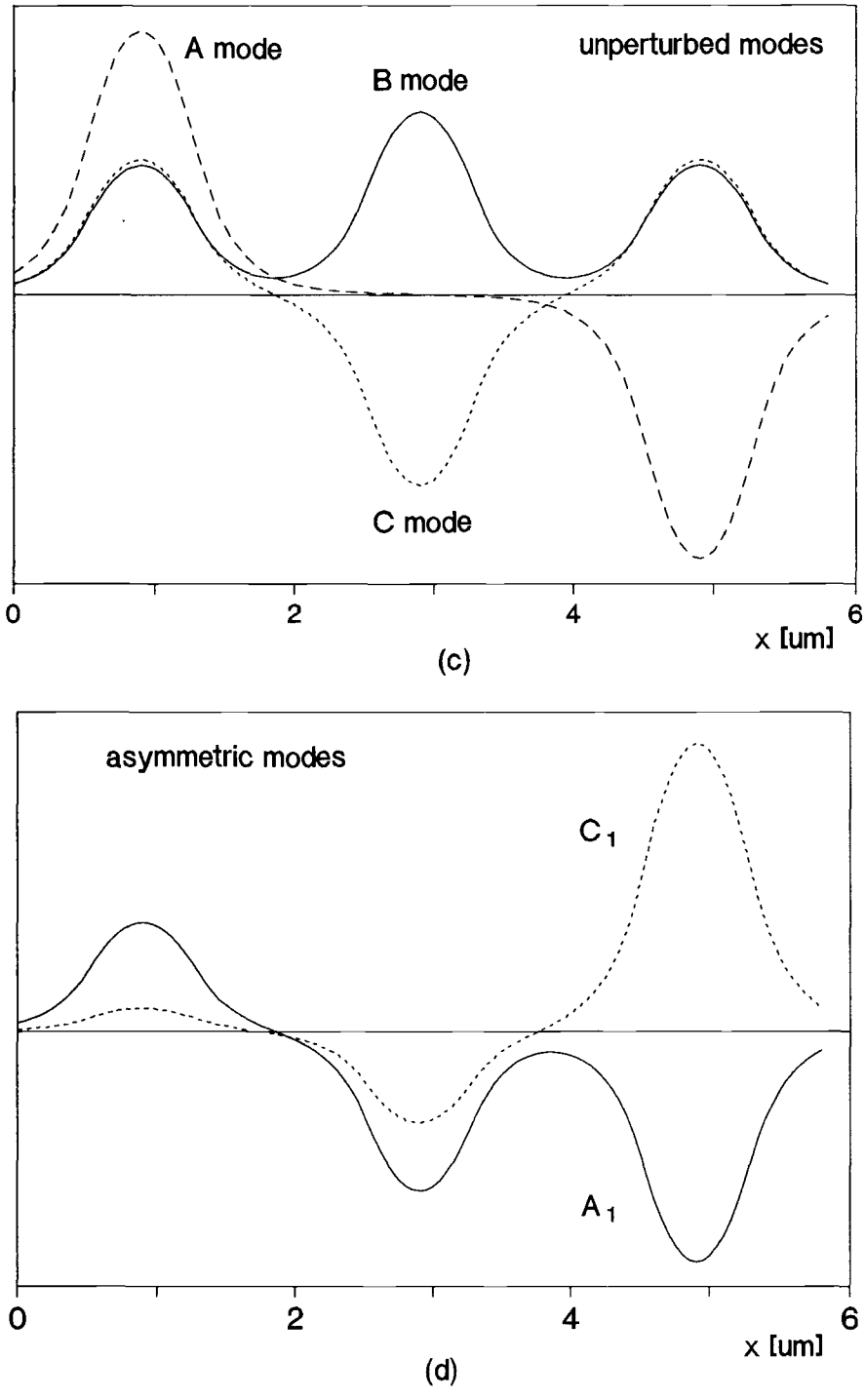


Fig. 5-9. Field distributions of (c) symmetric modes (branches B and C) and an antisymmetric mode (branch A) and (d) asymmetric modes (branches $A_1$ and $C_1$).

Power dependent switching behavior can be explained by the combination of perturbed modes as described in section 4-3. In this section, to calculate perturbed modes, we consider saturation effects only. All the calculations are based on an assumption that only the small change of the refractive index of the nonlinear medium is allowed. The number of modes involved in this calculation depends upon input conditions. Therefore, different switching characteristics are expected for different input conditions.

### 5.4.1 Center Waveguide Excitation

At low power, the extended matrix method gives the values effective indices $\beta_A$ = 3.5190121, $\beta_B$ = 3.5191300, and $\beta_C$ = 3.5188916. When the center waveguide is excited, as in the case of linear three-waveguide couplers, only B mode and C mode are superposed so that the total field at z = 0 conforms the input condition. A linear coupling length $L_c$ is calculated from $\pi/k_o(\beta_B - \beta_C)$ and $L_c \approx 1.703$ mm. Procedure for calculating perturbed modes are same as the one described in section 4.3. Typical field distributions of B and C modes are shown in Fig. 5-10(a) with the maximum dielectric constant change of 0.031 for saturable media. Fig. 5-10(b) shows that how fast the propagation constants of the modes converge. Fractional output power distributions at $L = L_c$ and $L = 2.8 \times L_c$ are shown in Fig. 5-10(c). Since saturation of refractive index and effective index and

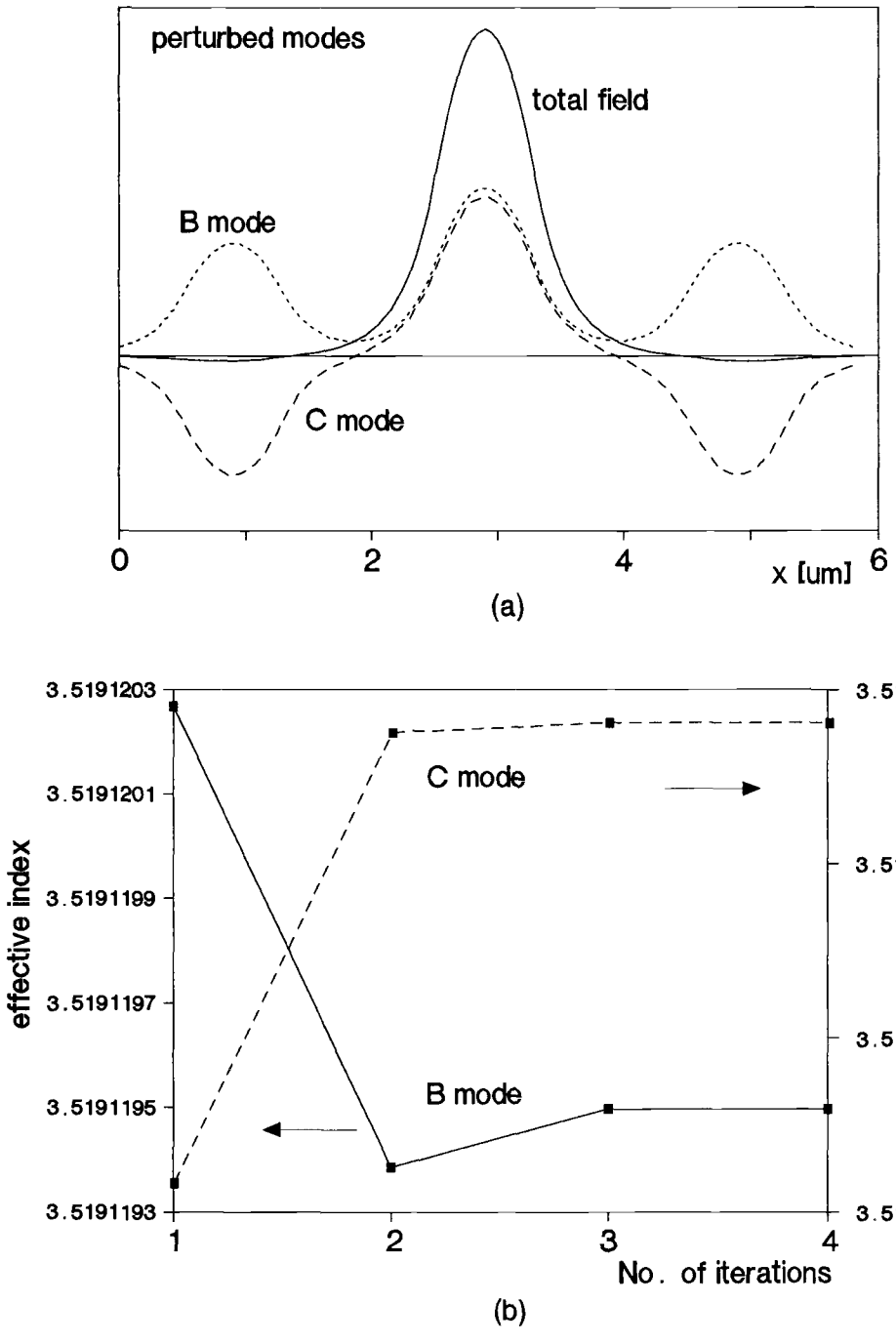


Fig. 5-10. (a) Field distributions of perturbed B mode, C mode, and the total field which conforms center guide input. (b) Convergence scheme of effective indices for perturbed B and C modes vs. No. of iterations.

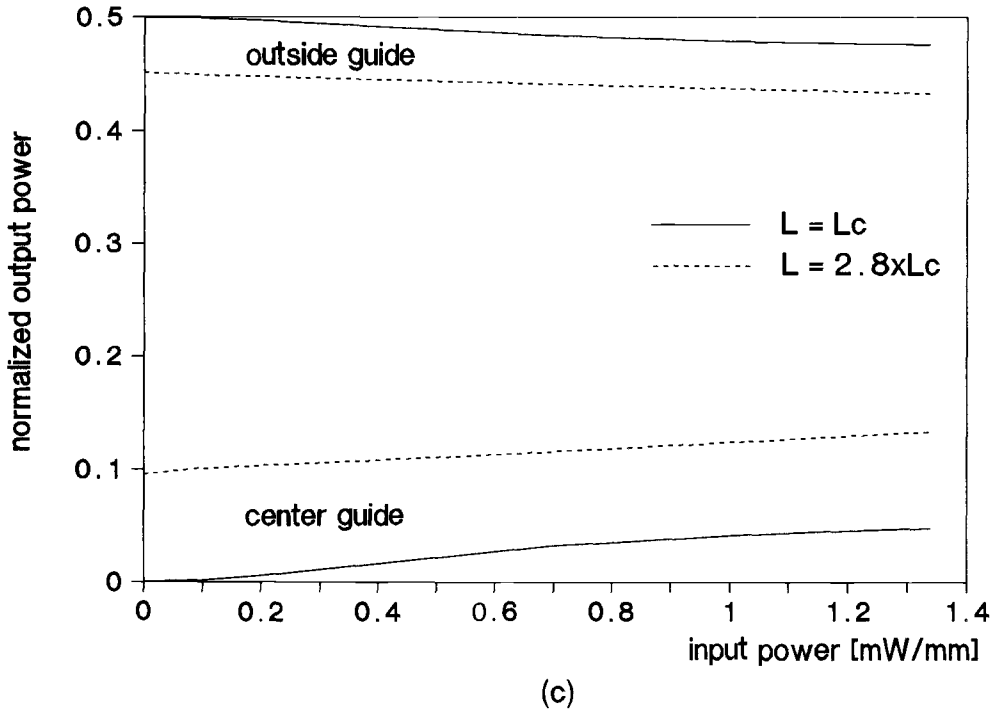


Fig. 5-10. (c) Normalized output power distributions of the coupler at two differnt guide lengths for the case of excitation of the center guide.

the ability of C mode to cancel the field of B mode in outer waveguide regions prevent switching from being strongly power dependent, switching characteristics is weakly power dependent or quasi-linear.

### 5.4.2 Excitation of An Outside Waveguide

With saturation effects considered, all three modes are involved when an outside guide is excited (asymmetrical excitation). Procedure for finding the three perturbed modes which can satisfy the input condition are illustrated in Appendix C. The perturbed modes become asymmetric in the presence of other modes, because the amplitude of A mode is additive in calculation of the refractive index of a nonlinear coupling medium and subtractive in the other coupling medium. These perturbed modes are shown in Fig. 5-11(a). Power dependent switching characteristics of the nonlinear directional coupler with asymmetrical excitation for guide length $L = L_c$ and $L = 2.8 \times L_c$ are shown in Fig. 5-11(b) and (c). Coupling length is power dependent and also saturates as the power increases. $L_c$ is a linear coupling length calculated for the central guide excitation. $P_1$, $P_2$, and $P_3$ denote the fractional output power emerging from the outside guide (input guide), the central guide, and the other outside guide, respectively. Output power distributions can be varied for waveguides with different guide length.

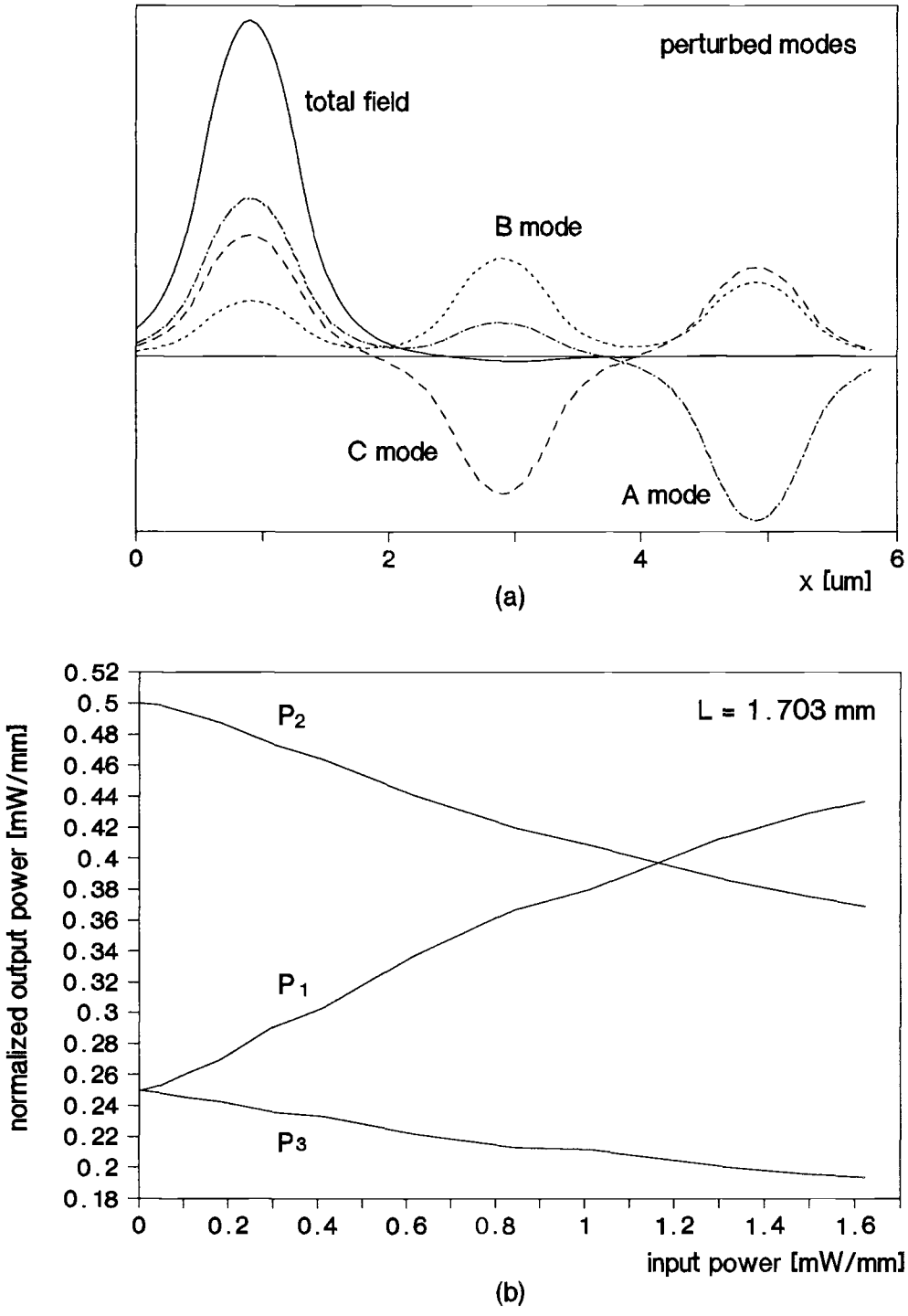


Fig. 5-11. (a) Field distributions of perturbed modes and the total field which conform the outside guide input. (b) Power dependent switching characteristics of the coupler at guide length $L = L_c$ for excitation of an outer guide.

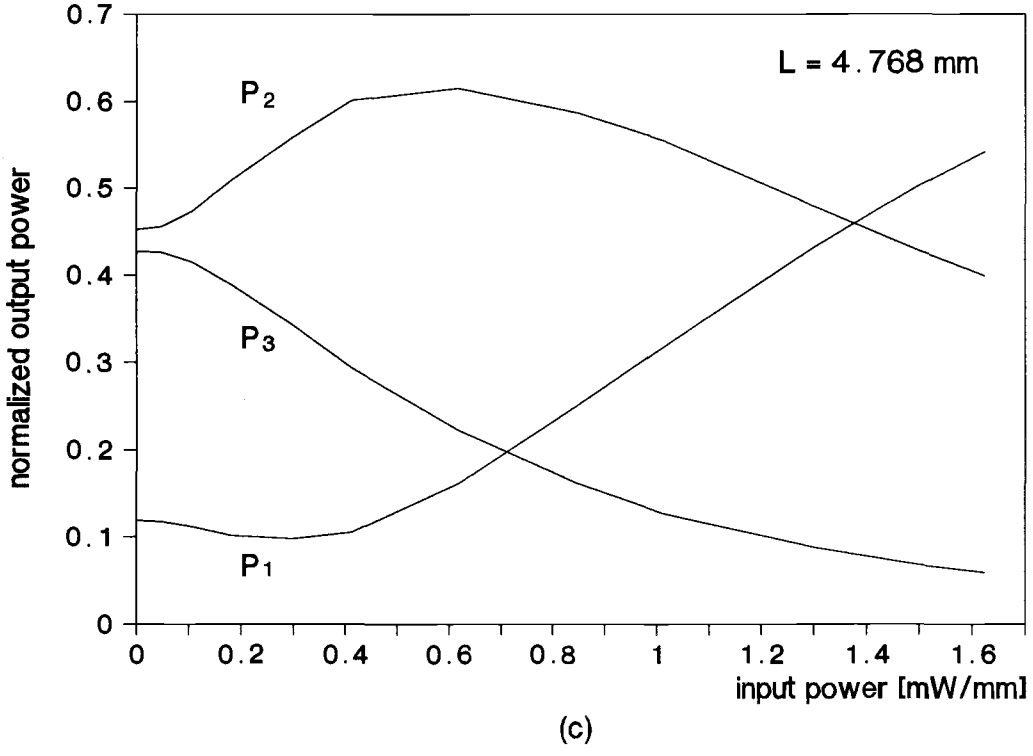


Fig. 5-11. (c) Power dependent switching characteristics of the coupler at guide length L = 2.8 x $L_c$ for the asymmetric excitation.

## 5.5 Concluding Remarks

Power dependent switching characteristics of a two-waveguide coupler with a multiple quantum well medium obtained from the extended matrix method with saturation effects considered has shown to be in agreement with published experimental data. Power dependent dispersion characteristics of unperturbed modes for a two-waveguide coupler with two semi-infinite self-focusing nonlinear media has been compared with analytical solutions. The numerical results has also shown that most of power remains in one waveguide for an asymmetric two-waveguide coupler regardless of input conditions at high input powers and that for identical three-waveguide couplers with two multiple quantum well coupling media, switching characteristics are dependent on input conditions. Steps for finding perturbed modes of a nonlinear three-waveguide coupler are described in Appendix C.

# CHAPTER 6

# CONCLUSIONS AND SUGGESTIONS FOR FUTURE WORK

## 6.1 Conclusions

Closed form expressions for multiport network functions, such as impedance matrix parameters and scattering parameters, of multiple coupled optical waveguides have been derived in terms of normal mode parameters of the coupled systems. The procedures for the evaluation of these normal mode parameters have also been presented. This normal mode analysis has been used to study the propagation characteristics of general two-waveguide and symmetric three-waveguide couplers for both sets of TE and TM modes. For matched systems, the numerical results of the normal mode analysis are, as expected, in good agreement with those obtained by the coupled mode theory.

The method presented in the thesis, however, is applicable for arbitrary terminations and is readily applied to the case of multiple coupled waveguides. For lower order systems with two or three individual waveguides, the expressions for impedance matrix parameters and scattering parameters are found in a convenient closed form leading to efficient CAD compatible models. The

method can be applied to investigate structure terminations often encountered in interconnecting optical components since the formulation is quite general and can be applied to numerous guided wave structures including optical waveguides and microwave components.

The conventional matrix method, which has been designed to study three-layer nonlinear waveguides, has been modified to analyze five-layer nonlinear waveguides with Kerr-like nonlinear coupling media. A two-level saturation model has been incorporated with the matrix method to consider the saturation effects of nonlinear media. The numerical results obtained for a multiple quantum well two-waveguide coupler are seen to be in agreement with the published experimental data. The matrix method has also been applied to a three-waveguide coupler with multiple quantum well coupling media and the results indicate that the six port optical device exhibits nonlinear switching behavior when an outside guide is excited and a quasi-linear switching behavior when the center guide is excited.

The nonlinear directional couplers can be used as fast all-optical switches and all-optical logic gates which perform logic functions such as AND and XOR. The matrix method can be applied to analyze couplers with non-Kerr-like nonlinear media.

## 6.2 Suggestions for Future Work

There are a few areas which should be investigated for development and improvement of the analyses of multiple coupled linear and nonlinear waveguides. Some suggestions for future study are summarized in the following paragraphs.

Analyses and design procedures for multiport components which consist of more than three individual waveguides can be devised for possible applications in multiple optical components including optical interconnects. The normal mode analysis can be extended to investigate lossy and graded index linear coupled waveguides and three-dimensional structures consisting of multiple coupled waveguides having finite rectangular crosssection.

The matrix method should also be extended to analyze the nonlinear couplers with lossy and saturable coupling media. Experimental work to characterize the refractive index of useful nonlinear media including saturation effect is warranted, since only few measurements of the optical properties are available. Experimental work including fabrication and testing of two-waveguide and three-waveguide couplers with multiple quantum well coupling media must be undertaken so that the accuracy and the

validity range of the matrix method can be checked and the optical circuits can be physically realized.

# REFERENCES


[1] Zh. I. Alferov, V. M. Andreev, E. L. Portnoi, and M. K. Trukan, "AlAs-GaAs Heterojunction Injection Lasers with a Low Room-Temperature Threshold," *Sov. Phys. - Semicond.*, vol. 3, No. 9, pp. 1107-1110, Mar., 1970.

[2] M. B. Panish, I. Hayashi, and S. Sumski, "Double-Heterostructure Injection Lasers with Room Temperature Thresholds as Low as 2300 A/cm$^2$," *Appl. Phys. Lett.*, Vol. 16, No. 8, pp. 326-327, Apr., 1970.

[3] I. Hayashi, M. B. Panish, P.W. Foy, and S. Sumski, "Junction Lasers which Operate Continuously at Room Temperature," *Appl. Phys. Lett.*, vol. 17, No. 3, pp.109-111, Aug., 1970.

[4] F. P. Kapron, D. B. Keck, and R. D. Maurer, "Radiation Losses in Glass Optical Waveguides," *Appl. Phys. Lett.*, vol. 17, No. 10, pp. 423-425, Nov., 1970.

[5] D. N. Payne and W. A. Gambling, "Zero Material Dispersion in Optical Fibers," *Electron. Lett.*, vol. 11, No. 8, pp. 176-178, Apr., 1975.

[6] M. Horiguchi, "Spectral Losses of Low-OH-Content Optical Fibers," *Electron. Lett.*, vol. 12, No. 12, pp. 310-312, Jun., 1976.

[7] T. Miya, Y. Terunuma, T. Hosaka, and T. Miyashita, "Ultimate Low-Loss Single-Mode Fibre at 1.55 $\mu$m," *Electron. Lett.*, vol. 15, No. 4, pp. 106-108, Feb., 1979.

[8] J. J. Hsieh, "Room-Temperature Operation of GaInAsP/InP Double-Heterostructure Diode Lasers Emitting at 1.1 $\mu$m," *Appl. Phys. Lett.*, vol. 28, No. 5, pp. 283-285, Mar., 1976.

[9] K. Oe, K. Sugiyama, "GaInAsP-InP Double Hetero-structure Lasers Prepared by a New LPE Apparatus," *Japan. J. Appl. Phys.*, vol. 15, pp. 2003-2004, Oct., 1976.

[10] Y. Itaya, Y. Suematsu, and K. Iga, "Carrier Lifetime Measurement of GaInAsP/InP Double-Heterostructure Lasers," *Japan. J. Appl. Phys.*, vol. 16, pp. 1057-1058, 1977.

[11] T. Yamamoto, K. Sakai, S. Akiba, and Y. Suematsu, "$In_{1-x}Ga_xAs_yP_{1-y}$ DH Lasers Fabricated on InP (100) Substrate," *IEEE J. Quantum Electron.*, vol. QE-14, No. 2, pp. 95-98, Feb., 1978.

[12] B. I. Miller, J. H. McFee, R. J. Martin, and P. K. Tien, "Room-Temperature Operation of Lattice-Matched InP/$Ga_{0.47}In_{0.53}As$/InP Double-Heterostructure Lasers Grown by MBE," *Appl. Phys. Lett.*, vol. 33, pp. 44-47, 1978.

[13] S. Arai, Y. Itaya, Y. Suematsu, K. Kishino, and S. Katayama, "Conditions of LPE Growth for Lattice Matched GaInAsP/InP DH Lasers with (100) Substrate in the Range of 1.2-1.5 $\mu$m," *Japan. J. Appl. Phys.*, vol. 17, pp. 2067-2068, 1978.

[14] A. Doi, T. Fukuzawa, M. Nakamura, R. Ito, and k. Aiki, "InGaAsP/InP Distributed-Feedback Injection Lasers Fabricated by One-Step Liquid Phase Epitaxy," *Appl. Phys. Lett.*, vol. 35, No. 6, pp. 441-443, Sep. 1979.

[15] K. Takahei, H. Hagai, and H. Kawaguchi, "Low Temperature Liquid Phase Epitaxy Growth for Room-Temperature CW Operation of 1.55 $\mu$m InGaAsP/InP Double Heterostructure Lasers," *Appl. Phys. Lett.*, vol. 36, No. 4, pp. 309-310, Feb., 1980.

[16] K. Utaka, K. Kobayashi, K. Kishino, and Y. Suematsu, "1.5-1.6 $\mu$m GaInAsP/InP Integrated Twin-Guide Lasers with First-Order Distributed Bragg Reflectors," *Electron. Lett.*, vol. 16, No. 12, pp. 455-456, Jun., 1980.

[17] O. Mikami, "1.55 $\mu$m GaInAsP/InP Distributed Feedback Lasers," *Japan. J. Appl. Phys.*, vol. 20, No. 7, pp. L488-L490, Jul., 1981.

[18] W. E. Martin, "A New Waveguide Switch/Modulator for Integrated Optics," *Appl. Phys. Lett.* vol. 26, No. 10, pp. 562-564, May, 1975.

[19] H. Kawaguchi, "GaAs Rib-Waveguide Directional Coupler Switch with Schottky Barriers," *Electron. Lett.*, vol. 14, No. 13, pp. 387-388, Jun., 1978.

[20] F. J. Leonberger, "High-Speed Operation of $LiNbO_3$ Electro-Optic Interferometric Waveguide Modulators," *Opt. Lett.*, vol. 5, No. 7, pp.312-314, Jul., 1980.

[21] R. C. Alferness, N. P. Economou, and L. L. Buhl, "Fast Compact Optical Waveguide Switch Modulator," *Appl. Phys. Lett.*, vol. 38, No. 15, Feb., 1981.

[22] J. P. Donnelly, N. L. DeMeo, G. A. Ferrante, K. B. Nichols, and F. J. O'Donnell, "Optical Guided-Wave Gallium Arsenide Monolithic Interferometer," *Appl. Phys. Lett.*, vol. 45, No. 4, pp. 360-362, Aug., 1984.

[23] H. Inoue, K. Hiruma, K. Ishida, H. Sato, and H. Matsumura, "Switching Characteristics of GaAs Directional Coupler Optical Switches," *Appl. Opt.*, vol. 25, No. 9, pp. 1484-1490, May, 1986.

[24] H. Takeuchi, K. Nagata, H. Kawaguchi, and K. Oe, "GaAs/ AlGaAs Directional Coupler Switch with Submillimetre Device Length," *Electron. Lett.*, vol. 22, No. 23, pp. 1241-1243, Nov., 1986.

[25] H. F. Taylor, "Frequency-Selective Coupling in Parallel Dielectric Waveguides," *Opt. Commun.*, vol. 8, No. 4, pp. 421-425, Aug., 1973.

[26] H. A. Haus and C. G. Fonstad, Jr., "Three-Waveguide Couplers for Improved Sampling and Filtering," *IEEE J. Quantum Electron.*, vol. QE-14, No. 12, pp. 2321-2325, Dec., 1981.

[27] R. C. Alferness and R. V. Schmidt. "Tunable Optical Waveguide Directional Coupler Filter," *Appl. Phys. Lett.* vol. 33, No. 2, pp. 161-163, Jul., 1978.

[28] J. R. Pierce, "Coupling of Modes of Propagation," *J. Appl. Phys.*, vol. 25, No. 2, pp. 179-183, 1954.

[29] S. E. Miller, "Coupled Wave Theory and Waveguide Applications," *Bell Syst. Tech. J.*, vol. 33, pp. 661-719, 1954.

[30] D. Marcuse, "The coupling of Degenerate Modes in Two Parallel Dielectric Waveguides," *Bell Syst. Tech. J.*, vol. 50, pp. 1791-1816, 1971.

[31] D. Marcuse, "Coupled Mode Theory of Round Optical Fibers," *Bell Syst. Tech. J.*, vol. 52, pp. 817-842, 1973.

[32] A. W. Snyder, "Coupled Mode Theory for Optical Fibers," *J. Opt. Soc. Amer.*, vol. 62, pp. 1267-1277, 1972.

[33] A. Yariv, "Coupled-Mode Theory for Guided Optics," *IEEE J. Quantum Electron.*, vol. QE-9, No. 9, pp. 919-933, Sep., 1973.

[34] H. Kogelnik, "Theory of Dielectric Waveguides", *Integrated Optics*, T. Tamir, Ed., New York: Springer-Verlag, ch2., 1975.

[35] L. Goldberg and S. H. Lee, "Optically Activated Switch/ Modulator Using a Photoconductor and Two Channel Waveguide," *Radio Science*, vol. 12, No. 4, pp. 537-542, Jul.-Aug., 1977.

[36] H. F. Taylor, "Guided Wave Electrooptic Devices for Logic and Computation," *Appl. Opt.*, vol. 17, No. 10, pp. 1493-1498, May, 1978.

[37] A. Hardy and W. Streifer, "Coupled Mode Theory of Parallel Waveguide," *J. Lightwave Tech.*, vol. LT-3, No. 5, pp. 1135-1146, Oct., 1985.

[38] A. Hardy and W. Streifer, "Coupled Mode Solutions of Multiwaveguide Systems," *IEEE J. Quantum Electron.*, vol. QE-22, No. 4, pp. 528-534, Apr., 1986.

[39] W. Streifer, M. Osinski, and A. Hardy, "Reformulation of the Coupled-Mode Theory of Multiwaveguide Systems," *J. Lightwave Tech.*, vol. LT-5, No. 1, pp. 1-4, Jan., 1987.

[40] H. A. Haus, W. P. Huang, S. Kawakami, and N. A. Whitaker, "Coupled-Mode Theory of Optical Waveguides," *J. Lightwave Tech.*, vol. LT-5, No. 1, pp. 16-23, Jan., 1987.

[41] H. A. Haus, W. P. Huang, and A. W. Snyder, "Coupled-Mode Formulations," *Opt. Lett.*, vol. 14, No. 21, pp. 1222-1224, Nov., 1989.

[42] H. A. Haus and W. P. Huang, "Coupled-Mode Theory," *Proc. IEEE*, vol. 79, No. 10, pp. 1505-1518, Oct., 1991.

[43] C. Vassallo, "About Coupled-Mode Theories for Dielectric Waveguides," *J. Lightwave Technol.*, vol. LT-6, No. 2, pp. 294-303, Feb., 1988.

[44] V. K. Tripathi, "Asymmetric Coupled Transmission Lines in an Inhomogeneous Medium," *IEEE Trans. Microwave Theory and Tech.*, vol. MTT-23, No. 9, pp. 734-739, Sep., 1975.

[45] V. K. Tripathi, "Equivalent Circuits and Characteristics of Inhomogeneous Nonsymmetrical Coupled-Line Two-Port Circuits," *IEEE Trans. Microwave Theory and Tech.*, vol. MTT-25, pp. 140-142, Feb., 1977.

[46] V. K. Tripathi, "On the Analysis of Symmetrical Three-Line Micro-Strip Circuits," *IEEE Trans. Microwave Theory and Tech.*, vol. MTT-25, No. 9, pp. 726-729, Sep., 1978.

[47] V. K. Tripathi, "The Scattering Parameters and Directional Coupler Analysis of Characteristically Terminated Three-Line Structures in an Inhomogeneous Medium," *IEEE Trans. Microwave Theory and Tech.*, vol. MTT-29, No. 1, pp. 22-26, Jan., 1981.

[48] Y. K. Chin, *Analysis and Applications of Multiple Coupled Line Structures in an Inhomogeneous Medium*, Ph.D. dissertation, Oregon State University, Corvallis, OR, U.S.A., May., 1982.

[49] V. K. Tripathi and J. B. Rettig, "A SPICE Model for Multiple Coupled Microstrips and Other Transmission Lines," *IEEE Trans. Microwave Theory Tech.*, pp. 1513-1518, Dec., 1985.

[50] V. K. Tripathi, "A Dispersion Model for Coupled Microstrips," *IEEE Trans. Microwave Theory Tech.*, pp. 66-71, Jan., 1986.

[51] A. S. Mohammed, *Analysis and Modeling of Electrically Long MESFET and Coupled Schottky Lines*, Ph.D. dissertation, Oregon State University, Corvallis, OR, U.S.A., Dec., 1987.

[52] V. K. Tripathi and A. Biswas, "Coplanar and Broadside Coupled Finline Six Port Hybrids," *Proc. European Microwave Conference*, Budapest, Hungary, Sep., 1990.

[53] Y. K. Chin, H. S. Chang, and V. K. Tripathi, "Application of Interdigitated DC Blocks/Transformers in Amplifier Design," *Proc. 3rd Int. Symp. on Recent Advances in Mirowave Technology*, pp. 532-535, Reno, Nevada, U.S.A., Aug., 1991.

[54] V. K. Tripathi, Y. K. Chin, H. S. Chang, and N. Orhanovic, "Coupled Line Multiports," *Proc. IEEE ISCAS*, May., 1992.

[55] C. T. Seaton, J. D. Valera, R. L. Shoemaker, G. I.

Stegeman, J. Chilwell, and D. Smith, "Anomalous Nonlinear Guided Wave Cut-Off Phenomena," *Appl. Phys. Lett.*, vol. 45, No. 11, pp. 1162-1163, Dec., 1984.

[56] E. W. Van Stryland, H. Vanherzeele, M. A. Woodall, M. J. Smirl, S. Guha, T. F. Boggess, "Two Photon Absorption, Nonlinear Refraction, and Optical Limiting in Semiconductors," *Opt. Engr.*, vol. 24, No. 4, pp. 613-623, Jul./Aug., 1985.

[57] C. T. Seaton, G. I. Stegeman, and H. G. Winful, "Nonlinear Guided Wave Applications," *Opt. Eng.*, vol. 24, No. 24, pp. 593-599, Jul./Aug., 1985.

[58] S. M. Jensen, "The Nonlinear Coherent Coupler," *IEEE J. Quantum Electron.*, vol. QE-18, No. 10, pp. 1580-1583, Oct., 1982.

[59] D. A. B. Miller, D. S. Chemla, D. J. Eilenberger, P. W. Smith, A. C. Gossard, and W. T. Tsang, "Large Room-Temperature Optical Nonlinearity in GaAs/$Ga_{1-x}$ $Al_x$As Multiple Quantum Well Structures," *Appl. Phys. Lett.*, vol. 41, No. 8, pp. 679-681, Oct., 1982.

[60] D. S. Chemla and D. A. B. Miller, "Room-Temperature Excitonic Nonlinear-Optical Effects in Semiconductor Quantum-Well Structures," *Opt. Soc. Amer.*, vol. 2, No. 7, pp. 1155-1173, Jul., 1985.

[61] P. LiKamWa, J. E. Sitch, N. J. Mason, J. S. Roberts, and P. N. Robson, "All Optical Multiple-Quantum-Well Waveguide Switch," *Electron. Lett.*, vol. 21, No. 1, pp. 27-28, Jan., 1985.

[62] A. K. Ghatak, K. Thyagarajan, and M. R. Shenoy, "Numerical Analysis of Planar Optical Waveguides Using Matrix Approach," *J. Lightwave Tech.*, vol. LT-5, No. 5, pp. 660-667, May, 1987.

[63] M. R. Ramadas, R. K. Varshney, K. Thyagarajan, and A. K. Ghatak, "A Matrix Approach to Study the Propagation Characteristics of a General Nonlinear Planar Waveguide," *J. Lightwave Tech.*, vol. LT-7, No. 12, pp. 1901-1904, May, 1987.

[64] M. Cada and J. D. Begin, "An Analysis of a Planar Optical Directional Coupler with a Lossless Kerr-Like Coupling Medium," *IEEE J. Quantum Electron.*, vol. QE-26, No. 2, pp. 361-371, Feb., 1990.

[65] B. P. Keyworth and M. Cada, "All-Optical Switching in a GaAs-Based Multiple Quantum Well Directional Coupler," *Can. J. Phys.*, vol. 67, pp. 408-411, 1989.

[66] P. R. Berger, P. K. Bhattacharya, and S. Gupta, "A Waveguide Directional Coupler with a Nonlinear Medium," *IEEE J. Quantum Electron.*, vol. QE-27, No. 3, pp. 788-795, Mar., 1991.

[67] U. Langbein, F. Lederer, T. Perschel, and H.-E. Ponath, "Nonlinear Guided Waves in Saturable Nonlinear Media," *Opt. Lett.*, vol. 10, No. 11, pp. 571-573, Nov., 1985.

[68] G. I. Stegeman, C. T. Seaton, C. N. Ironside, T. Cullen, and A. C. Walker, "Effects of Saturation and Loss on Nonlinear Directional Couplers," *Appl. Phys. Lett.*, vol. 50, No. 16, pp. 1035-1037, Apr., 1987.

[69] E. Caglioti, S. Trillo, S. Wabnitz, and B. Daino, "Power-Dependent Switching in A Coherent Nonlinear Directional Coupler in the Presence of Saturation," *Appl. Phys. Lett.*, vol. 51, No. 5, pp. 293-295, Aug., 1987.

[70] G. I. Stegeman, E. Caglioti, S. Trillo, and S. Wabnitz, "Parameter Trade-Offs in Nonlinear Directional Couplers: Two Level Saturable Nonlinear Media," *Opt. Comm.*, vol. 63, No. 5, pp.281-284, Sep., 1987.

[71] E. Caglioti, S. Trillo, S. Wabnitz, and G. I. Stegeman, "Limitations to All-Optical Switching Using Nonlinear Couplers in the Presence of Linear and Nonlinear Absorption and Saturation," *J. Opt. Soc. Am. B*, vol. 5, No. 2, pp. 472-482, Feb., 1988.

[72] B. Daino, G. Gregori, and S. Wabnitz, "Stability Analysis of Nonlinear Coherent Coupling," *J. Appl. Phys.*, vol. 58, No. 12, pp. 4512-4514, Dec., 1985.

[73] Y. Chen, "Solution to Full Coupled Wave Equations of Nonlinear Coupled Systems," *IEEE J. Quantum Electron.*, vol. QE-25, No. 10, pp.2149-2153, Oct., 1989.

[74] X. J. Meng and N. Okamoto, "Improved Coupled-Mode Theory for Nonlinear Directional Couplers," *IEEE J. Quantum Electron.*, vol. QE-27, No. 5, pp. 1175-1181, May, 1991.

[75] G. I. Stegeman, C. T. Seaton, C. N. Ironside, T. Cullen, and A. C. Walker, "Effects of Saturation and Loss on Nonlinear Directional Couplers," *Appl. Phys. Lett.*, vol. 50, No. 16, pp. 1035-1037, Apr., 1987.

[76] E. Caglioti, S. Trillo, S. Wabnitz, and G. I. Stegeman, "Limitations to All-Optical Switching Using Nonlinear Couplers in the Presence of Linear and Nonlinear Absorption and Saturation," *J. Opt. Soc. Am. B*, vol. 5, No. 2, pp. 472-482, Feb., 1988.

[77] A. Yariv, *Optical Electronics*, 3rd Ed. New York:CBS College Publishing, Ch. 13, 1985.

[78] R. Levy, "Transmission-Line Directional Couplers for Very Broad Band Operation," *Proc. Inst. Elec. Eng.* vol. 112, pp. 469-476, Mar., 1965.

[79] R. E. Collin, *Field Theory of Guided Waves*, York, PA:McGraw-Hill, Ch. 6, 1960.

[80] T. Itoh, *Numerical Technique for Microwave and Millimeter-Wave Passive Structures*, New York:Wiley, Ch. 11, 1989.

[81] N. N. Akhmediev, "Novel Class of Nonlinear Surface Waves:Asymmetric Modes in a Symmetric Layered Structure," *Sov. Phys. JETP*, vol. 56, No. 2, pp. 299-303, Aug., 1982.

[82] F. Lederer, U. Langbein, and H.-E. Ponath, "Nonlinear Waves Guided by a Dielectric Slab:1. TE-Polarization," *Appl. Phys. B*, vol. 31, pp. 69-73, 1983.

[83] U. Langbein, F. Lederer, and H.-E. Ponath, "A New Type of Nonlinear Slab-Guided Waves," *Opt. Commun.*, vol. 46, pp. 167-169, Jul., 1983.

[84] C. T. Seaton, J. D. Valera, R. L. Shoemaker, G. I. Stegeman, J. T. Chilwell, and S. D. Smith, "Calculations of Nonlinear TE Waves Guided by Thin Dielectric Films Bounded by Nonlinear Media," *IEEE J. Quantum Electron.*, vol. QE-21, NO. 7, pp. 774-783, Jul., 1985.

[85] M. Abramowitz and J. A. Stegun, *Handbook of Mathematical Functions*, Appl. Math. Series 55, Washington, DC: Nat. Bureau Standards, pp. 569-607, 1964.

[86] D. F. Lawden, *Elliptic Functions and Applications*, Appl. Math. Sciences 80, Springer-Verlag, New York, Chap. 3, 1989.

[87] A. D. Boardman and P. Egan, "Optically Nonlinear Waves in Thin Films," *IEEE J. Quantum Electron.*, vol. QE-22, No. 2, pp. 319-324, Feb., 1986.

[88] T. Sakakibara and N. Okamoto, "Nonlinear TE Waves in a Dielectric Slab Waveguide with Two Optically Nonlinear Layers," *IEEE J. Quantum Electron.*, vol. QE-23, No. 12, pp. 2084-2088, Dec., 1987.

[89] S. Shin, E. M. Wright, and G. I. Stegeman, "Nonlinear TE Waves of Coupled Waveguides Bounded by Nonlinear Media," *J. Lightwave Technol.*, vol. LT-6, No. 6, pp. 977-983, Jun., 1988.

[90] D. Marcuse, "Directional Couplers Made of Non-identical Asymmetric Slabs. Part I: Synchronous Couplers," *J. Lightwave Technol.*, vol. LT-5, No. 1, pp. 113-118, Jan., 1987.

# APPENDICES

# APPENDIX A

## The Impedance Matrix for TM Modes

General expressions for the impedance matrix of an asymmetric n-waveguide can be obtained by methods similar to those described in section 2.4. Fields are expressed as

$$h_j = \sum_{i=1}^{n} A_i R_{ji} e^{-j\beta_i z} + A_{n+1} R_{ji} e^{j\beta_i z} \qquad \text{(A-1)}$$

$$e_j = \sum_{i=1}^{n} A_i R_{ji} Z_{ji} e^{-j\beta_i z} - A_{n+i} R_{ji} Z_{ji} e^{j\beta_i z} \qquad \text{(A-2)}$$

where

$$Z_{ji} = \pm \left. \frac{e_j}{h_j} \right|_i = \frac{\beta_i}{\omega \epsilon_j} \qquad \text{(A-3)}$$

for which j and i represent,respectively, the guides and modes, and where $Z_{ji}$ is the wave impedance of guide j for mode i. A positive sign indicates waves travelling +z direction, whereas a negative sign indicates waves propagating -z direction. The fields at input and output ends of the coupler are

$$\begin{bmatrix} H_1 \\ H_2 \\ \cdot \\ \cdot \\ H_n \\ -H_{n+1} \\ -H_{n+2} \\ \cdot \\ \cdot \\ -H_{2n} \end{bmatrix} = \begin{bmatrix} [M_H] & [M_H] \\ & \\ & \\ & \\ -[M_H]\,[e^{-j\theta_i}]_d & -[M_H]\,[e^{j\theta_i}]_d \end{bmatrix} \begin{bmatrix} A_1 \\ A_2 \\ \cdot \\ \cdot \\ A_n \\ A_{n+1} \\ A_{n+2} \\ \cdot \\ \cdot \\ A_{2n} \end{bmatrix} \qquad \text{(A-4)}$$

and

$$\begin{bmatrix} E_1 \\ E_2 \\ \cdot \\ \cdot \\ E_n \\ E_{n+1} \\ E_{n+2} \\ \cdot \\ \cdot \\ E_{2n} \end{bmatrix} = \begin{bmatrix} [M_E] & -[M_E] \\ & \\ & \\ & \\ [M_E]\,[e^{-j\theta_i}]_d & -[M_E]\,[e^{j\theta_i}]_d \end{bmatrix} \begin{bmatrix} A_1 \\ A_2 \\ \cdot \\ \cdot \\ A_n \\ A_{n+1} \\ A_{n+2} \\ \cdot \\ \cdot \\ A_{2n} \end{bmatrix} \qquad \text{(A-5)}$$

where $[M_E]$ and $[M_H]$ are the eigenvectors corresponding to eigenvalues and d denotes a diagonal matrix. The eigenvectors are

$$[M_H] = \begin{bmatrix} R_{11} & R_{12} & \cdots & R_{1n} \\ R_{21} & R_{22} & \cdots & R_{2n} \\ \vdots & & & \vdots \\ R_{n1} & R_{n2} & \cdots & R_{nn} \end{bmatrix}, \qquad [M_E] = \begin{bmatrix} R_{11}Z_{11} & R_{12}Z_{12} & \cdots & R_{1n}Z_{1n} \\ R_{21}Z_{21} & R_{22}Z_{22} & \cdots & R_{2n}Z_{2n} \\ \vdots & & & \vdots \\ R_{n1}Z_{n1} & R_{n2}Z_{n2} & \cdots & R_{nn}Z_{nn} \end{bmatrix}$$

(A-6)

Eqs. (A-4) and (A-5) can be rewritten as $[H] = [T_H][A]$ and $[E] = [T_E][A]$. The impedance matrix can be obtained by substituting $[A] = [T_E]^{-1}[H]$ into eq. (A-5). The electric field and magnetic field relationships are then

$$[E] = \begin{bmatrix} [M_E] & -[M_E] \\ [M_E]\,[e^{-j\theta_i}]_d & -[M_E]\,[e^{j\theta_i}]_d \end{bmatrix} \begin{bmatrix} [M_H] & [M_H] \\ -[M_H]\,[e^{-j\theta_i}]_d & -[M_H]\,[e^{j\theta_i}]_d \end{bmatrix}^{-1} [H]$$

(A-7)

By rearranging eq. (A-7), the impedance matrix is then

$$[Z] = \begin{bmatrix} [M_E] & [0] \\ [0] & [M_E] \end{bmatrix} \begin{bmatrix} [U] & -[U] \\ [e^{-j\theta_i}]_d & -[e^{j\theta_i}]_d \end{bmatrix} \begin{bmatrix} [U] & [U] \\ -[e^{-j\theta_i}]_d & -[e^{j\theta_i}]_d \end{bmatrix}^{-1} \begin{bmatrix} [M_H] & [0] \\ [0] & [M_H] \end{bmatrix}$$

$$= -\begin{bmatrix} [M_E] & [0] \\ [0] & [M_E] \end{bmatrix} \begin{bmatrix} [jcot\theta_i]_d & [jcsc\theta_i]_d \\ [jcsc\theta_i]_d & [jcot\theta_i]_d \end{bmatrix} \begin{bmatrix} [M_H]^{-1} & [0] \\ [0] & [M_H]^{-1} \end{bmatrix}$$

$$= -\begin{bmatrix} [M_E]\,[jcot\theta_i]_d[M_H]^{-1} & [M_E]\,[jcsc\theta_i]_d[M_H]^{-1} \\ [M_E]\,[jcsc\theta_i]_d[M_H]^{-1} & [M_E]\,[jcot\theta_i]_d[M_H]^{-1} \end{bmatrix} \qquad \text{(A-8)}$$

Eq. (A-8) represents a general expression of the impedance matrix for TM modes of a n-waveguide coupler; the admittance matrix can be obtained similarly.

For a two-waveguide coupler, $[M_E]$ and $[M_H]$ are given by

$$[M_E] = \begin{bmatrix} Z_{m11} & Z_{m12} \\ R_c Z_{m21} & R_\pi Z_{m22} \end{bmatrix}, \qquad [M_H] = \begin{bmatrix} 1 & 1 \\ R_c & R_\pi \end{bmatrix} \qquad \text{(A-9)}$$

where $Z_{m11} = \beta_c/\omega\epsilon_{g1}$, $Z_{m12} = \beta_\pi/\omega\epsilon_{g1}$, $Z_{m21} = \beta_c/\omega\epsilon_{g2}$, and $Z_{m22} = \beta_\pi/\omega\epsilon_{g2}$. $\epsilon_{g1}$ and $\epsilon_{g2}$ are dielectric constants of guide 1 and guide 2. From eq. (A-8), the impedance matrix parameters are then easily obtained as

$$\begin{aligned}
Z_{11} &= Z_{33} = R_\pi Z_{m11}\cot\theta_1 - R_c Z_{m12}\cot\theta_2 \\
Z_{12} &= Z_{34} = -Z_{m11}\cot\theta_1 + Z_{m12}\cot\theta_2 \\
Z_{21} &= Z_{43} = R_c R_\pi Z_{m21}\cot\theta_1 - R_c R_\pi Z_{m22}\cot\theta_2 \\
Z_{22} &= Z_{44} = -R_c Z_{m21}\cot\theta_1 + R_c Z_{m12}\cot\theta_2 \\
Z_{13} &= Z_{31} = R_\pi Z_{m11}\csc\theta_1 - R_c Z_{m12}\csc\theta_2 \\
Z_{14} &= Z_{32} = -Z_{m11}\csc\theta_1 + Z_{m12}\csc\theta_2 \\
Z_{23} &= Z_{41} = R_c R_\pi Z_{m21}\csc\theta_1 - R_c R_\pi Z_{m22}\csc\theta_2 \\
Z_{24} &= Z_{44} = -R_c Z_{m21}\csc\theta_1 + R_c Z_{m12}\csc\theta_2
\end{aligned} \qquad \text{(A-10)}$$

Here, $-j/\Delta$ was assumed and $\Delta = R_{\pi} - R_{c}$. It is noted that $R_{c}$ and $R_{\pi}$ are the elements of the magnetic field eigenvectors.

# APPENDIX B

## Comments on Measuring Elements of Eigenvectors

We have defined $R_c$ and $R_\pi$ as the ratios of amplitudes of the fields in guide 2 to the fields in guide 1 for the two modes of a two-waveguide structure where the structural parameters of a guide are close to those of the other, as described in chapter 2. Another definition for these normal mode parameters can be made for an asymmetric two-waveguide as already shown in Fig. 2-1. The parameters are $n_1 = n_3 = n_5 = 3.2$, $n_2 = 3.3$, $n_4 = 3.35$, $d = W_1 = 1$ $\mu$m, and $\lambda = 1.5$ $\mu$m. Complete power exchange between guides can be achieved for this asymmetric structure by controlling $W_2$ and $W_2$ is found to be 0.4734 $\mu$m [90]. TE modes of the coupler are shown in Fig. B-1(a).

Synchronism of the two guides is expected from the field distributions. We extend the regions of guide 1 and guide 2 to the first half and to the other half of the coupler, respectively. Power associated with the field distribution is proportional to integration of $E_y^2$ across the structure. $R_c$ and $R_\pi$ must be related to field amplitudes rather than power. Then, $R_c$ and $R_\pi$ can be defined as

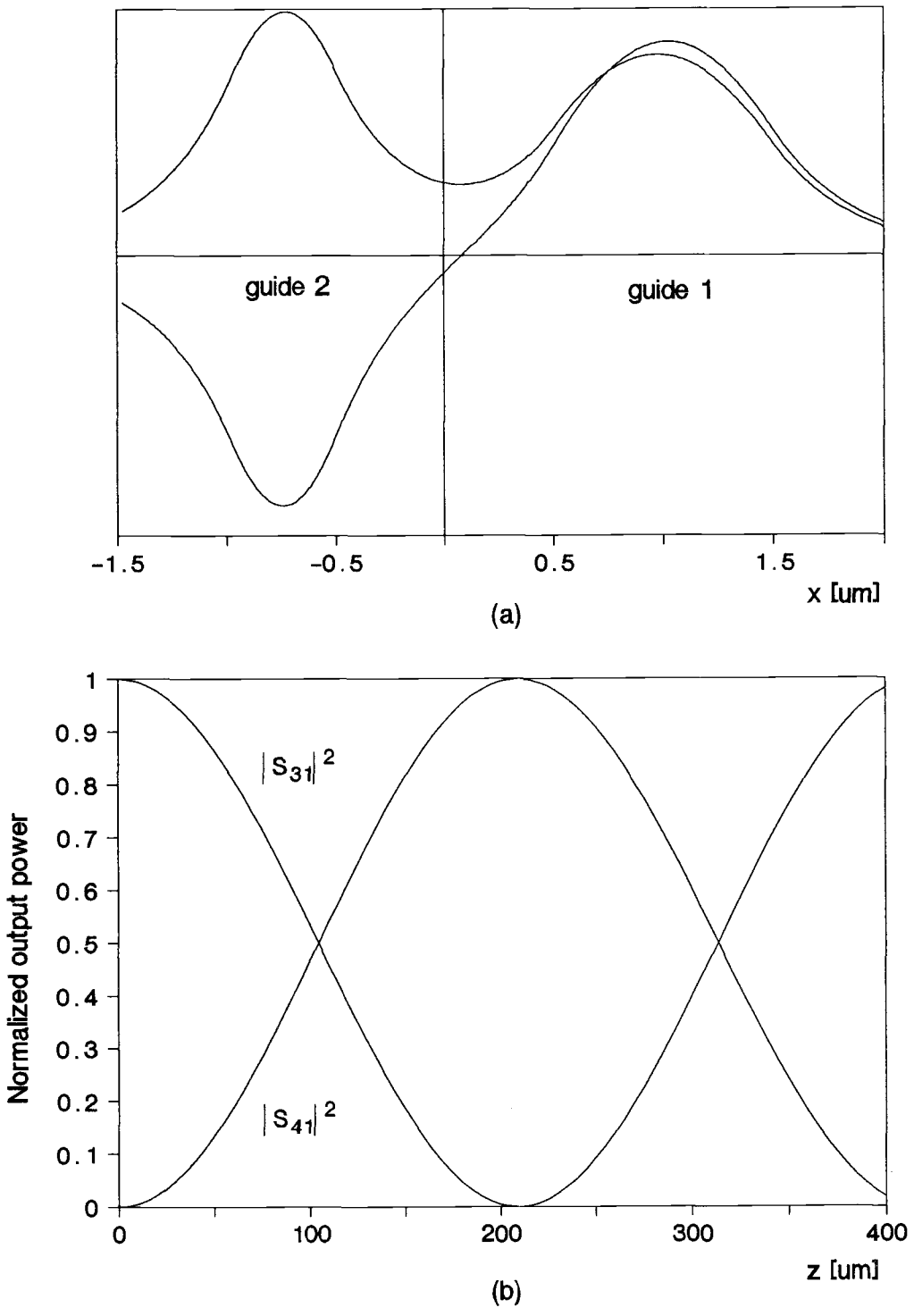


Fig. B-1. (a) TE modes of an asymmetric two-waveguide coupler. (b) Power distribution of the coupler.

$$R_{c,\pi} = \pm\sqrt{\int_{-\infty}^{0} |E_{c,\pi}|^2 \, dx} \; / \; \sqrt{\int_{0}^{\infty} |E_{c,\pi}|^2 \, dx} \qquad \text{(B-1)}$$

where a positive sign and a negative sign indicate c mode and $\pi$ mode, respectively. Based on this definition, power distribution of the coupler is calculated from the normal mode analysis and is shown in Fig. B-1(b).

# APPENDIX C

## Perturbed Modes of A Three-Waveguide Coupler

The matrix method can be used to analyze a three-waveguide coupler with two nonlinear coupling media in a similar manner as described for a two-waveguide coupler in section 4.3. Total field can be expressed as the sum of three perturbed modes such that $E(x,z) = Y_A(x,z) + Y_B(x,z) + Y_C(x,z)$. By expressing each perturbed modes as $Y_m(x,z) = y_m(x) \exp(-jk_o\beta_m z)$ for m = A, B, and C, a nonlinear wave equation results in three simultaneous nonlinear differential equations:

$$d^2y_A/dx - k_A^2y_A + \alpha k_o^2 F y_A = 0 \qquad (C\text{-}1)$$

$$d^2y_B/dx - k_B^2y_B + \alpha k_o^2 F y_B = 0 \qquad (C\text{-}2)$$

$$d^2y_C/dx - k_C^2y_C + \alpha k_o^2 F y_C = 0 \qquad (C\text{-}3)$$

where F is a function of three modal fields and their propagation constants and is given by

$$F = y_A^2 + y_B^2 + y_C^2 + 2y_Ay_B\cos\theta_{AB} + 2y_By_C\cos\theta_{BC} + 2y_Ay_C\cos\theta_{AC}. \qquad (C\text{-}4)$$

$k_m^2 = k_o^2(\beta_m^2 - n_o^2)$ and $\theta_{mn} = k_o(\beta_m - \beta_n)z$ for m, n = A, B, C and for $m \neq n$. The field in the $i^{th}$ nonlinear medium is given by

$$y_{m,i} = A_{m,i}\cosh[k_{m,i}(x-d_{i-1})] + B_{m,i}\sinh[k_{m,i}(x-d_{i-1})] \qquad (C\text{-}5)$$

It is convenient to calculate the propagation constants and the field distributions for the perturbed modes at the input end (z = 0). When we assume a subscript i for the $i^{th}$ nonlinear layer, F and $n^2$ can then be written as

$$F = (y_A + y_B + y_C)^2 \text{ and } n^2 = n_o^2 + \alpha F^2_{avg}. \qquad (C\text{-}6)$$

To obtain an initial field $y_A$ for mode A, the initial value of $n^2$ is evaluated from

$$n^2 = n_o^2 + \alpha(y_B + y_C + A_A)^2_{avg} \ , \qquad (C\text{-}7)$$

where $(y_B + y_C + A_A)^2_{avg}$ is expressed as

$$\begin{aligned}(y_B + y_C + A_A)^2_{avg} &= A_A^2 + \frac{1}{2}(A_B^2 - B_B^2 + A_C^2 - B_C^2) \\ &+ \frac{1}{4\Delta_B}[(A_B^2 + B_B^2)\sinh 2\Delta_B + 2A_BB_B(\cosh 2\Delta_B - 1) \\ &+ 8A_A(A_B\sinh\Delta_B + B_B(\cosh\Delta_B - 1))] + \frac{1}{4\Delta_C}[(A_C^2 + B_C^2)\sinh 2\Delta_B \\ &+ 2A_CB_C(\cosh 2\Delta_C - 1) + 8A_A(A_C\sinh\Delta_C + B_C(\cosh\Delta_C - 1))] \\ &+ \frac{1}{\Delta_{B+C}}[(A_BA_C + B_BB_C)\sinh\Delta_{B+C} + (B_BA_C + A_BB_C)(\cosh\Delta_{B+C} - 1)] \\ &+ \frac{1}{\Delta_{B-C}}[(A_BA_C - B_BB_C)\sinh\Delta_{B-C} + (B_BA_C - A_BB_C)(\cosh\Delta_{B-C} - 1)]\end{aligned} \qquad (C\text{-}8)$$

and where $\Delta_{B,C} = k_{B,C}\Delta x$ and $\Delta_{B\pm C} = (k_B \pm k_C)\Delta x$. Perturbed A mode $y_A$ in the presence of other two modes is obtained based on the value of the dielectric constant calculated from eq. (C-7). The refractive index of the $i^{th}$ nonlinear layer can then be calculated from

$$n^2 = n_o^2 + \alpha(y_A + y_B + y_C)^2_{avg} = n_o^2 + \alpha G^2_{avg}, \qquad (C\text{-}9)$$

$G^2_{avg}$ is rewritten for computational purpose as

$$
\begin{aligned}
G_{avg}^2 = {} & \frac{1}{2}(A_A^2 - B_A^2 + A_B^2 - B_B^2 + A_C^2 - B_C^2) \\
& + \frac{1}{4\Delta_A}[(A_A^2 - B_A^2)\,sinh2\Delta_i + 2A_{AB_A}(cosh2\Delta_A - 1)] \\
& + \frac{1}{4\Delta_B}[(A_B^2 + B_B^2)\,sinh2\Delta_B + 2A_BB_B(cosh2\Delta_B - 1)] \\
& + \frac{1}{4\Delta_C}[(A_C^2 + B_C^2)\,sinh2\Delta_C + 2A_CB_C(cosh2\Delta_C - 1)] \\
& + \frac{1}{\Delta_{A+B}}[(A_AA_B + B_AB_B)\sinh\Delta_{A+B} + (B_AA_B + A_AB_B)(\cosh\Delta_{A+B} - 1)] \\
& + \frac{1}{\Delta_{A-B}}[(A_AA_B - B_AB_B)\sinh\Delta_{A-B} + (B_AA_A - A_AB_B)(\cosh\Delta_{A-B} - 1)] \\
& + \frac{1}{\Delta_{B+C}}[(A_BA_C + B_BB_C)\sinh\Delta_{B+C} + (B_BA_C + A_BB_C)(\cosh\Delta_{B+C} - 1)] \\
& + \frac{1}{\Delta_{B-C}}[(A_BA_C - B_BB_C)\sinh\Delta_{B-C} + (B_BA_C - A_BB_C)(\cosh\Delta_{B-C} - 1)] \\
& + \frac{1}{\Delta_{A+C}}[(A_AA_C + B_AB_C)\sinh\Delta_{A+C} + (B_AA_C + A_BB_C)(\cosh\Delta_{A+C} - 1)] \\
& + \frac{1}{\Delta_{A-C}}[(A_AA_C - B_AB_C)\sinh\Delta_{A-C} + (B_AA_C - A_AB_C)(\cosh\Delta_{A-C} - 1)]
\end{aligned}
\tag{C-10}
$$

where $\Delta_{m\pm n} = (k_m \pm k_n)\Delta x$ for m, n = A, B, C and for $m \neq n$. The steps of calculating perturbed modes are summarized as

1. The initial value of the nonlinear refractive index for mode A is calculated from eq. (C-7) in the presence of other modes.
2. A mode function $y_A$ is obtained from eq. (C-1).
3. Calculate the refractive index from eq. (C-9).
4. Repeat steps 2 and 3 until the refractive index converges.
5. B and C modes are obtained from eq. (C-2) and eq. (C-3), respectively by following steps 1 through 4.